공학박사 학위논문

Active Learning Methods and Applications to Reliability Analysis and Optimization of Complex Structural Systems

복잡 구조시스템의 신뢰성 해석 및 최적화를 위한
능동학습 개발 및 적용

2022년 8월

서울대학교 대학원

건설환경공학부

김 정 호

Active Learning Methods and Applications to Reliability Analysis and Optimization of Complex Structural Systems

복잡 구조시스템의 신뢰성 해석 및 최적화를 위한
능동학습 개발 및 적용

지도교수 송 준 호

이 논문을 공학박사 학위논문으로 제출함
2022년 8월

서울대학교 대학원
건설환경공학부
김 정 호

김정호의 공학박사 학위논문을 인준함
2022년 8월

위 원 장 김 호 경 (인)

부 위 원 장 송 준 호 (인)

위 원 채 윤 병 (인)

위 원 이 영 주 (인)

위 원 전 준 호 (인)

Abstract

To secure the resilience of the modern society, structural systems should achieve a proper level of reliability in the processes of design and maintenance decisions. Such procedures can assure the reliability of structural systems by preventing the risk of unexpected failures. Thus, appropriate strategies are required for reliability assessment and optimization to support the decision-making process of structural systems. However, reliability assessment generally needs to evaluate the system's performance repeatedly and thus may result in high computational costs. This issue is exacerbated especially when the structural system requires complex and high-dimensional models to describe the system's performance accurately. To effectively design and assess complex structural systems under various uncertainties, this dissertation introduces active learning frameworks for reliability assessment and reliability-based design optimization (RBDO) using adaptive surrogate models of system performance trained by computational simulation data and presents numerical applications.

First, an efficient active learning-based reliability assessment framework is developed. The proposed Probability-Adaptive Kriging in *n*-Ball (PAK-B^n) method predicts the limit-state surfaces using Gaussian process (GP) model, also known as Kriging, and adaptively trains the surrogate model using active learning. The proposed PAK-B^n incorporates the probabilistic density of the random variable space into the adaptive training procedure of identifying the surrogate limit-state surface. In addition, alternative sampling in *n*-ball domain is used as the candidate points for statistical learning, and the best candidate for training is determined in terms of

influence on the reliability estimation. The numerical examinations are carried out to demonstrate the efficiency and applicability of the proposed PAK-B^n method.

Although PAK-B^n is effective for reliability problems up to around 10 random variables, its applications are limited in high-dimensional problems, which are often needed to evaluate the reliability of structural systems subjected to natural and human-made hazards, e.g., wind loads, earthquakes, and collisions. To tackle such challenge and extend the applicability to stochastic dynamical systems, an active learning-based heteroscedastic Gaussian process (AL-HGP) is developed. Considering uncertainties arising from the structural system and the environmental wind loads, the proposed formulation by a mixture distribution of Gaussian densities, each of which represents the conditional distribution of the maximum response, enables estimation of first-passage probability using GP-based surrogates with heteroscedastic noises. In addition, an adaptive training process for surrogates can identify the best experimental designs achieving efficient convergence. The examples of engineering applications demonstrate the performance of the proposed AL-HGP method.

Next, the active learning framework is further developed for RBDO problems that aim to identify the optimal reliable design of complex structures. A new RBDO method, termed quantile surrogates by adaptive Gaussian process (QS-AGP), employs quantile surrogates of the limit-state functions to identify the admissible domain concerning reliability requirement. The GP-based quantile surrogates are trained adaptively through an exploration-exploitation trade-off based on inherent randomness and the model uncertainty of the surrogate. The adaptive training process in QS-AGP guides the computational simulations toward the domain, which

makes the greatest contribution to the optimization process. It is found that the proposed QS-AGP requires fewer performance function evaluations in achieving convergence to a reliable optimum design than existing RBDO approaches.

Finally, to promote the application of the ideas in QS-AGP to high-dimensional engineering systems, a new RBDO method termed, quantile surrogates and sensitivity by adaptive Gaussian process (QS^2-AGP) is developed. To this end, a non-sampling-based procedure is proposed for efficient estimation of the quantile surrogates based on input uncertainties and model error of surrogates. Moreover, to perform quantile-surrogate-based RBDO without relying on pre-generated design samples, the parameter sensitivity of the quantile surrogate is implemented. The computational efficiency of the proposed QS^2-AGP is demonstrated by a variety of RBDO examples including a large number of design parameters.

The performance of the proposed methods is demonstrated by numerical examples incorporating high-fidelity computational simulations. The compelling results confirm the merits and potential of the outcomes of this study, which will eventually enhance the resilience of modern engineering systems facilitated by reliability assessment and reliability-based optimization for design and maintenance decisions.

Keyword: Active learning, Decision-making, Design of experiment, Gaussian process, Reliability analysis, Reliability-based design optimization, Risk-informed decision, Optimization, Surrogate model, Stochastic loads

***Student Number*:** 2016-26343

Table of Contents

List of Figures

List of Tables

Chapter 1. Introduction

1.1 Motivation

The modern infrastructures are inevitably affected by the uncertainties, arising from lack of data, modeling approximations, or inherent randomness in the systems and their environment. Such uncertainties may have a significant impact on the system performance, which may induce catastrophic damage or losses. With the growing complexity of modern engineering systems, it is essential to manage the impact of such uncertainties in their processes of design and performance assessment. Thus, appropriate strategies are required for reliability assessment and design optimization to support the decision-making process of structures and other engineering systems.

To assure the reliability of structural systems, structural reliability analysis and reliability-based design optimization (RBDO) have been widely studied and applied (Du and Chen 2004; Der Kiureghian and Ditlevsen 2009; Dubourg *et al*. 2011; Zhang *et al*. 2017). Reliability analysis aims to assess the effects of uncertainties by estimating the associated failure probability with respect to some relevant limit state functions. RBDO aims to achieve reliable optimal design of systems whose optimal solution satisfies given reliability constraints. To evaluate the reliability in the processes of designing and assessing structural systems, researchers developed various methods which can be categorized as classical first and second-order reliability methods (FORM, SORM; Der Kiureghian 2022), simulation-based strategies (Au and Beck 2004; Kurtz and Song 2013; Wang *et al*. 2019), and surrogate-based approaches (Echard *et al*. 2011; Marelli and Sudret 2018).

However, the reliability evaluation generally requires repetitive structural analyses and thus may result in high computational costs. These enormous computational costs might hamper their engineering practice applications that often entail challenging and time-consuming simulations, e.g., nonlinear dynamic structural analyses, finite element simulations. This issue can be exacerbated when the engineering system requires complex and high-dimensional models to describe the system's performance accurately.

To address the issue, some researchers have investigated various machine learning algorithms to alleviate the computational burden caused by time-consuming structural analysis procedures. One of the compelling approaches to increase the computational efficiency for complex engineering analyses is the surrogate model approach (Jones *et al*. 1998; Dubourg *et al*. 2011; Zhang *et al*. 2017; Kim *et al*. 2020). A surrogate model, also termed a meta-model, approximates the results of expensive computational simulations based on the training dataset of input-output pairs. The accuracy and efficiency of the surrogate-based predictions rely on the training data collection and their learning strategies. Thus, the surrogate models and its applications need to be developed from the viewpoint of structural reliability and reliability-based design optimization.

This dissertation aims to address the computational challenges in reliability assessment and RBDO applications by improving the accuracy of predictions and extending the applicability to more practical engineering systems. To this end, the Gaussian process (GP) model, which is one of the machine learning-based surrogate model, are employed as a tool to predict the structural responses and quantify the prediction uncertainties. To improve the efficiency and accuracy in surrogate-based

predictions, an active learning algorithm is utilized to train the surrogate models by adaptively selecting the simulation points. Through the active learning frameworks developed using GP-based surrogate models, it is possible to assess the reliability and achieve reliable optimal design of complex engineering systems with significantly reduced computational costs and dataset.

1.2 Objectives and scopes

The research described in this dissertation aims to achieve four goals: (1) developing an active learning framework for reliability assessment of challenging and complex engineering systems, (2) extending the method to high-dimensional reliability problems that incorporates the stochastic sequences of wind excitations, (3) enabling RBDO applications for decision-making, and (4) facilitating the applications to high-dimensional RBDO problems.

The dissertation first focuses on developing an active learning reliability method, termed probability-adaptive Kriging in *n*-ball (PAK-B^n). The main objective of PAK-B^n is to carry out an adaptive selection of simulation points, i.e., adaptive training of Kriging surrogates, with low computational costs from a reliability analysis standpoint. Next, to estimate the reliability of structures subjected to stochastic wind excitations, an active-learning-based heteroscedastic Gaussian process (AL-HGP) method is developed by incorporating high-dimensional sequences of stochastic winds. Next, a new active learning-based RBDO method, quantile surrogates by adaptive Gaussian process (QS-AGP) is developed using quantile-based formulation to identify the probability-feasible design domain. Finally, an extension is made to promote the applications of QS-AGP to high-

dimensional RBDO problems in which the number of design parameters is considerably large. The extended method is referred to as quantile surrogates and sensitivity by adaptive Gaussian process (QS^2-AGP) because the sensitivity-based optimization algorithm is employed to handle a large number of design parameters without requiring any random samples.

Compared with the existing reliability analysis and RBDO methods, the proposed active learning-based methods have the following benefits: (1) accurate estimation of the reliability of structures including stochastic dynamical systems is obtained with significantly less computational efforts; (2) the optimal reliable design of structural systems can be efficiently identified considering various uncertainties in engineering systems and/or their environment; (3) the high-dimensional reliability and RBDO problems can be solved without losing the benefits and merits of the proposed methods; (4) the methods successfully deal with high-fidelity and time-consuming computational simulations, e.g., finite element analyses; (5) it is possible to deal with challenging engineering systems featuring highly nonlinear performance functions, various distribution types, and complexity; and (6) the proposed risk-informed design frameworks can be employed for the recent performance-based engineering frameworks and decision-making for modern structural systems under various disasters.

1.3 Organization

The dissertation is organized into six chapters. Chapters 2 and 3 address the development of active learning reliability methods, i.e., PAK-B^n and AL-GHP, for assessing structural reliability for both static and dynamic systems. In Chapters 4 and

5, the proposed active learning-based RBDO methods are introduced to handle a considerably large number of design parameters. More details on the specific subjects covered in each chapter are presented below.

Chapter 2 describes the development of PAK-B^n method that improves the efficiency and accuracy of reliability analysis by incorporating the probabilistic density of the random variable space into the adaptive procedure of identifying the surrogate limit-state surface. In addition, samples distributed uniformly inside the *n*-ball domain are used as the candidate points to enrich the experimental design, and the best candidate for simulation is determined in terms of influence on the failure probability estimation. The efficiency and accuracy of the proposed PAK-B^n method are demonstrated by several reliability examples characterized by highly non-linear limit-state functions, small failure probability, multiple design points, and engineering applications. The results confirm that the method facilitates convergence to the failure probability with a smaller number of function evaluations.

Chapter 3 begins with a discussion on the reliability measures of structural systems against stochastic loads caused by natural and man-made hazards, e.g., wind loads, earthquakes, and collisions, which lead to a high-dimensional reliability analysis problem. Since the PAK-B^n method in Chapter 2 has limitations in the high-dimensional applications, a new AL-HGP method is introduced to efficiently estimate the reliability under stochastic excitations. The AL-HGP introduces an alternative formulation using the conditional distribution of the maximum response to handle the high-dimension of stochastic excitation sequences. The method employs the Gaussian-process-based surrogate model with heteroscedastic noises to fit the distribution parameter functions considering uncertainties arising from the

structural system and the environmental loads. In addition, an adaptive training process for surrogates is introduced to identify the best experimental designs achieving efficient convergence. The numerical examples of an eight-story building and a transmission tower demonstrate that the proposed method can produce accurate estimation results with fewer structural simulations than existing methods.

Chapter 4 describes the RBDO problem that incorporates various uncertainties into the design optimization of structures and other engineering systems. Many RBDO methods have been developed, but their practical applications can be limited if the reliability consideration entails a large number of evaluations of performance functions, especially for those requiring time-consuming simulations. To overcome the challenge, this chapter proposes a new RBDO method that employs quantile surrogates of the performance functions to identify the admissible domain, termed the probability-feasible design domain. Gaussian process models of the quantile surrogates are updated adaptively through an exploration-exploitation trade-off based on inherent randomness and the model uncertainty of the surrogate. The method guides the computational simulations toward the domain in which the quantile estimation can make the greatest contribution to the optimization process. The validity and efficiency of the proposed RBDO method using QS-AGP are demonstrated using several numerical examples. The results confirm that QS-AGP facilitates convergence to a reliable optimum design with a significantly reduced number of function evaluations compared to existing RBDO approaches.

Chapter 5 extends the applicability of the QS-AGP method in Chapter 4 to high-dimensional RBDO applications. Since QS-AGP uses pre-generated design samples to check whether the design samples satisfy the reliability requirements, the

approach could be computationally expensive in high-dimensional applications that may require an insurmountable memory. To alleviate this difficulty, a new quantile surrogate-based RBDO framework is proposed in this chapter. To this end, a non-sampling-based procedure is proposed for efficient estimation of the quantile surrogates based on both input uncertainties and model error of surrogates. Moreover, to perform quantile-surrogate-based RBDO without relying on pre-generated design samples, the parameter sensitivity of the quantile surrogate is implemented. The computational efficiency of the proposed QS^2-AGP is demonstrated by a variety of RBDO examples featuring up to 15 design parameters.

Finally, Chapter 6 provides a summary of the developments and discusses the major findings. This dissertation is concluded by discussions on current limitations, requirements, and recommended topics for future research.

Chapter 2. Active Learning-based Reliability Analysis Using Probability-Adaptive Kriging in *n*-Ball (PAK-B^n)

2.1 Introduction

Complexity of today's engineering systems inevitably makes the computational simulation of their performance challenging and time-consuming. Since structural reliability analysis methods generally repeat such computational simulations, it is essential to reduce the number of function evaluations required to achieve reliable estimates. In research efforts to fulfill this aim, adaptive Kriging methods have gained significant interest because of their desirable properties and accuracy of the surrogate model (Jones *et al*. 1998; Echard *et al*. 2010; Dubourg *et al*. 2011; Zhang *et al*. 2017). However, the existing adaptive Kriging approaches may not be flexible enough to fit the complex shape and orientation of the critical points especially when a structural reliability problem has small failure probability of complex failure domains (Wen *et al*. 2016; Lelièvre *et al*. 2018). Thereby, the adaptive Kriging needs to guide the simulation data to the vicinity of limit-state surface while giving priorities to critical regions from the viewpoint of reliability analysis.

This chapter first presents a brief overview of structural reliability problem and basic theories of Gaussian process model. The overview includes the AK-MCS method that is one of the most widely used active learning reliability method and its limitations. Next, details of the new adaptive Kriging method, PAK-B^n, will be introduced: (1) alternative sampling in *n*-ball, (2) new learning function, and (3) the

adaptive algorithm for reliability analysis. Through numerical examples of challenging reliability problems, the proposed approach will be tested in terms of (1) robustness against multiple design points and high non-linearity of limit-state functions, and (2) accuracy and efficiency with respect to the number of function evaluations for various levels of failure probability. In each example, the final experimental designs and the identified limit-state surface will be visualized to provide further insight. Lastly, a summary of the results and concluding remarks are provided (Kim and Song 2020).

2.2 Kriging-based reliability analysis

2.2.1 Structural reliability analysis

In a reliability problem described by an n-vector of basic random variables, $\mathbf{X}$, the failure probability P_f is defined as the n-fold integral

$$P_f = \int_{G(\boldsymbol{x})\leq 0} f_{\mathbf{X}}(\boldsymbol{x})\, d\boldsymbol{x} \tag{2.1}$$

where $f_{\mathbf{X}}(\boldsymbol{x})$ is the joint probability density function (PDF) of $\mathbf{X}$; and $G(\boldsymbol{x})$ is the limit-state function whose negative sign indicates the occurrence of the failure event of interest. In general structural reliability problems, the computation of Eq. (2.1) can be a difficult task since the integration of $f_{\mathbf{X}}(\boldsymbol{x})$ over the failure domain is time-consuming, and/or identifying the limit-state surface, i.e., $\{\boldsymbol{x}|G(\boldsymbol{x}) = 0\}$ is challenging. Thus, various methods have been developed in order to assess structural reliability efficiently but without compromising accuracy.

The first and second order reliability methods (FORM, SORM) are the most widely used reliability methods, which estimate the failure probability based on

approximation of the limit-state surface at the richest point in terms of probability density, termed design point or most probable point (MPP) (Der Kiureghian 2022). However, in this approach, finding the design point is quite difficult in some problems, and the error caused by approximating limit-state surface can be significant if the function shows a high level of nonlinearity, or has multiple design points or critical regions (Kim and Song 2018). Figure 2.1 shows an example of design point for a component reliability problem with two random variables. As an alternative, Monte Carlo Simulation (MCS) is often used to estimate the failure probability based on computational simulations at sample points, and known to be robust against the type and dimension of a given reliability problem. On the other hand, MCS may require a large number of function evaluations especially in small failure probability problems. In order to reduce the variance of the failure probability estimated by MCS, various alternatives, e.g., Importance Sampling, Directional Simulation, Subset Simulation, and Line Sampling (Nie and Ellingwood 2000; Au and Beck 2001; Schuëller *et al*. 2004; Kurtz and Song 2013), have been proposed.

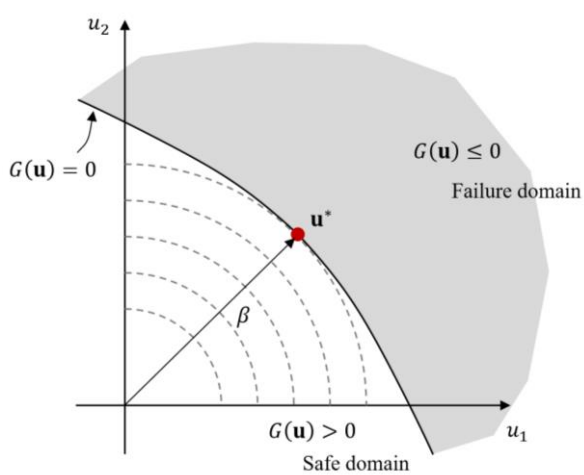

Figure 2.1 Design point for a component reliability problem with two random variables

In order to construct an accurate Kriging model with a small set of simulation points, many adaptive schemes have been developed and used for optimization and reliability assessment (Jones *et al*. 1998; Echard *et al*. 2010). A Kriging approach is considered "adaptive" when the information from the prior stages is utilized in selecting the next experiment points, i.e., the values of $\boldsymbol{x}$ where the function $G(\boldsymbol{x})$ will be actually evaluated. Echard *et al*. (2010) proposed an adaptive Kriging method that can efficiently estimate the failure probability by pursuing adaptive design of experiments in surrogate model construction. In their approach termed AK-MCS, the limit-state function is evaluated for only a small subset of Monte Carlo samples, and drastically decreases the number of function calls compared to other surrogate-based methods. In each iteration, the next point for function evaluation is adaptively selected based on the learning function $U(\boldsymbol{x})$ representing the trade-off between Kriging mean and variance. The sample point with the minimum $U(\boldsymbol{x})$ is selected as the next point to enrich the experimental design. Several other methods, e.g., AK-OIS, AK-SS and AK-SYS (Fauriat and Gayton 2014; Huang *et al*. 2016; Zhang *et al*. 2020), were also developed to improve the efficiency of adaptive Kriging method.

During the adaptive refinement process of the Kriging surrogate model, the influence of the misclassification error depends on relative importance of the corresponding locations. In reliability problems, critical domains such as areas including the design point are important for accurate estimation of failure probability and reliability index. Therefore, adaptive refinement focusing on such critical domains is desired. Since the learning function $U(\boldsymbol{x})$ in AK-MCS is defined in terms of the Kriging mean and variance only, the relative importance of $\boldsymbol{x}$, which is determined by the corresponding probability density, is not incorporated into the

adaptive procedure. Furthermore, it is noted that the assessment of low failure probability is still challenging even when an adaptive Kriging method is used. When the failure probability is extremely low (e.g., $10^{-3}\sim10^{-7}$), a large size of MCS sample populations are required to identify the failure region, which may cause a memory problem.

2.2.2 Basic theories of Gaussian process model

A Gaussian process model, also known as Kriging, has been widely used to construct a surrogate of a complex function based on the function evaluations at a few input points, which are selected among samples through so-called Design of Experiment (DoE) process. The main assumption behind the GP-based surrogates is that the response at the input $\boldsymbol{x}$, $y(\boldsymbol{x})$ is the realization of a Gaussian process (Rasmussen and Willians 2006; Rasmussen and Nickisch 2015), that is,

$$y(\boldsymbol{x})\sim GP\big(m(\boldsymbol{x}), k(\boldsymbol{x},\boldsymbol{x}';\boldsymbol{\Theta})\big) \tag{2.2}$$

where $m(\boldsymbol{x}) = \mathrm{E}[y(\boldsymbol{x})]$ is the mean function; $k_y(\boldsymbol{x},\boldsymbol{x}') = \mathrm{E}\big[\big(y(\boldsymbol{x}) - m(\boldsymbol{x})\big)\big(y(\boldsymbol{x}') - m(\boldsymbol{x}')\big)\big]$ is the covariance function (or "kernel" function); and $\boldsymbol{\Theta}$ is a set of parameters that characterize the process, often termed hyperparameters. For example, Matérn class of covariance function (Rasmussen and Willians 2006), adopted in this study, is defined as

$$k(\boldsymbol{x},\boldsymbol{x}';\boldsymbol{\Theta}) = \frac{\sigma_f^2}{2^{\nu-1}\Gamma(\nu)}\left(\frac{\sqrt{2\nu}\|\boldsymbol{d}\|}{l}\right)^{\nu} K_\nu\left(\frac{\sqrt{2\nu}\|\boldsymbol{d}\|}{l}\right) \tag{2.3}$$

where K_ν and $\Gamma(\cdot)$ are respectively the modified Bessel function of order ν, which is usually set to $\nu = 3/2$ or $\nu = 5/2$ (Rasmussen and Willians 2006), and

the gamma function; $\|\boldsymbol{d}\| = \|\boldsymbol{x} - \boldsymbol{x}'\|$ denotes the distance between the two inputs $\boldsymbol{x}$ and $\boldsymbol{x}'$; and σ_f^2 and l are the hyperparameters in $\boldsymbol{\Theta}$, respectively denote the process variance and correlation length. Figure 2.2 denotes the Matérn class of covariance functions and corresponding realizations of Gaussian process with different parameters of correlation length l.

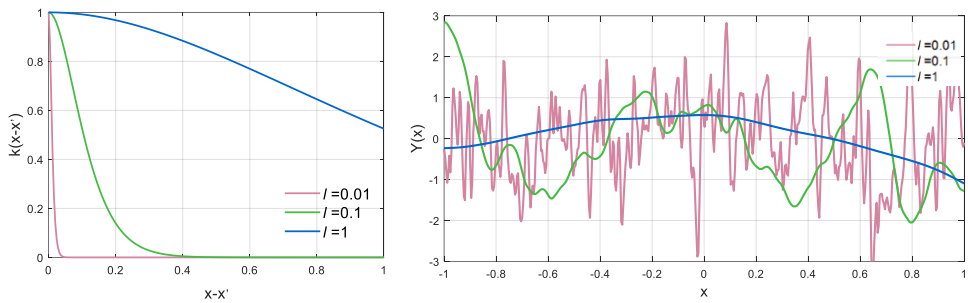

(a) (b)

Figure 2.2 Examples of Matérn class covariances for different correlation length parameters: (a) covariance functions, and (b) realization of Gaussian process

In using GP model, it is typically assumed that the observations $\mathcal{Y}$ include the Gaussian noise, i.e.,

$$\mathcal{Y} = y(\boldsymbol{x}) + \varepsilon \tag{2.4}$$

where ε denotes the Gaussian noises that are statistically independent and identically distributed with fixed variance σ_n^2. Given the n pair of the training set $\boldsymbol{\mathcal{D}} = \{\boldsymbol{x}_{\boldsymbol{\mathcal{D}}}, \boldsymbol{\mathcal{Y}}_{\boldsymbol{\mathcal{D}}}\}$, i.e., input points $\boldsymbol{x}_{\boldsymbol{\mathcal{D}}} = [\boldsymbol{x}_1, \dots, \boldsymbol{x}_n]^{\mathrm{T}}$ and corresponding noisy observations $\boldsymbol{\mathcal{Y}}_{\boldsymbol{\mathcal{D}}} = [\mathcal{Y}(\boldsymbol{x}_1), \dots, \mathcal{Y}(\boldsymbol{x}_n)]^{\mathrm{T}}$, the computational simulation results at the selected DoE points representing material properties, the optimal estimates of the hyperparameters, $\widehat{\boldsymbol{\Theta}}$ can be obtained by the maximum likelihood estimation (MLE) method (Rasmussen and Williams 2006) as

$$\widehat{\boldsymbol{\Theta}} = \underset{\boldsymbol{\Theta}}{\operatorname{argmax}} \ln p(\boldsymbol{y_D}|\boldsymbol{w_D}, \boldsymbol{\Theta}) \text{ where} \tag{2.5a}$$

$$\ln p(\boldsymbol{y_D}|\boldsymbol{w_D}, \boldsymbol{\Theta}) = -\frac{1}{2}\boldsymbol{y_D}^{\mathrm{T}}(\boldsymbol{K} + \sigma_n^2\boldsymbol{I})^{-1}\boldsymbol{y_D} - \frac{1}{2}\ln|\boldsymbol{K} + \sigma_n^2\boldsymbol{I}| - \frac{n}{2}\ln(2\pi) \tag{2.5b}$$

where $\boldsymbol{K}$ is the covariance matrix whose element is determined as $K_{i,j} = k(\boldsymbol{x}_i, \boldsymbol{x}_j)$, $i, j = 1, \ldots, n$; and $\boldsymbol{I}$ is the $(n \times n)$ identity matrix.

Then, the GP model with the estimated model parameters can predict the response at unexplored input points. Consider a prediction point $\boldsymbol{x}_*$ whose response is unknown yet. The GP-based estimate of y at a new point $\boldsymbol{x}_*$ and corresponding prediction variance are respectively given as the conditional mean $\mu_{\hat{Y}}(\boldsymbol{x}_*)$ and variance $\sigma_{\hat{Y}}^2(\boldsymbol{x}_*)$ of the Gaussian distribution

$$p\left(y_*|\boldsymbol{x}_*, \boldsymbol{x_D}, \boldsymbol{y_D}, \widehat{\boldsymbol{\Theta}}\right) \sim N\left(\mu_{\hat{Y}}(\boldsymbol{x}_*), \sigma_{\hat{Y}}^2(\boldsymbol{x}_*)\right) \text{ with} \tag{2.6}$$

$$\mu_{\hat{Y}}(\boldsymbol{x}_*) = m(\boldsymbol{x}_*) + \boldsymbol{k}_*^{\mathrm{T}}(\mathbf{K} + \sigma_n^2\mathbf{I})^{-1}\left(\boldsymbol{y_D} - m(\boldsymbol{x_D})\right) \tag{2.7}$$

$$\sigma_{\hat{Y}}^2(\boldsymbol{x}_*) = k_{**} - \boldsymbol{k}_*^{\mathrm{T}}(\mathbf{K} + \sigma_n^2\mathbf{I})^{-1}\boldsymbol{k}_* \tag{2.8}$$

where $\boldsymbol{k}_* = [k(\boldsymbol{x}_*, \boldsymbol{x}_1), \ldots, k(\boldsymbol{x}_*, \boldsymbol{x}_n)]^{\mathrm{T}}$ denotes the covariance matrix between the prediction location $\boldsymbol{x}_*$ and n observed points $\boldsymbol{x_D}$; and $k_{**} = k(\boldsymbol{x}_*, \boldsymbol{x}_*)$. The GP model not only provides the mean estimate $\mu_{\hat{Y}}(\boldsymbol{x}_*)$ but also quantifies the uncertainty of the prediction by $\sigma_{\hat{Y}}^2(\boldsymbol{x}_*)$. It is also noted that the prediction variance is usually negligible near the observation points because of the correlation described by the covariance function. For example, a typical visualization of the predictive mean and variance of Gaussian process given observations is provided in Figure 2.3. In this research, the GPML Toolbox (Rasmussen and Nickisch 2015) in MATLAB® is utilized to build the GP model and obtain the predictions.

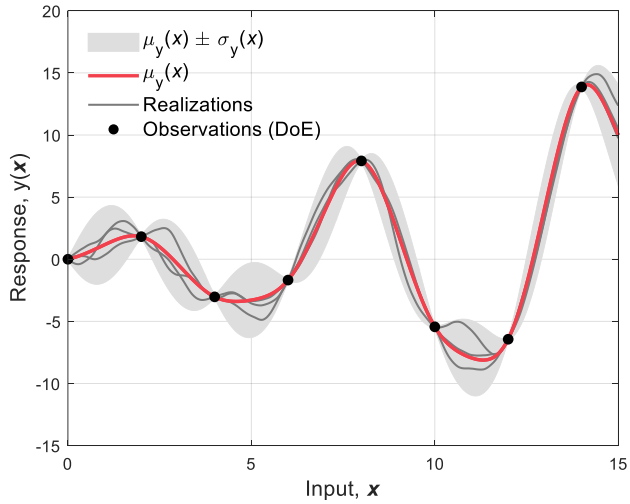

Figure 2.3 Example Gaussian process model and predictions

2.2.3 Reliability analysis using adaptive Kriging methods

When constructing a Kriging model, the number of DoE points should be sufficiently large to achieve an accurate surrogate. However, this may entail large computational costs especially when the evaluation of the original function is computationally expensive. For an efficient enrichment in DoE, a number of adaptive methods have been developed in recent years to add points sequentially based on the information from the previous iterations (Picheny *et al*. 2010; Dubourg *et al*. 2011; Marelli and Sudret 2018). The main goal of such an adaptive scheme is to identify the region in the input space whose exploration is expected to be most effective in terms of Kriging modeling.

To compute the failure probability efficiently using an adaptive Kriging approach, Echard *et al*. (2011) proposed to combine Kriging and Monte Carlo simulation. The method, termed AK-MCS, first generates Monte Carlo sample points with respect to the probability density function. To assess the importance of

each Monte Carlo sample based on previous simulation results, the *learning function* is defined as

$$U(\boldsymbol{x}) = \frac{|\mu_{\hat{G}}(\boldsymbol{x})|}{\sigma_{\hat{G}}(\boldsymbol{x})} \tag{2.9}$$

where $\mu_{\hat{G}}(\boldsymbol{x})$ and $\sigma_{\hat{G}}(\boldsymbol{x})$ respectively denote the Kriging (mean) prediction and corresponding standard deviation. AK-MCS selects the Monte Carlo sample minimizing the learning function as the next simulation point. Since the minimum value of $U(\boldsymbol{x})$ indicates that $\mu_{\hat{G}}(\boldsymbol{x})$ is close to zero and $\sigma_{\hat{G}}(\boldsymbol{x})$ is large, the learning function guides AK-MCS to explore the region which is expected to close to the limit-state surface, but requires more simulations to reduce the prediction uncertainty. This active learning process is continued until the stopping criterion, e.g., $\min\big(U(\boldsymbol{x})\big) \geq 2$, is satisfied, i.e., until the probability of correct classification of each MCS sample is reduced to $1 - \Phi(-2) = 0.9772$. As the size of the initial MCS population becomes large enough to guarantee a small coefficient of variation, the failure probability is estimated as $\hat{P}_f = n_{\hat{G}<0}/n_{MC}$ where $n_{\hat{G}<0}$ and n_{MC} respectively denote the number of MCS points whose Kriging predictions indicate failure, and the size of initial MCS population.

Since the learning function in Eq. (2.9) guides the sample selection toward the vicinity of the limit-state surface, i.e., the surface discerning the failure and safe domain, AK-MCS can facilitate finding an effective DoE for the purpose of reliability analysis. In particular, the exploration-exploitation trade-off enables the algorithm to identify the limit-state surface efficiently. Several other active-learning methods have been later proposed to further reduce the number of evaluations of the original limit-state function, e.g., AK-SS (combining with subset simulation), AK-

SYS (for system reliability), AK-OIS (combining with importance sampling), metaAK-IS (combining meta-IS algorithm) (Dubourg *et al*. 2013; Cadini *et al*. 2014; Fauriat and Gayton 2014; Huang *et al*. 2016; Zhang *et al*. 2020).

2.3 Proposed method: PAK-B^n

The aforementioned adaptive Kriging method, AK-MCS, uses Monte Carlo samples as candidate points for Kriging prediction. The active-learning process is carried out using the Kriging predictions of the learning function at the sample points. It is noted that when a structural reliability problem has small failure probability or complex failure domains, such adaptation may not be flexible enough to fit the complex shape and orientation of the critical points (Wen *et al*. 2016; Lelièvre *et al*. 2018). Therefore, in this chapter, a new adaptive reliability analysis method named PAK-B^n is proposed by re-defining the learning function and using alternative sampling in *n*-ball instead of Monte Carlo sampling. In particular, the exploration-exploitation trade-off on the limit state surface is now extended to incorporate probabilistic density of each sample to identify the sample point in the vicinity of the limit-state surface that contributes most to the failure probability. In other words, the adaptive Kriging guides the DoE to the vicinity of limit-state surface while giving priorities to critical regions from the viewpoint of reliability analysis. Note that, in this chapter, the term 'sample' refers to a candidate point sampled for the purpose of active-learning, while the term 'simulation' means actual evaluation of the true function at the sample selected by the active-learning process.

2.3.1 Alternative sampling for adaptive selection of simulation point

In AK-MCS, Monte Carlo sample points $\boldsymbol{x}$ are generated with respect to the probabilistic density of random variables, $f_{\mathbf{x}}(\boldsymbol{x})$. Hereafter, it is assumed that, the random variable space has been transformed to the standard normal space (Der Kiureghian 2022), and $f_{\mathbf{x}}(\boldsymbol{x})$ denotes the joint probability density function of n uncorrelated standard normal random variables. Then, the integral in Eq. (2.1) is estimated as $\hat{P}_f = n_{\hat{G}<0}/n_{MC}$, i.e., based on whether the Gaussian process predicts each MC sample is in the failure domain or not. Most of the generated samples, however, are located in the vicinity of the peak of the density of random variables, e.g., mean point for the multivariate Gaussian random variables, which naturally restricts the domain to explore. As a result, a limit-state surface showing complex shape or located far from the peak may not be captured by Monte Carlo population.

Thus, PAK-B^n adopts samples from the uniform density in the domain of n-ball, i.e., samples uniformly distributed over the interior of an n-dimensional hypersphere of radius R, whose volume is denoted as $V_{\mathcal{B}}(R)$. PAK- B^n adopts the n-ball domain in order to (1) promote a balanced search in the uncorrelated standard normal space whose density $f_{\mathbf{x}}(\boldsymbol{x})$ is rotationally-symmetric; and (2) facilitate adaptive expansion of the domain in terms of the radius R. In addition, the uniform density is selected, instead of the original density $f_{\mathbf{x}}(\boldsymbol{x})$ to promote effective Kriging-based identification. Figure 2.4 compares the 10^5 random samples generated by MCS and those by proposed n-ball approach in a three-dimensional space of random variables.

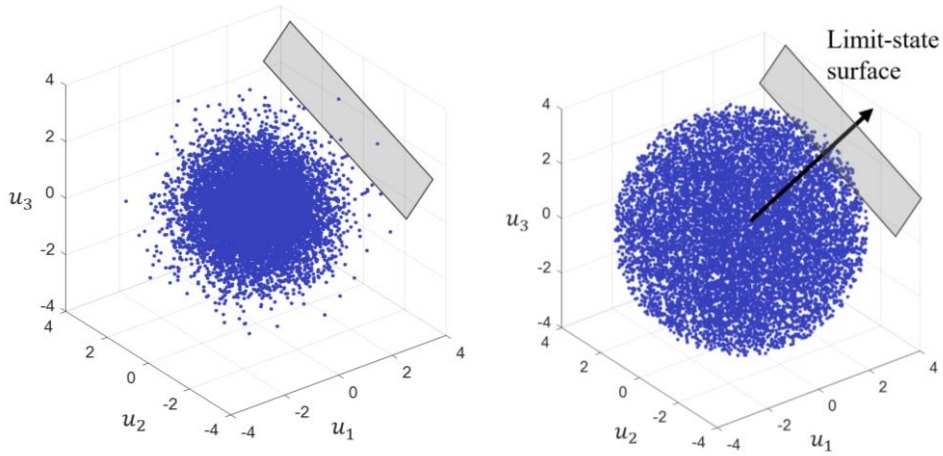

(a) (b)

Figure 2.4 Random samples generetaed by (a) MCS and (b) *n*-ball sampling

To incorporate the alternative (uniform) sampling density, Eq. (2.1) is re-formulated as

$$P_f = \int \left[\frac{I_{\{G(\boldsymbol{x})\leq 0\}} f_{\mathbf{x}}(\boldsymbol{x})}{h_{\mathbf{x}}(\boldsymbol{x})}\right] h_{\mathbf{x}}(\boldsymbol{x})\, d\boldsymbol{x} = E_h\left[\frac{I_{\{G(\boldsymbol{x})\leq 0\}} f_{\mathbf{x}}(\boldsymbol{x})}{h_{\mathbf{x}}(\boldsymbol{x})}\right] \tag{2.10}$$

where $I_{\{G(\boldsymbol{x})\leq 0\}}$ is the binary indicator function which gives "1" if the limit-state function $G(\boldsymbol{x})$ is negative or zero, and "0" otherwise; and $E_h[\cdot]$ denotes the mathematical expectation with respect to the alternative density $h_{\mathbf{x}}(\boldsymbol{x})$, i.e., the joint PDF of the uniform distribution in the *n*-ball, which is defined as $h_{\mathbf{x}}(\boldsymbol{x}) = 1/V_{\mathcal{B}}(R)$ if $\|\boldsymbol{x}\|_2 \leq R$ and $h_{\mathbf{x}}(\boldsymbol{x}) = 0$ otherwise. From samples $\boldsymbol{x}_i, i = 1, \ldots, N$ generated from $h_{\mathbf{x}}(\boldsymbol{x})$, the failure probability is then estimated as

$$P_f \cong \frac{V_{\mathcal{B}}(R)}{N} \sum_{i=1}^{N} \left[I_{\{\hat{G}(\boldsymbol{x}_i)\leq 0\}} f_{\mathbf{x}}(\boldsymbol{x}_i)\right] \tag{2.11}$$

where it is noted that the index function is defined in terms of the response predicted by the Kriging model, $\hat{G}(\boldsymbol{x}_i)$. The volume of the *n*-ball, $V_{\mathcal{B}}(R)$ is derived as

$$V_{\mathcal{B}}(R) = \frac{\pi^{\frac{n}{2}}}{\Gamma\left(\frac{n}{2}+1\right)} R^n \tag{2.12}$$

The variance of the failure probability estimate can be derived as

$$\begin{aligned} Var\left[\widehat{P_f}\right] &= \frac{1}{N}\left(\frac{1}{N}\sum_{i=1}^{N}\left[I_{\{\hat{G}(\boldsymbol{x}_i)\le 0\}}\left(\frac{f_{\mathbf{x}}(\boldsymbol{x}_i)}{h_{\mathbf{x}}(\boldsymbol{x}_i)}\right)^2\right] - \widehat{P_f}^2\right) \\ &= \frac{1}{N}\left(\frac{V_{\mathcal{B}}^2(R)}{N}\sum_{i=1}^{N}\left[I_{\{\hat{G}(\boldsymbol{x}_i)\le 0\}} f_{\mathbf{x}}(\boldsymbol{x}_i)^2\right] - \widehat{P_f}^2\right) \end{aligned} \tag{2.13}$$

The coefficient of variation δ_{P_f} of the failure probability estimate is estimated as

$$\delta_{P_f} = \frac{\sqrt{Var\left[\widehat{P_f}\right]}}{\widehat{P_f}} \tag{2.14}$$

To further improve convergence, this study employs low-discrepancy samples, often termed quasi-random samples. One of the most widely used quasi-random sequence called "Sobol and Halton sequence" is adopted. The improvement of the convergence rate by low-discrepancy of samples in structural reliability problems has been discussed in the literature (Caflisch 1998; Wang and Fang 2003).

2.3.2 Determining radius of *n*-ball sampling domain

Unlike general importance sampling methods requiring a proper selection of sampling density parameters, the only initial assumption required by the proposed sampling scheme is the radius of the *n*-ball, denoted by $R^{(1)}$. A small radius may yield inaccurate estimate if the sampling domain cannot properly cover the failure domain. On the other hand, a large radius may require unnecessarily large computational costs. Thus, PAK-B^n aims to identify a proper radius of the *n*-ball by increasing the radius with the increment ΔR until the failure probability estimate is

converged.

Let $R^{(k)}$ denote the n-ball radius used for the k-th round of the reliability analysis. From Eq. (2.11), the corresponding estimate of the failure probability is

$$\widehat{P_f}^{(k)} = \frac{V_{\mathcal{B}}\left(R^{(k)}\right)}{N_{total}^{(k)}} \sum_{i=1}^{N_{total}^{(k)}} \left[I_{\{\hat{G}(\boldsymbol{x}_i)\leq 0\}} f_{\mathbf{x}}(\boldsymbol{x}_i)\right] \tag{2.15}$$

where $N_{total}^{(k)}$ is the total number of the generated samples accumulated over k rounds. To determine whether additional round of analysis is needed, new N_{k+1} samples are generated in the domain $R^{(k)} < R \leq R^{(k)} + \Delta R$. Using the Kriging predictions at $N_{total}^{(k+1)} (= N_{total}^{(k)} + N_{k+1})$ sample points, the failure probability is estimated using Eq. (2.15). Since this task is to check the needs for expanding the ball, no actual function evaluations are needed.

The convergence is checked in terms of the relative increment of the reliability index instead of the failure probability. This is to avoid numerical issues caused by low failure probability. In particular, using the generalized reliability index $\hat{\beta}_g = -\Phi^{-1}\left(\hat{P}_f\right)$, the convergence condition is formulated as

$$\left|\frac{\hat{\beta}_g^{(k)} - \hat{\beta}_g^{(k+1)}}{\hat{\beta}_g^{(k)}}\right| < \epsilon_{tol} \tag{2.16}$$

where $\hat{\beta}_g^{(k)}$ and $\hat{\beta}_g^{(k+1)}$ respectively denote the generalized reliability index after the k-th round and that based on $N_{total}^{(k+1)}$ Kriging predictions discussed above; and ϵ_{tol} is a specified tolerance value. From the experience, it is recommended to choose a tolerance value in the range $10^{-5} < \epsilon_{tol} < 10^{-3}$ depending on the target level of accuracy. Geometric illustration of convergence criteria for determining proper radius is given in Figure 2.5.

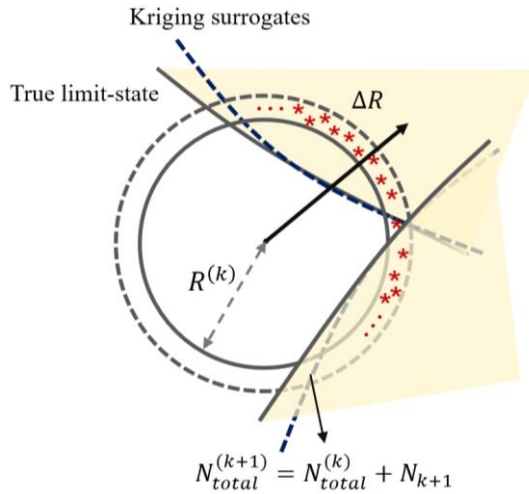

Figure 2.5 Geometric representations of convergence criteria in PAK-B^n method

It is noted that the *n*-ball samples refer to candidate points for statistical learning, and the actual evaluation is performed on a sample point that is selected by the active-learning process. Therefore, compared to the conventional response surface methodology that builds a second order mathematical response model based on a factorial or fractional factorial design with center points, termed central composite design (Myers *et al*. 2004), the proposed adaptive Kriging model can achieve efficient experimental designs from the viewpoint of reliability analysis.

2.3.3 Learning function for probability-adaptive Kriging

To enrich DoE by adaptive Kriging, it is important to take into account relative contributions of samples to the failure probability. In other words, the learning criteria should be defined so as to fit limit-state surface sufficiently well especially in the region that contributes most to the failure probability P_f. This chapter propose

a new learning function to facilitate this *probability-adaptive* Kriging, which guides the search process to the most enriched areas named critical regions having significant effects on P_f. Multiplying Eq. (2.9) by a penalty function $\gamma(\boldsymbol{x})$, the learning function of the probability-adaptive Kriging is defined as

$$\alpha(\boldsymbol{x}) = \frac{|\mu_{\hat{G}}(\boldsymbol{x})|}{\sigma_{\hat{G}}(\boldsymbol{x})} \cdot \gamma(\boldsymbol{x}) \tag{2.17}$$

where $\gamma(\boldsymbol{x})$ is introduced to discourage the search toward less-critical domains. For a sample $\boldsymbol{x}_i$ in the k-th round, the penalty function is defined as

$$\gamma(\boldsymbol{x}_i) = \begin{cases} \dfrac{\left|R(\boldsymbol{x}_i) - \hat{R}^*\right|}{R^{(k)}} & \Delta_{c.p} \geq tol \\ 1 & \Delta_{c.p} < tol \end{cases} \tag{2.18}$$

where $R(\boldsymbol{x}_i)$ denotes the Euclidean distance of $\boldsymbol{x}_i$ from the origin; $\hat{R}^*$ is the estimated distance from the origin to the nearest failure point (termed "critical point" in this chapter); and $\Delta_{c.p}$ is the distance between the critical points identified in the current and previous learning-steps. If $\Delta_{c.p}$ is larger than the specified tolerance, i.e., $\Delta_{c.p} \geq tol$, which means that the estimated location of the critical point has shown a critical change, the penalty function discourages the search toward samples relatively far from the critical point. If $\Delta_{c.p}$ is small, on the other hand, the penalty function is equal to one to reduce Eq. (2.17) back to Eq. (2.9), which means that the same trade-off between mean and standard deviation as AK-MCS is used. The distance to the critical point can be estimated by Kriging predictions, i.e.,

$$\hat{R}^* = \|\hat{\boldsymbol{x}}^*\|_2 \quad where\ \hat{\boldsymbol{x}}^* = \underset{\boldsymbol{x}_i}{\operatorname{argmax}}\left[I_{\{\hat{G}(\boldsymbol{x}_i)\leq 0\}} f_{\mathbf{x}}(\boldsymbol{x}_i)\right] \tag{2.19}$$

where $\|\cdot\|_2$ denotes 2-norm, i.e., Euclidean distance; $\hat{G}(\boldsymbol{x}_i)$ is the limit-state function value estimated by the Kriging prediction at $\boldsymbol{x} = \boldsymbol{x}_i$; and $\hat{\boldsymbol{x}}^*$ represents the

critical point in the space.

In summary, the left-hand side term in Eq. (2.17) guides the search to the vicinity of target limit-state surface $\{\boldsymbol{x}|G(\boldsymbol{x})=0\}$ while the right-hand side term guides toward the critical regions which have significant impact on the failure probability. Through the learning process, $\alpha(\boldsymbol{x})$ leads samples near the critical point with a priority. Next, as the variance of the searched regions is reduced, the learning guides the search toward less critical areas.

2.4 Algorithm of PAK-B^n

The algorithm of the proposed PAK-B^n is summarized as follows (see Figure 2.6 for the flowchart):

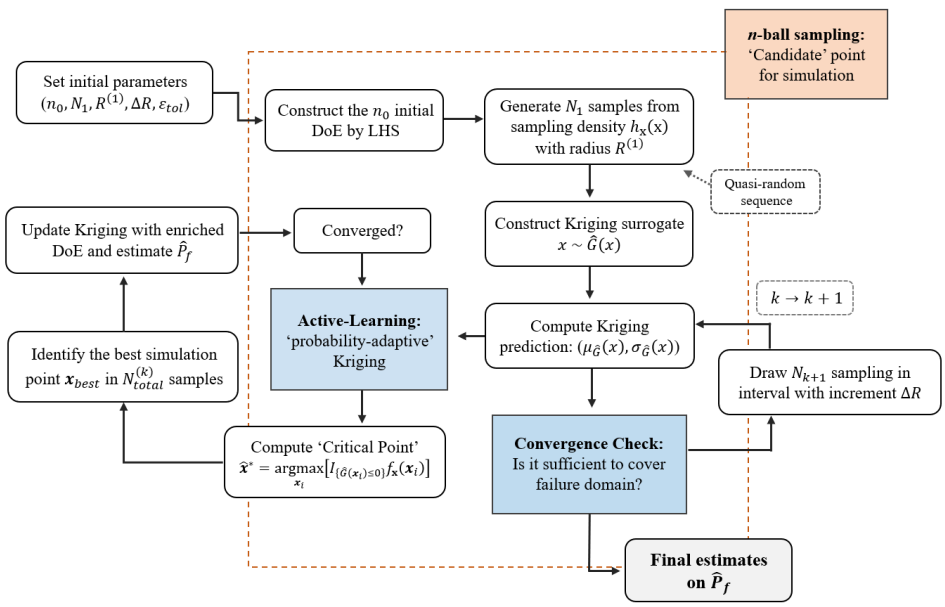

Figure 2.6 Flowchart of PAK-B^n algorithm

1. *Construct the initial DoE*: n_0 samples $\boldsymbol{x}=[\boldsymbol{x}_1,\ldots,\boldsymbol{x}_{N_0}]^{\mathrm{T}}$ are generated by Latin Hypercube Sampling (LHS) in the standard normal space. The

domain of LHS is set to $\|\boldsymbol{x}\|_1 \leq d_{LHS}$. The limit-state function $G(\boldsymbol{x})$ is evaluated on these points to construct the initial DoE of the adaptive-Kriging model. The size of initial DoE, n_0 needed to ensure an accurate estimation tends to increase with the dimension of the random variables. The sample size $n_0 = 10\sim30$ if dimension $n \leq 10$, and $n_0 = 2n + 1$ otherwise, seems a reasonable choice from the author's experience for the investigated examples.

2. *Generate samples in design space*: Generate N_i samples according to the sampling density $h_{\mathbf{x}}(\boldsymbol{x}) = 1/V_{\mathcal{B}}(R)$ if $\|\boldsymbol{x}\|_2 \leq R^{(i)}$ and $h_{\mathbf{x}}(\boldsymbol{x}) = 0$ otherwise. These sample populations are used as candidate locations for active-learning. The initial population size $N_1 = 10^4\sim10^5$ seems to be a good trade-off from the experience.
3. *Construct Kriging model*: Construct a Kriging model at the sample points using the current DoE. In this chapter, GPML toolbox in MATLAB® is utilized for this purpose. The Matérn class of auto-correlation function in Eq. (2.3) is chosen as the correlation model (see Section 2.2.2 for more details).
4. *Perform active-learning process*: Identify the sample point where the learning function $\alpha(\boldsymbol{x})$ in Eq. (2.17) is minimized as the next best simulation point. The DoE is enriched by acquiring function evaluation at the point to update the Kriging model. The enrichment of DoE, i.e., evaluating the function at the best points, continues until the stopping condition is satisfied. The stopping condition for the active-learning process is $\Delta\hat{\beta}_g < \varepsilon_{\beta_{tol}}$, which means that the estimated generalized reliability

index $\hat{\beta}_g$ converges. Note that this stopping condition differs from the convergence criteria described in the following.

5. *Check the convergence criteria*: Once the active-learning process is terminated, its corresponding convergence condition in Eq. (2.16) is computed to guess whether the increase in the radius would affect the failure probability estimate. If the procedure fails to achieve convergence, go back to Step 2 to create additional samples in the expanded *n*-ball and repeat the steps described above until the convergence is achieved.
6. *End of PAK-B^n*: If the convergence criteria is satisfied, PAK-B^n stops and provides the estimate of the failure probability in the current size of *n*-ball as the final estimate.

2.5 Numerical examples

The proposed PAK-B^n procedure and its performance are demonstrated by numerical examples. Examples of series and parallel systems are introduced to check the performance in system reliability problems. Also investigated are examples featuring small failure probability, high non-linearity, e.g., a large curvature around design point, and multiple design points. Then, applications to engineering systems, e.g., nonlinear oscillator and cantilever tube, are provided to examine the effects of dimension and distribution type on the performance of the proposed method. The number of initial DoE, n_0 is set to 10, with LHS bound $d_{LHS} = 6$, and the initial radius and interval of sampling domain are set to $R^{(1)} = 5$, and $\Delta R = 0.2$ respectively. The initial number of population is $N_1 = 50{,}000$.

2.5.1 Applications to benchmark reliability problems

2.5.1.1 Series system with multiple design points

First, consider a series system with three design points, whose limit-state function is given as (Cadini *et al* 2014; Dubourg *et al*. 2014)

$$G(\boldsymbol{x}) = \min \begin{Bmatrix} c - 1 - x_2 + \exp(-x_1^2/10) + (x_1/5)^4 \\ c^2/2 - x_1 \cdot x_2 \end{Bmatrix} \tag{2.20}$$

where x_1 and x_2 are uncorrelated standard normal variables; and c is an integer parameter. The limit-state function features three design points whose coordinates are $\boldsymbol{x}^{*(1)} = [0, c]^{\mathrm{T}}$, $\boldsymbol{x}^{*(2)} = \left[c/\sqrt{2}, c/\sqrt{2}\right]^{\mathrm{T}}$, and $\boldsymbol{x}^{*(3)} = \left[-c/\sqrt{2}, -c/\sqrt{2}\right]^{\mathrm{T}}$. Figure 2.7 shows the final experimental designs and the identified limit-state surface for the parameter $c = 4$.

The analysis results by PAK-B$^{\mathrm{n}}$ method are presented in Table 2.1, which shows the typical number of function calls and the corresponding failure probability representing more than 20 independent runs of analysis. The results are compared to those by crude MCS and several other widely used reliability methods reported in (Echard *et al*. 2011; Der Kiureghian 2022). The accuracy and efficiency of the different methods are compared in terms of N_{call}, i.e., the number of actual function evaluations required to estimate the failure probability, the failure probability P_f, the coefficient of variation of the failure probability, δ_{P_f}, and the generalized reliability index β_g. N_{call} in the tables denotes the total number of simulations. For AK-MCS and PAK-B$^{\mathrm{n}}$, N_{call} is the sum of the initial DoE (n_0) points and the number of the simulations during the active-learning process described in Section 2.3.3. FORM approximation for series system (Der Kiureghian 2022) is calculated

as $P_f(E_{sys}) = 1 - \Phi_m(\boldsymbol{\beta}, \mathbf{R})$ where $\boldsymbol{\beta} = [\beta_1, \dots, \beta_m]^{\mathrm{T}}$, i.e., the vector of the reliability indices from m individual component reliability analyses by FORM, $\mathbf{R}$ is the matrix of correlation coefficients between the standard normal random variables representing the component failure events, and Φ_m is the m-variate standard normal CDF. Since the system has four components, i.e. $m = 4$, the number of simulations of four FORM analyses, each of which use the mean as the starting point, are summed up to obtain N_{call}.

A parametric study is performed with respect to the parameter c. Since the three design points are located with the common distance from the origin, i.e., $\|\boldsymbol{x}^*\| = c$, a larger parameter yields a lower failure probability. The results by crude MCS estimations are considered reference values here. It is seen that PAK-B^n saves a significant amount of function evaluations compared to the other sampling-based approaches while producing results similar to the reference value $P_{f,MCS}$. It is worth noting that the performance of PAK-B^n is not hampered by low failure probability thanks to sampling in the n-ball. In Table 2.1, the numbers in the parentheses represent those of initial MCS samples. Note that the AK-MCS requires a large number of samples when $c = 5$, more than 10^8 samples, which may result in memory problems and inaccurate estimations.

The final experimental designs are shown in Figure 2.7. Using the initial DoE points, represented by black circles, the initial surrogate model is constructed. The red-cross markers are the most suitable training sample points selected at each iteration according to the learning function in Eq. (2.17). The blue solid and black dotted lines represent the true limit-state function and Kriging prediction using the

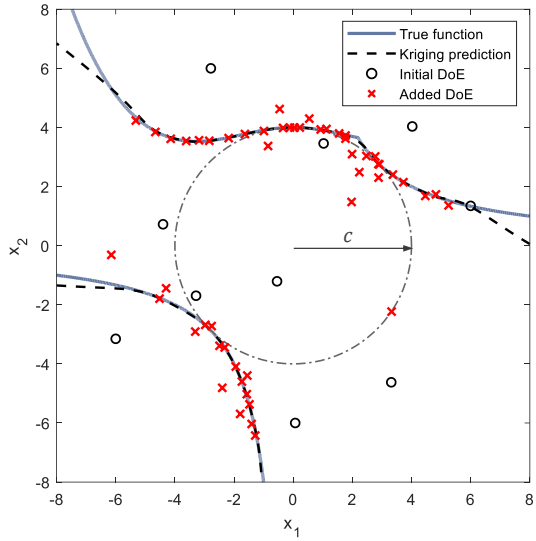

Figure 2.7 Final experimental designs for series system with multiple design points (c=4).

final DoE respectively. Most of the selected sample points reside around the true limit-state surface, especially in the critical regions near the three design points, which helps to construct an effective surrogate model for reliability analysis purpose.

Table 2.1 Comparison between the results by PAK-B^n and those by several reliability analysis methods for series system example

Case	Method	N_{call}	P_f	δ_{P_f} (%)	β_g
c=3	MCS	1.20×10^5	3.47×10^{-3}	4.89	2.70
	AK-MCS	10+85 (10^5)	3.52×10^{-3}	4.40	2.69
	PAK-B^n	**10+32**	$\mathbf{3.38 \times 10^{-3}}$	**1.67**	**2.71**
c=4	MCS	4.60×10^6	8.94×10^{-5}	4.93	3.75
	AK-MCS	10+101 (10^5)	8.33×10^{-5}	4.85	3.76
		10+106 (10^6)	8.79×10^{-5}	4.92	3.75
	PAK-B^n	**10+52**	$\mathbf{9.01 \times 10^{-5}}$	**1.80**	**3.75**
c=5	MCS	4.30×10^8	9.48×10^{-7}	4.95	4.76
	AK-MCS	-	-	-	-
	PAK-B^n	**10+70**	$\mathbf{9.02 \times 10^{-7}}$	**1.91**	**4.77**

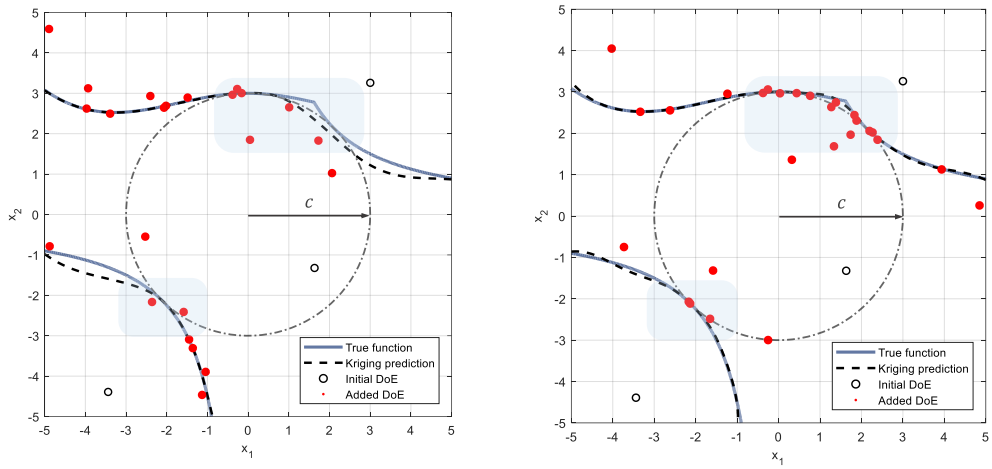

(a) (b)

Figure 2.8 Close-ups of final steps of DoE for series system with multiple design points using (a) $U(\boldsymbol{x})$, and (b) $\alpha(\boldsymbol{x})$ as the learning function

To further clarify the proposed adaptive search process, Figure 2.8 provides the close-ups of the last step results that are respectively trained by the learning functions $U(\boldsymbol{x})$ and $\alpha(\boldsymbol{x})$ given the same conditions. It is confirmed that $U(\boldsymbol{x})$ tries to capture the limit-state function and surface overall while the proposed learning function guides the search so that more simulations are performed in the critical regions. Therefore, the critical regions from the viewpoint of failure probability estimation is enriched with a priority, which leads to more efficient estimation of the failure probability.

Figure 2.9 shows the angle of the position vectors representing the critical points identified during the iteration procedure. The horizontal dash-dotted lines represent the locations of the design points having the angles $\theta = \pi/4, \pi/2$, and $-3\pi/4$ (rad) in polar coordinate. The asterisks show the estimated locations of the critical points, i.e., $\hat{\boldsymbol{x}}^*$ in Eq. (2.19) at each iteration. It is shown that all critical

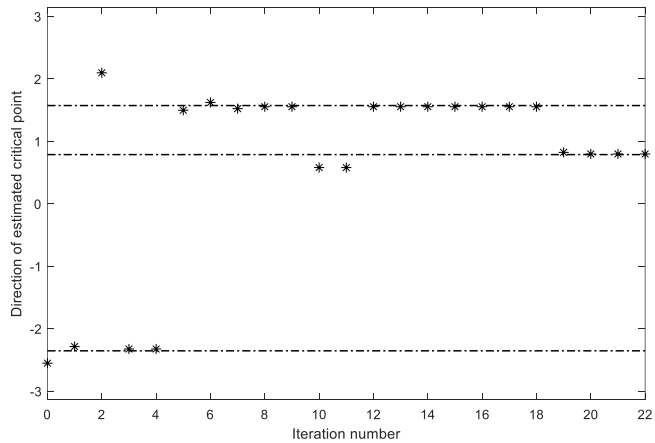

Figure 2.9 Direction of critical points estimated through iterations for series system example (c=3).

areas near the three design points are well identified by the probability-adaptive-learning of PAK-B^n, which performs computational simulations predominantly in critical regions of the reliability analysis problem.

2.5.1.2 Parallel system with small failure probability

In the next numerical example, PAK-B^n is applied to a parallel system with two components (Kurtz and Song 2013) whose limit-state function is

$$G(\boldsymbol{x}) = \max[x_1^2 - 8x_2 + 16, -16x_1 + x_2^2 + 32] \tag{2.21}$$

where x_1 and x_2 are uncorrelated standard normal variables. Figure 2.10(a) shows the limit-state surface and the "joint" design point discussed in Kurtz and Song (2013). The limit-state function shows highly nonlinear feature that is sharply concave in the direction away from the origin in the uncorrelated standard normal space. Figure 2.10(b) and (c) illustrate the adaptive simulations using the learning

functions $\alpha(\boldsymbol{x})$ and $U(\boldsymbol{x})$ respectively after 9 iterations. In particular, the yellow markers represent the best simulation points identified based on the red circular markers from the previous simulations. The comparison between Figures 2.10(b) and (c) clearly shows that the proposed learning function $\alpha(\boldsymbol{x})$ guides the search toward the critical area near the joint design point. The final experimental designs trained by the proposed PAK-B^n is given in Figure 2.11.

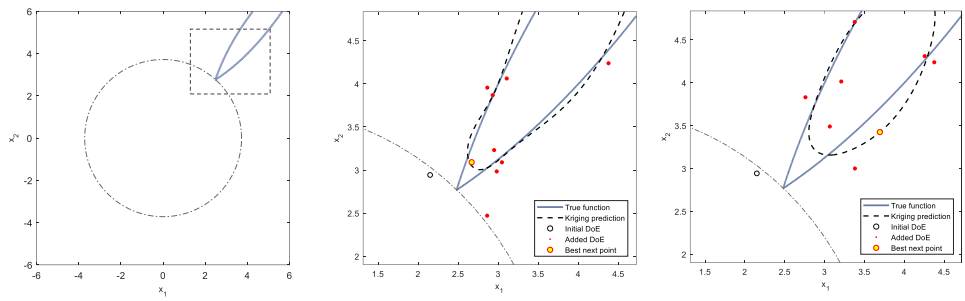

(a) (b) (c)

Figure 2.10 (a) The limit-state surface of a parallel system example, and adaptation of DoE over 9 iterations using (b) the probability-adaptive learing function $\alpha(\boldsymbol{x})$, and (c) the learning function $U(\boldsymbol{x})$

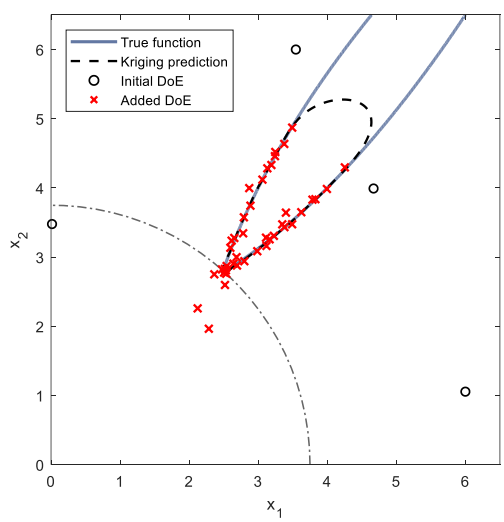

Figure 2.11 Final experimental designs for parallel system example

Table 2.2 presents the estimated failure probabilities along with the number of function evaluations. The MCS results are obtained using 1.70×10^7 sample population. The FORM approximation is performed as $P_f(E_{sys}) = \Phi_m(-\boldsymbol{\beta}, \mathbf{R})$. Due to the strong non-linearity, the FORM approximation shows large error. It is noted that in AK-MCS method, even with a large number of initial MCS samples ($\sim 10^7$), cannot provide a reliable estimate since the learning process terminates if the failure cases are not identified in the initial iteration procedure. It is also shown that the choice of the initial radius of domain $R^{(1)}$ does not significantly affect the performance of PAK-B^n.

Table 2.2 Comparison between the results by PAK-B^n and those by several reliability analysis methods for parallel system example

Method	Initial parameter	N_{call}	P_f	δ_{P_f} (%)	β_g
MCS		1.70×10^7	6.23×10^{-6}	9.72	4.37
FORM		4	5.18×10^{-4}	-	3.28
AK-MCS		-	0	-	-
PAK-B^n	$R^{(1)} = 4.0$	**10+48**	$\mathbf{5.90 \times 10^{-6}}$	**9.92**	**4.38**
	$R^{(1)} = 5.0$	**10+43**	$\mathbf{6.56 \times 10^{-6}}$	**9.62**	**4.36**
	$R^{(1)} = 6.0$	**10+33**	$\mathbf{6.08 \times 10^{-6}}$	**9.93**	**4.37**

2.5.2 Applications to engineering systems

2.5.2.1 Dynamic response of a non-linear oscillator

As an engineering application example, the non-linear undamped single degree of freedom (SDOF) system with bilinear restoring force. In figure 12, which is subjected to a rectangular load pulse, is investigated. The limit-state function is described as (Bucher and Bourgund 1990; Echard *et al*. 2011)

$$G(k_1, k_2, m, R, t_1, F_1) = 3R - z_{max}$$
$$= 3R - \left| \frac{2F_1}{m\omega_0^2} \sin\left(\frac{\omega_0 t_1}{2}\right) \right| \quad (2.22)$$

where k_1 and k_2 are the initial stiffness of the nonlinear springs; $\omega_0 = \sqrt{(k_1 + k_2)/m}$; t_1 and F_1 represent duration and amplitude of load pulse respectively; R denotes the displacement at which one of the springs yields; and z_{max} is the maximum displacement response of the system. This problem is selected to test PAK-B^n in real structural reliability problems described by a larger number of random variables, i.e., six. Table 2.3 summarizes types of distributions of all random variables and parameters. Table 2.4 shows that PAK-B^n method successfully deals with the dimension producing accurate results.

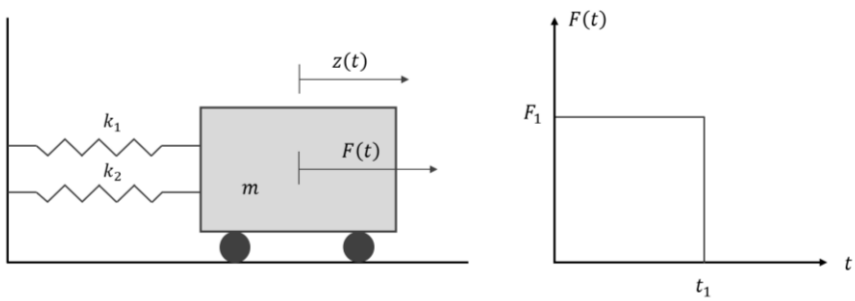

Figure 2.12 Non-linear oscilator subjected to a rectangular load pulse (Echard *et al*. 2011)

Table 2.3 Distribution type and parameters of the random variables

Random variables	Distribution	Mean	Standard deviation
m	Gaussian	1	0.05
k_1	Gaussian	1	0.1
k_2	Gaussian	0.1	0.01
R	Gaussian	0.5	0.05
t_1	Gaussian	1	0.2
F_1	Gaussian	0.6	0.2

Table 2.4 Comparison between the results by PAK-B^n and those by several reliability analysis methods for non-linear oscilator example

Method	N_{call}	P_f	δ_{P_f} (%)	β_g
MCS	1.0×10^6	5.46×10^{-4}	4.28	3.27
FORM	26	6.46×10^{-4}	-	3.22
AK-MCS	>300	5.49×10^{-4}	4.81	3.26
PAK-B^n	**20+106**	$\mathbf{5.50 \times 10^{-4}}$	**4.78**	**3.26**

2.5.2.2 Cantilever tube

The cantilever tube in Figure 2.13 is subjected to forces F_1, F_2 and P, and torsion T. The limit-state function is defined as (Du 2008; Xiao *et al*. 2018)

$$G(\boldsymbol{x}) = S_y - \sqrt{\sigma_x^2 + 3\tau_{zx}^2} \tag{2.23}$$

where S_y is the yield strength; and σ_{x} and τ_{zx} denote the normal stress and torsional stress on the top of surface of the tube at the origin respectively. The stresses σ_{x} and τ_{zx} are respectively derived as

$$\sigma_{\mathrm{x}} = \frac{P + F_1 \sin(\theta_1) + F_2 \sin(\theta_2)}{A} + \frac{Md}{2I} \tag{2.24a}$$

$$\tau_{zx} = \frac{Td}{2J} \tag{2.24b}$$

in which $M = F_1 L_1 \cos(\theta_1) + F_2 L_2 \cos(\theta_2)$; $A = (\pi/4)[d^2 - (d-2t)^2]$; $I = (\pi/64)[d^4 - (d-2t)^4]$; and $J = 2I$. Table 2.5 summarizes the properties of a total of nine random variables.

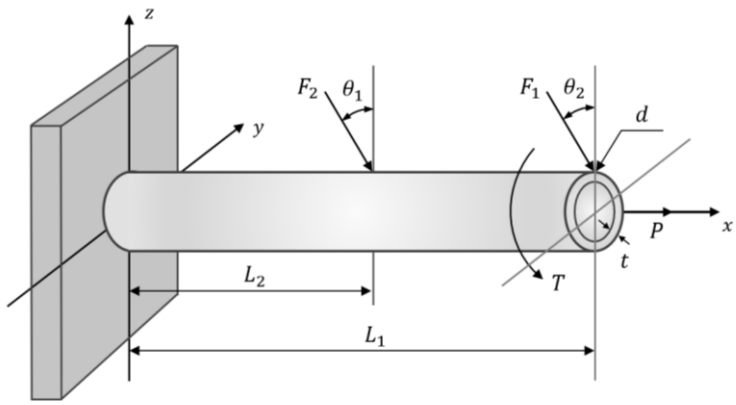

Figure 2.13 A cantilever tube (Du 2008)

Table 2.5 Distribution type and parameters of the random variables

Random variables	Distribution	Parameter1*	Parameter2*
$t\ (mm)$	Gaussian	5	0.1
$d\ (mm)$	Gaussian	42	0.5
$L_1\ (mm)$	Uniform	119.75	120.25
$L_2\ (mm)$	Uniform	59.75	60.25
$F_1\ (N)$	Gaussian	3000	300
$F_2\ (N)$	Gaussian	3000	300
$P\ (N)$	Gumbel	12000	1200
$T\ (N \cdot mm)$	Gaussian	90000	9000
$S_y\ (MPa)$	Gaussian	220	22

Note: Parameter1 and Parameter2 respectively denote the mean and standard deviation for Gaussian distribution, and location and scale parameters for Gumbel distribution, and the lower and upper bounds for Uniform distributions.

Table 2.6 shows that PAK-B^n needs only $168\ (= 50 + 118)$ function calls to obtain accurate estimation results while the AK-MCS demands more than 400 function evaluations.

While the proposed method is effective for engineering applications shown in the Section 2.5.2, the performance may degenerate if the random variables of engineering problem feature extreme value distribution types, e.g., Weibull and Gumbel, which requires a highly nonlinear transformation to uncorrelated standard

normal space and thus makes a response far away from the Gaussian distribution. This feature has usually been observed in nonlinear dynamical systems with hysteretic behavior and thus need to be further investigated.

Table 2.6 Comparison between the results by PAK-B^n and those by other methods for cantilever tube example

Method	N_{call}	P_f	δ_{P_f} (%)	β_g
MCS	2.0×10^6	2.19×10^{-4}	4.77	3.52
AK-MCS	>400	2.21×10^{-4}	4.58	3.51
PAK-B^n	**50+118**	$\mathbf{2.22 \times 10^{-4}}$	**4.75**	**3.51**

2.6 Summary

This chapter proposed a probability-adaptive Kriging method based on sampling in *n*-ball (PAK-B^n method), for structural reliability analysis. The main objective of PAK-B^n is to carry out an adaptive selection of simulation points with low computational costs from reliability analysis standpoint. The method utilized a new learning criterion designed to identify important points that are located in the vicinity of the limit-state surface and, at the same time, contribute most to the failure probability. This probability-adaptive procedure further reduced the number of computational simulations by utilizing samples uniformly distributed in an *n*-ball domain as candidate sets of simulation, and adaptively determining a proper radius of *n*-ball that achieves efficient convergence.

Accuracy and efficiency of the proposed method were demonstrated through several benchmarks reliability problems: a system problem with high non-linearity, small failure probability and multiple design points, and general engineering problems with moderate dimension. In each example, the proposed method needs a

small number of limit-state function evaluations to achieve accurate and converged estimates. PAK-B^n is expected to effectively deal with such challenging and time-consuming problems in practical engineering with robustness against the types of limit-state surface.

Chapter 3. First-Passage Probability Estimation under Stochastic Wind Excitations Using Active Learning

3.1 Introduction

Structural failures caused by natural or human-made hazards may induce catastrophic damage or losses. Thus, it is essential to evaluate the reliability of structural systems against stochastic excitations, e.g., wind loads, earthquake ground motions, and collisions, for managing the risk. The first-passage probability, i.e., the probability of the event that maximum structural response over a given time interval exceeds a prescribed threshold, is of great engineering interest as a reliability measure of a system under such conditions. It is crucial to consider the variability arising from the external stochastic excitations and the uncertainties associated with the structural systems and hazard models in evaluating the first-passage probability (Au and Beck 2003; Suksuwan and Spence 2018; Kanjilal *et al*. 2021).

In general, evaluating the first-passage probability is challenging because it requires multidimensional integration of a random process over time. No exact solution of this probability exists in general cases, and thus many attempts have been made to derive approximate solutions including system-reliability-based methods, simulation approaches, surrogate approaches (Lutes and Sarkani 2004; Andrieu-Renaud *et al*. 2004; Zuev *et al*. 2012; Yang *et al*. 2017; Chun *et al*. 2019; Wang *et al*. 2019; Kanjilal *et al*. 2021; Yi and Song 2021). A primary challenge in employing surrogate models for stochastic dynamical systems is incorporating the high-

dimensional sequences used for describing desirable time or frequency-domain characteristics of stochastic excitations (Gidaris *et al*. 2015; Suksuwan and Spence 2018; Jensen *et al*. 2020). This leads to a high-dimensional reliability analysis problem, which may degenerate the performance of surrogate-based approximations in the first-passage probability estimation.

To employ surrogate models without exacerbating performance, a new active learning-based heteroscedastic Gaussian process (AL-HGP) method is proposed in this chapter. To this end, the proposed method alternatively formulates the first-passage probability as a mixture distribution of Gaussian densities, each of which represents the conditional distribution of the maximum response. This procedure employs a GP model with heteroscedastic noises to fit the distribution parameters of mixture distribution, considering uncertainties arising from the structural system and the environmental wind loads. In addition, the framework trains the surrogates through an adaptive selection of simulation points in terms of their influence on the estimation of the first-passage probability given threshold level.

This chapter first provides a brief overview of the first-passage probability problem and stochastic wind-field model used to generate the random excitations of wind forces. Next, the following details of the proposed AL-HGP method are introduced: (1) an alternative formulation of the first-passage probability, (2) distribution parameter function estimations by a heteroscedastic GP model, (3) corresponding active-learning-based training process of surrogates, and (4) the adaptive learning algorithm of AL-HGP. The several numerical examples demonstrate the efficiency and applicability of the proposed AL-HGP method. Lastly, a summary of the results and concluding remarks are provided (Kim *et al*. Under

review).

3.2 Background

3.2.1 First-passage probability problem

The first-passage probability, commonly utilized as a reliability measure of structural systems subject to stochastic excitations, refers to the probability that the maximum response exceeds a prescribed threshold within a given time interval $t \in [0, \tau]$. A general mathematical formulation of the probability is

$$p_f(u_0; \tau) = P(\max_{0<t\leq\tau} |u(\boldsymbol{X}, \boldsymbol{Z}, t)| \geq u_0) \tag{3.1}$$

where $|\cdot|$ denotes absolute value expression; u_0 is the prescribed threshold on the response; and $u(\cdot)$ is the response time history, which is assumed to be affected by the two vectors of random variables $\boldsymbol{X}$ and $\boldsymbol{Z}$. First, the "basic" random variables $\boldsymbol{X} \in \mathbb{R}^{n_x}$ include time-invariant random parameters associated with the structural system, such as damping ratios and story stiffnesses, and the wind hazard model, e.g., 3-second gust wind speed and turbulence intensity. On the other hand, the "environmental" random variables $\boldsymbol{Z} \in \mathbb{R}^{n_z}$ characterize the stochasticity of the wind loads in the time or frequency domains. Thus $\boldsymbol{X}$ and $\boldsymbol{Z}$ are assumed to be independent of each other. Note that $\boldsymbol{x}$ and $\boldsymbol{z}$, respectively, denote the realizations of the random vectors $\boldsymbol{X}$ and $\boldsymbol{Z}$. The failure domain $\mathcal{F}$ is defined as the event that the maximum structural response exceeds a prescribed threshold, i.e., $\mathcal{F} = \{(\boldsymbol{x}, \boldsymbol{z}) : \max_{0<t\leq\tau} |u(\boldsymbol{x}, \boldsymbol{z}, t)| \geq u_0\}$.

Eq. (3.1) can be computed by the following multidimensional integral by using the indicator function of the failure domain:

$$p_f = \int \int I_{\mathcal{F}}(\boldsymbol{x}, \boldsymbol{z}) f_{\boldsymbol{X}}(\boldsymbol{x}) f_{\boldsymbol{Z}}(\boldsymbol{z})\, d\boldsymbol{x} d\boldsymbol{z} \tag{3.2}$$

where $f_{\mathbf{x}}(\boldsymbol{x})$ and $f_{\boldsymbol{Z}}(\boldsymbol{z})$, respectively, denote the joint probability density functions (PDFs) of the random vectors $\boldsymbol{X}$ and $\boldsymbol{Z}$; and $I_F(\boldsymbol{x}, \boldsymbol{z})$ is the binary indicator function which gives "1" if $(\boldsymbol{x}, \boldsymbol{z}) \in \mathcal{F}$ and "0" otherwise. The integral in Eq. (3.2) incorporates the PDF of environmental random variables $f_{\boldsymbol{Z}}(\boldsymbol{z})$, which often involves the sequence of stochastic excitation. This makes the reliability estimation a high-dimensional problem (generally more than hundreds), which may forbid the efficient assessment of the structural system's reliability (Alibrandi 2014; Suksuwan and Spence 2018). Moreover, the complexity of the failure event hampers the practical implementation of Eq. (3.2). It has been known that no exact solution exists for general cases, and thus the assessment of the first-passage probability entails a large number of dynamic simulations.

3.2.2 Stochastic wind-field model

Various modeling approaches have been developed for wind loads – data-driven methods, computational-fluid-dynamics (CFD), and stochastic simulation methods (Wood *et al*. 2001; Chen and Kareem 2004; Wang *et al*. 2013; Spence *et al*. 2016). In this chapter, the stochastic wind-field model is adopted to characterize the stochastic nature of wind excitations. Based on the conventional quasi-steady theory, the stochastic wind load at the *i*th location can be expressed as (Li and Kareem 1993; Spence *et al*. 2016)

$$f_i(t) = \frac{1}{2}\rho_a C_D A_i (\bar{V}(h_i) + v(h_i, t))^2 \cong \rho_a C_D A_i \bar{V}(h_i) v(h_i, t) \tag{3.3}$$

where h_i is the height of interest, e.g., the top of a building structure; A_i is the

tributary area at h_i; ρ_a is the air density; C_D is the drag coefficient; $\bar{V}(h_i)$ denotes the temporal average of the wind speed at h_i; and $v(h_i, t)$ denotes the zero-mean fluctuating component of the wind speed at h_i. Based on ASCE 07, the temporal average of the wind speed at h_i is given as (ASCE 2017)

$$\bar{V}(h_i) = V_b \bar{b} \left(\frac{h_i}{10}\right)^{\bar{a}} \tag{3.4}$$

where $\bar{a}$ and $\bar{b}$ are the constants characterizing the exposure condition; and V_b is the basic wind speed (or 3-second gust wind speed).

The along-wind velocity fluctuation component at h_i, i.e., $v(h_i, t)$ in Eq. (3.4) can be defined through the power spectral density (PSD) model in the frequency domain (Kaimal *et al*. 1972; Cheynet *et al*. 2018)

$$S_i(\omega) = v_*^2 \frac{a_s h_i}{\bar{V}(h_i)} \frac{1}{\left(1 + b_s \frac{\omega h_i}{\bar{V}(h_i)}\right)^{5/3}} \tag{3.5}$$

where ω denotes the turbulence frequency; a_s and b_s are the spectrum coefficients; and v_* is the friction velocity of the wind flow, defined as

$$v_* = V_b \bar{b} \frac{\kappa_a}{\ln(10/h_0)} \tag{3.6}$$

where κ_a is the von Kármán constant; and h_0 is the roughness height at the site of interest. To incorporate the correlation between the fluctuating wind components at arbitrary heights h_i and h_k, the following coherence function (Davenport, 1972) is incorporated:

$$\gamma_{ik}(\omega) = \exp\left[-\frac{\omega C_z |h_i - h_k|}{0.5[\bar{V}(h_i) + \bar{V}(h_k)]}\right] \tag{3.7}$$

in which $\gamma_{ik}(\omega)$ denotes the exponentially decaying coherence function between

the two stochastic wind processes $v(h_i,t)$ and $v(h_k,t)$; and C_z is the decay coefficient. Then, the spectral models in Eqs. (3.5)-(3.7) constitute the cross-PSD matrix $\boldsymbol{S}(\omega)$ whose element is defined as follows:

$$S_{ik}(\omega) = \sqrt{S_i(\omega)S_k(\omega)}\gamma_{ik}(\omega) \tag{3.8}$$

3.2.3 Simulation of stochastic wind time history

Because the cross-PSD matrix $\boldsymbol{S}(\omega)$ is Hermitian and positive definite, the matrix can be decomposed by a lower triangular matrix $\boldsymbol{H}(\omega)$ and the transpose of its complex conjugate $\boldsymbol{H}^*(\omega)$, i.e., $\boldsymbol{S}(\omega) = \boldsymbol{H}(\omega)\boldsymbol{H}^*(\omega)^{\mathrm{T}}$ using the Cholesky decomposition method. Then, the components of the m-variate (representing m different locations) wind vector process $\boldsymbol{v}(t)$ can be simulated by the spectral representation method (Deodatis 1996), defined as

$$v(h_i,t) = 2\sum_{r=1}^{m}\sum_{s=1}^{n_s}|H_{ir}(\omega_{rs})|\sqrt{\Delta\omega}\cos[\omega_{rs}(t) - \alpha_{ir}(\omega_{rs}) + \phi_{rs}], \quad \begin{matrix} \\ i = 1,\dots,m \end{matrix} \tag{3.9}$$

where H_{ir} is an element of the lower triangular matrix $\boldsymbol{H}(\omega)$; $\Delta\omega$ is the discretization resolution in frequency; n_s is the total number of sampling points; and $\omega_{rs} = (s-1)\Delta\omega + r\Delta\omega/m, s = 1,\dots,n_S$. ϕ_{rs} describes the m sequences of n_s independent random phase angles uniformly distributed over the range of $[0,2\pi]$; and α_{ir} is the complex phase angle of the simulated time histories, defined as

$$\alpha_{ir}(\omega) = \tan^{-1}\frac{\mathrm{Im}[H_{ir}(\omega)]}{\mathrm{Re}[H_{ir}(\omega)]} \tag{3.10}$$

where $\mathrm{Re}[\cdot]$ and $\mathrm{Im}[\cdot]$ are the real and imaginary parts of the complex number,

respectively. In particular, the elements of random phase angles ϕ_{rs} characterize the inherent randomness of stochastic wind excitations and belong to the environment random vector $\boldsymbol{Z}$ in Eq. (3.1) and Eq. (3.2). Figure 3.1 shows the comparison between the normalized target PSD model for along-wind velocity in Eq. (3.5) with the normalized PSD of a randomly generated sample by spectral representation method in Section 3.2.3.

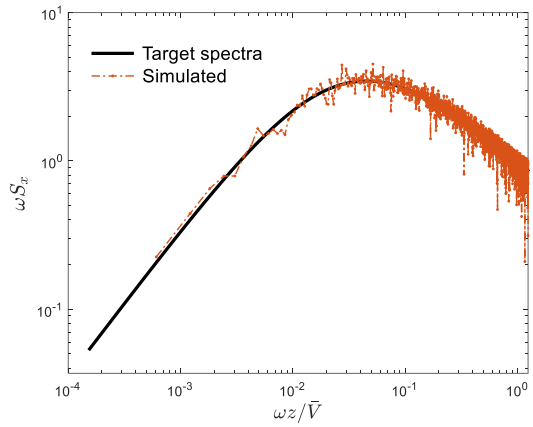

Figure 3.1 Comparisons between target and simulated normalized PSD of the wind velocity

3.3 Challenges in employing surrogate models for stochastic dynamical systems

A Gaussian process model, also known as Kriging, is often used to construct a surrogate of a complex function, e.g., response of a nonlinear structural system, based on training datasets of input-output pairs. In the first-passage probability problem in Eq. (3.1), the response quantity of interest might be the absolute value of maximum displacement response, i.e., $\mathcal{M} \equiv \max_{0<t\leq\tau} |u(\boldsymbol{X}, \boldsymbol{Z}, t)|$ which could be predicted using surrogates. Thus, one can directly collect the pair of the training set

by obtaining the structural responses $\mathcal{M}$ at the input points of all-inclusive random vectors in Eq. (3.1), i.e., $\boldsymbol{W} = [\boldsymbol{X}, \boldsymbol{Z}]^{\mathrm{T}}$. However, the high dimensionality of the input parameters associated with wind's stochastic characteristics, $\boldsymbol{Z}$ often makes predictions using such an approach infeasible. Therefore, it is desirable to handle the influences of the two random vectors $\boldsymbol{X}$ and $\boldsymbol{Z}$ on first-passage failure probability separately (Gidaris *et al*. 2015; Kanjilal *et al*. 2021).

The proposed method thus aims to address the aforementioned first-passage probability problem by developing a surrogate-based method to consider variabilities arising from the external wind excitation and structural system parameters. In addition, an adaptive surrogate training process is developed to identify the experimental design, effectively reducing the computational costs (Dubourg *et al*. 2011; Zhang *et al*. 2017; Wang and Broccardo 2020). To this end, the proposed AL-HGP introduces an alternative first-passage probability formulation whose distribution parameter functions are identified by a heteroscedastic Gaussian process model. An active learning framework is also introduced to train the surrogates through an adaptive selection of simulation points achieving efficient convergence.

3.4 Development of active learning-based heteroscedastic Gaussian process (AL-HGP)

3.4.1 Alternative formulation using conditional distribution

To handle the influences of the two random vectors $\boldsymbol{X}$ and $\boldsymbol{Z}$ on first-passage failure probability separately, the probability of failure in Eq. (3.2) is alternatively expressed using the conditional first-passage probability given the outcomes of the

basic random variables without loss of generality, i.e.,

$$p_f = \int_{\boldsymbol{x}_* \in \mathbb{R}^{n_x}} p_{f|\boldsymbol{X}}(\boldsymbol{x}_*) f_{\boldsymbol{X}}(\boldsymbol{x}_*)\, d\boldsymbol{x}_* \tag{3.11}$$

where $p_{f|\boldsymbol{X}}(\boldsymbol{x}_*)$ is the conditional first-passage probability given $\boldsymbol{x} = \boldsymbol{x}_*$, expressed as

$$p_{f|\boldsymbol{X}}(\boldsymbol{x}_*) = \int_{\boldsymbol{z} \in \mathbb{R}^{n_z}} I_{\mathcal{F}}(\boldsymbol{x}_*, \boldsymbol{z}) f_{\boldsymbol{Z}}(\boldsymbol{z})\, d\boldsymbol{z} \tag{3.12}$$

where $I_{\mathcal{F}}(\cdot)$ is the indicator function introduced in Eq. (3.2). The conditional probability in Eq. (3.12) describes the influence of the variability stemming from stochastic sequences on a deterministic structure represented by $\boldsymbol{x} = \boldsymbol{x}_*$.

This conditional probability is usually approximated as follows using the lognormal distribution, which is commonly utilized within the performance-based wind engineering framework (Ellingwood *et al*. 2004; Masoomi *et al*. 2018; Subgranon and Spence 2021; Abdelhady *et al*. 2022):

$$p_{f|\boldsymbol{X}}(\boldsymbol{x}_*) = 1 - P[\mathcal{M}(\boldsymbol{x}_*, \boldsymbol{z}) \leq u_0] = 1 - \Phi\left(\frac{\ln u_0 - \lambda(\boldsymbol{x}_*)}{\zeta(\boldsymbol{x}_*)}\right) \tag{3.13}$$

where $\mathcal{M}(\boldsymbol{x}_*, \boldsymbol{z})$ is the stochastic response of interest for a specific input $\boldsymbol{x}_*$; $\Phi(\cdot)$ denotes the cumulative distribution function (CDF) of the standard Gaussian distribution; and $\lambda(\cdot)$ and $\zeta(\cdot)$ are the mean and standard deviation of the natural logarithm of the response, respectively. Substituting Eq. (3.13) into Eq. (3.11), the first-passage probability can be estimated as

$$\begin{aligned} \hat{p}_f &= \int_{\boldsymbol{x}_* \in \mathbb{R}^{n_x}} \left[1 - \Phi\left(\frac{\ln u_0 - \lambda(\boldsymbol{x}_*)}{\zeta(\boldsymbol{x}_*)}\right)\right] f_{\boldsymbol{X}}(\boldsymbol{x}_*)\, d\boldsymbol{x}_* \\ &\cong 1 - \frac{1}{n_k} \sum_{k=1}^{n_k} \Phi\left(\frac{\ln u_0 - \lambda(\boldsymbol{x}_k)}{\zeta(\boldsymbol{x}_k)}\right) \end{aligned} \tag{3.14}$$

where $\boldsymbol{x}_k$ is the kth random sample generated from $f_{\boldsymbol{X}}(\boldsymbol{x})$, $k = 1, \ldots, n_k$. Eq. (3.14) computes the first-passage probability by a mixture of Gaussian densities, each of which is obtained at a random sample $\boldsymbol{x}_k$.

As a result of the conditional distribution based formulation and the lognormal distribution approximation, the first-passage probability problem can be solved by estimating the two distribution parameter functions $\lambda(\boldsymbol{x})$ and $\zeta(\boldsymbol{x})$. It is also noted that other distribution types, e.g., Gumbel distribution, Weibull distribution, can be adopted in this formulation using a proper transformation from the standard Gaussian space (Der Kiureghian 2022). A geometric representation of the proposed formulation of the first-passage probability is provided in Figure 3.2.

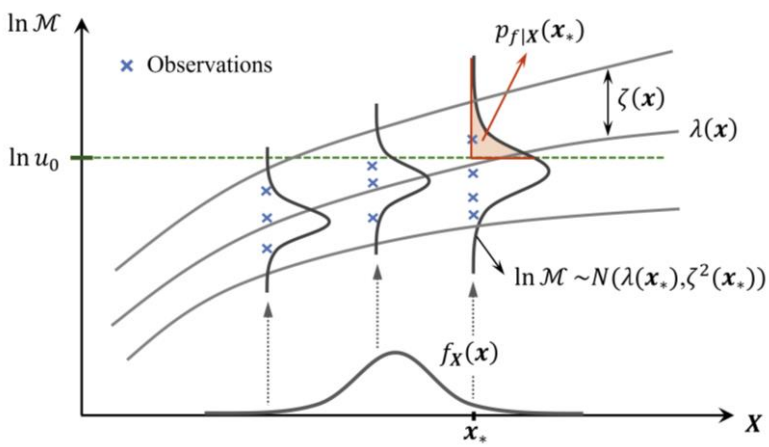

Figure 3.2 Conditional distribution based formulation of the first-passage probability

3.4.2 Estimation of distribution parameters

As discussed in Section 3.4.1, the distribution parameter functions in Eq. (3.14) describe the trends of the mean and standard deviation of the log-observations over the input space $\boldsymbol{x}$. A naive estimation of these parameters would require repetitive

dynamic simulations per each $\boldsymbol{x}$, which can be prohibitive in computational costs (Gidaris *et al*. 2015; Ghosh *et al*. 2018). Therefore, it is essential to estimate the distribution parameter functions with a minimal computational burden for efficient evaluations of the first-passage probability. The proposed AL-HGP predicts the distribution parameter functions by constructing GP-based surrogates, denoted by $\hat{\lambda}_{GP}(\boldsymbol{x})$ and $\hat{\zeta}_{GP}(\boldsymbol{x})$ as follows.

3.4.2.1 Heteroscedastic Gaussian process

Let us first consider the inputs of the simulations, $\boldsymbol{x}_{\mathcal{D}} = [\boldsymbol{x}_1, \dots, \boldsymbol{x}_n]^{\mathrm{T}}$ and the corresponding log-responses observed at independently sampled sequences of excitations, i.e., $\ln \boldsymbol{\mathcal{M}}_{\mathcal{D}} = [\ln \mathcal{M}(\boldsymbol{x}_1, \boldsymbol{z}_1), \dots, \ln \mathcal{M}(\boldsymbol{x}_n, \boldsymbol{z}_n)]^{\mathrm{T}}$. These observations exhibit a certain level of noise because of the uncertainties stemming from the stochastic characteristics of wind loads. Furthermore, the influence of the excitation sequences on the response varies across the input space $\boldsymbol{x}$, and thus the prediction model should incorporate the input-dependent noise (Kyprioti and Taflanidis 2021). This noise is not commonly assumed in the standard GP model that describes the additive noise with fixed variance, i.e., homoscedastic noise.

Therefore, the proposed method employs a GP model with input-dependent noise, i.e., heteroscedastic noise, to predict the distribution parameter functions. Let us consider the GP model in Eq. (2.4) in Section 2.2.2, that is, $\mathcal{Y} = y(\boldsymbol{x}) + \varepsilon$. Replacing the general output $\mathcal{Y}$ by the log-observation $\ln \mathcal{M}$, and introducing the Gaussian heteroscedastic noise $\varepsilon(\boldsymbol{x})$, the GP model is described as

$$\ln \mathcal{M} = y(\boldsymbol{x}) + \varepsilon(\boldsymbol{x}) \quad \text{where } \varepsilon(\boldsymbol{x}) \sim N(0, r(\boldsymbol{x})) \tag{3.15}$$

where $r(\boldsymbol{x}) = \exp(g(\boldsymbol{x}))$ is the variance of the heteroscedastic noise parameterized to ensure a positive value. The noise variance can be modeled by placing another GP prior $g(\boldsymbol{x}) \sim GP(\mu_0, k_g(\boldsymbol{x}, \boldsymbol{x}'))$. The model is then composed of two latent functions $y(\boldsymbol{x})$ and $g(\boldsymbol{x})$ with the augmented hyperparameters $\boldsymbol{\Theta}_A = \{\boldsymbol{\theta}_y, \boldsymbol{\theta}_g, \mu_0\}$, in which $\boldsymbol{\theta}_y$ and $\boldsymbol{\theta}_g$ respectively denote the hyperparameters for the kernel functions $k_y(\boldsymbol{x}, \boldsymbol{x}')$ and $k_g(\boldsymbol{x}, \boldsymbol{x}')$. Because of the additional latent function on the heteroscedastic noise, the marginal likelihood in Eq. (2.5), and the predictive distributions of response in Eqs. (2.6)-(2.8) are now analytically intractable.

3.4.2.2 Predictions of distribution parameters

Lázaro-Gredilla and Titsias (2011) introduced the marginalized variational (MV) bound to identify the best-factorized approximation of the predictions in terms of Kullback-Leibler (KL) divergence. Based on the MV approximation, a rigorous and analytically tractable lower bound of the exact marginal likelihood can be obtained in terms of two sets of parameters – mean vector $\boldsymbol{m}$ and covariance matrix $\boldsymbol{V}$ – as follows:

$$B_{MV}(\boldsymbol{m}, \boldsymbol{V}) = \ln f_N(\ln \boldsymbol{\mathcal{M}}_{\boldsymbol{\mathcal{D}}}; \boldsymbol{0}, \boldsymbol{K}_{\boldsymbol{y}} + \boldsymbol{R}) - \frac{1}{4}\mathrm{tr}(\boldsymbol{V}) - \mathrm{KL}(f_N(\boldsymbol{g}; \boldsymbol{m}, \boldsymbol{V}) \| f_N(\boldsymbol{g}; \mu_0 \boldsymbol{1}, \boldsymbol{K}_{\boldsymbol{g}})) \tag{3.16}$$

where $f_N(\cdot)$ is the PDF of a multivariate Gaussian distribution; $\boldsymbol{0}$ is the vector of zeros; $\boldsymbol{K}_{\boldsymbol{y}}$ and $\boldsymbol{K}_{\boldsymbol{g}}$ are the covariance matrices of $y(\boldsymbol{x})$ and $g(\boldsymbol{x})$, respectively; $\boldsymbol{R}$ is the diagonal matrix with elements $R_{i,i} = \exp\left(m_i - V_{i,i}/2\right), i = 1, \dots, n$; $\mathrm{tr}(\cdot)$ is a trace operator of the matrix; $\mathrm{KL}(\cdot)$ expresses the KL divergence between the two distributions; and $\boldsymbol{1}$ denotes the vectors of ones. Then, the optimal estimates of

the augmented hyperparameters, $\widehat{\boldsymbol{\Theta}}_A$ can be obtained by maximizing this lower bound. For an efficient optimization, a positive semi-definite diagonal matrix $\boldsymbol{\Lambda}$ can be introduced to re-parametrize the variational parameters $\boldsymbol{m}$ and $\boldsymbol{V}$ in a reduced order (Lázaro-Gredilla *et al*. 2013; Rogers *et al*. 2020).

Next, with the optimal hyperparameters, the predictive distribution at a new point $\boldsymbol{x}_*$, $p(\ln \mathcal{M}_*)$ can be computed by the following integral:

$$\begin{aligned} p(\ln \mathcal{M}_*) &= \int\int p(\ln \mathcal{M}_* | y_*, g_*) p(y_*) p(g_*)\, dy_*\, dg_* \\ &= \int f_N(\ln \mathcal{M}_*; a_*, c_*^2 + \exp(g_*)) f_N(g_*; \chi_*, \gamma_*^2)\, dg_* \end{aligned} \tag{3.17}$$

where $a_* = \boldsymbol{k}_{\boldsymbol{y}_*}^{\mathrm{T}} (\boldsymbol{K}_{\boldsymbol{y}} + \boldsymbol{R})^{-1} \ln \boldsymbol{\mathcal{M}}_{\mathcal{D}}$ and $c_*^2 = k_{y_{**}} - \boldsymbol{k}_{\boldsymbol{y}*}^{\mathrm{T}} (\boldsymbol{K}_{\boldsymbol{y}} + \boldsymbol{R})^{-1} \boldsymbol{k}_{\boldsymbol{y}_*}$ are respectively the posterior mean vector and covariance matrix of $y(\boldsymbol{x})$ while $\chi_* = \boldsymbol{k}_{\boldsymbol{g}*}^{\mathrm{T}} (\boldsymbol{\Lambda} - \frac{1}{2}\boldsymbol{I})\boldsymbol{1} + \mu_0$ and $\gamma_*^2 = k_{g**} - \boldsymbol{k}_{\boldsymbol{g}*}^{\mathrm{T}} (\boldsymbol{K}_{\boldsymbol{g}} + \boldsymbol{\Lambda}^{-1})^{-1} \boldsymbol{k}_{\boldsymbol{g}*}$ are those for $g(\boldsymbol{x})$. The predictive mean and standard deviation functions of $\ln \mathcal{M}_*$ at input point $\boldsymbol{x}_*$ then can be derived in terms of GP kernel functions as follows (Lázaro-Gredilla and Titsias 2011):

$$\hat{\lambda}_{GP}(\boldsymbol{x}_*) = \mathrm{E}_p[\ln \mathcal{M}_*] = a_* \tag{3.18}$$

$$\hat{\zeta}_{GP}(\boldsymbol{x}_*) = \sqrt{\mathrm{Var}_p[\ln \mathcal{M}_*]} = \sqrt{\exp(\chi_* + \gamma_*^2/2) + c_*^2} \tag{3.19}$$

where $\mathrm{E}_p[\cdot]$ and $\mathrm{Var}_p[\cdot]$ respectively denote the mathematical expectation and variance under $p(\ln \mathcal{M}_*)$. As a result, the predictive mean and standard deviation in Eqs. (3.18) and (3.19) serve as GP-based estimates of distribution parameter functions $\hat{\lambda}_{GP}(\boldsymbol{x})$ and $\hat{\zeta}_{GP}(\boldsymbol{x})$ respectively, under the heteroscedastic noise assumption. AL-HGP utilizes both predictions for estimating the first-passage probability in Eq. (3.14). The heteroscedastic GP model can predict the distribution

parameter functions without requiring repetitive simulations per each $\boldsymbol{x}$. It is also noted that AL-HGP needs to establish only one surrogate model to estimate both distribution parameter functions $\hat{\lambda}_{GP}(\boldsymbol{x}_*)$ and $\hat{\zeta}_{GP}(\boldsymbol{x}_*)$ and therefore, they do not need to be trained separately.

3.4.3 Adaptive training of surrogates

For efficiency, the proposed method employs an adaptive Design of Experiment (DoE) scheme (Dubourg *et al*. 2011; Zhang *et al*. 2017) to obtain surrogate-based predictions by as few dynamic simulations as possible. In detail, the proposed adaptive learning method iteratively refines the surrogates by computational simulations at locations recommended by a learning function instead of attempting to fit limit-state boundaries in the entire domain.

To effectively enrich the DoE, the learning function should be designed to guide the search process to DoE areas that would significantly improve the first-passage probability estimation. For this, the random samples $\boldsymbol{x}_k$ introduced in Eq. (3.14) are directly used as candidate points for the next DoE. In particular, the formulation in Eq. (3.14) introduces a mixture of n_k Gaussian CDFs evaluated at given threshold level u_0, each of which indicates the conditional probability of first-passage failure at the sample point $\boldsymbol{x}_k$. Note that each GP-based conditional failure probability at $\boldsymbol{x}_k$ directly presents the relative importance of the corresponding locations in terms of the total first-passage probability. Therefore, after constructing the surrogates based on the initial DoE points, AL-HGP selects the random sample that minimizes the learning function as the next simulation point, that is,

$$\boldsymbol{x}_{best} = \underset{\boldsymbol{x}_k}{argmax}\, p_{f|\boldsymbol{X}}(\boldsymbol{x}_k) = \underset{\boldsymbol{x}_k}{argmin}\, \Phi\left(\frac{\ln u_0 - \hat{\lambda}_{GP}(\boldsymbol{x}_k)}{\hat{\zeta}_{GP}(\boldsymbol{x}_k)}\right) \tag{3.20}$$

where $\hat{\lambda}_{GP}(\boldsymbol{x}_k)$ and $\hat{\zeta}_{GP}(\boldsymbol{x}_k)$ are the logarithmic mean and standard deviation in Eq. (3.18) and Eq. (3.19) estimated at $\boldsymbol{x} = \boldsymbol{x}_k$, respectively. Because the Gaussian CDF $\Phi(\cdot)$ is a monotonically increasing function, the logarithmic mean $\hat{\lambda}_{GP}(\cdot)$ in the numerator encourages computational simulations in the vicinity of the current maximum over the threshold. On the other hand, the logarithmic standard deviation $\hat{\zeta}_{GP}(\cdot)$ in the denominator promotes simulations at less-explored areas, especially for those under the threshold level (where the numerator is positive) because most of the observations are usually lower than the given threshold in typical first-passage probability problems. Therefore, the learning criteria help guide the search toward the regions that have a significant influence on the first-passage probability in terms of the given threshold level u_0, utilizing the GP-based predictions on distribution parameter functions.

To illustrate this point, Figure 3.3 shows the GP-based densities at two candidate points denoted by $\boldsymbol{x}_1$ and $\boldsymbol{x}_2$ respectively representing points with relatively large mean and small variability (standard deviation) and those with relatively small mean and large variability. Given the threshold level, the corresponding conditional failure probability at $\boldsymbol{x}_2$ is greater than that of $\boldsymbol{x}_1$, and thus AL-HGP method will prioritize $\boldsymbol{x}_2$ as the next point of the computational simulation.

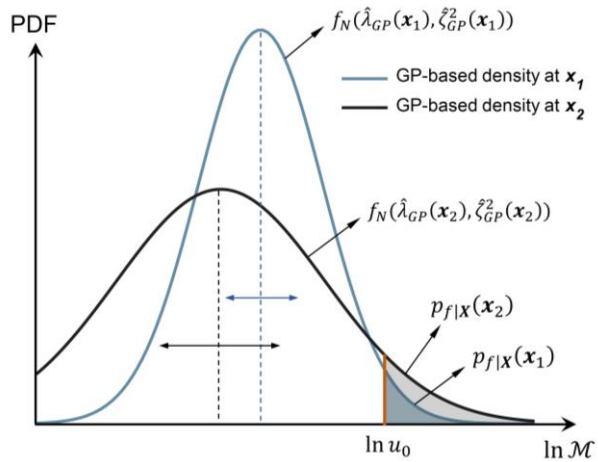

Figure 3.3 Illustration of conditional probabilities of failure for sample points ($\boldsymbol{x}_1$ and $\boldsymbol{x}_2$) using the GP-based densities giben threshold level

3.4.4 Convergence criteria

The proposed adaptive learning procedure updates the first-passage probability until satisfying the selected convergence criterion. Inspired by the CDF distance metric utilized for adaptive seismic fragility analysis (Chun *et al*. 2000; Kim *et al*. 2021), the proposed method employs the convergence criteria defined in terms of the *normalized probability distance* (NPD) as follows:

$$\varepsilon_i^{NPD} = \frac{\left(\int_0^1 (u_{i-1}^p - u_i^p)^2 \, dp\right)^{1/2}}{\mu_{u_i}} \tag{3.21}$$

where u_i^p denotes the p-quantile of the first-passage probability function in Eq. (3.14), i.e., the threshold level that makes the first-passage probability p, i.e., $\hat{p}_f(u^p) = p$, at the *i*th learning step. The denominator μ_{u_i} denotes the mean value of the quantiles from the *i*th iteration, normalizing the NPD. As shown in Figure 3.4, NPD considers the relative increment of the first-passage probability *curve*, capturing the differences in both mean and variability. This curve can be obtained by

calculating the proposed formulation in Eq. (3.14) at a set of thresholds using the trained surrogates at each learning step. Thus, the NPD quantifies the overall distance (or difference) between the first-passage probability curves identified in the current and previous learning steps.

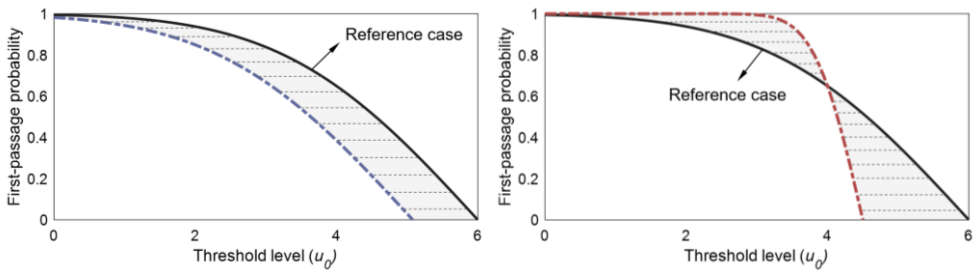

Figure 3.4 NPD measure capturing the difference in (a) mean and (b) variability of the first-passage probability curves

The AL-HGP monitors whether the NPD at two consecutive steps becomes *small* and *stagnant* as the learning process proceeds. To this end, the NPD value at the *i*th learning step, $\varepsilon_i^{(1)} = \varepsilon_i^{NPD}$ and the convergence "trend" defined as $\varepsilon_i^{(2)} = \left|\varepsilon_{i-1}^{(1)} - \varepsilon_i^{(1)}\right|$ are calculated at each iteration. If both $\varepsilon_i^{(1)}$ and $\varepsilon_i^{(2)}$ become smaller than the specified tolerances $\varepsilon_{tol}^{(1)}$ and $\varepsilon_{tol}^{(2)}$, respectively, the iteration is terminated.

3.4.5 Algorithm

The algorithm of the proposed AL-HGP is summarized as follows and illustrated by the flowchart in Figure 3.5:

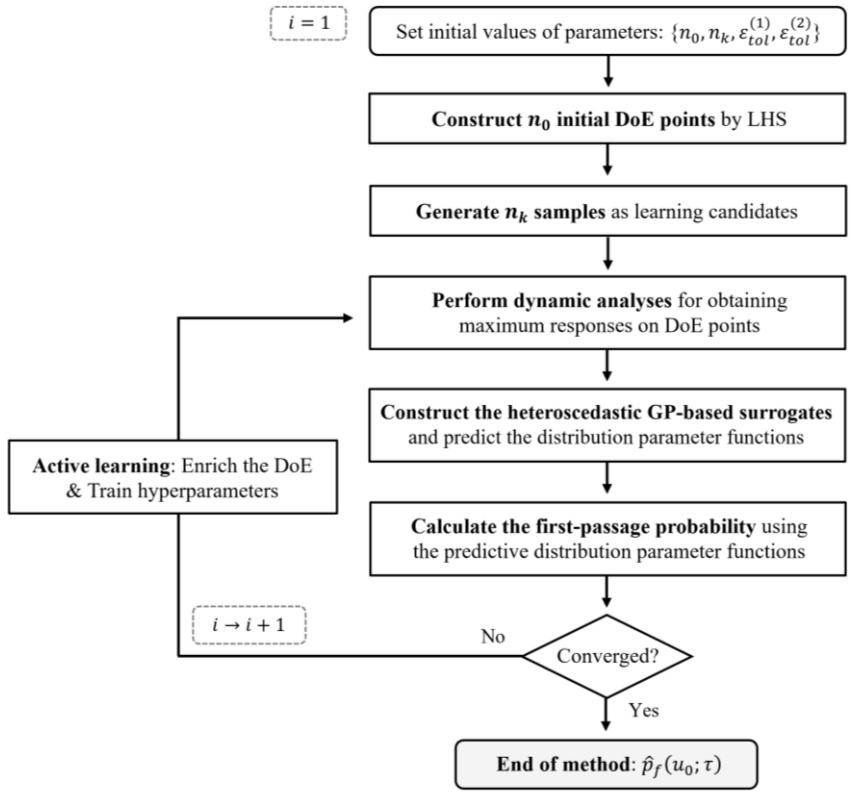

Figure 3.5 Flowchart of AL-HGP algorithm

1. *Construct the initial DoE points*: n_0 initial DoE samples $\boldsymbol{x_D} = [\boldsymbol{x}_1, \dots, \boldsymbol{x}_{n_0}]^{\mathrm{T}}$ are generated from the vector of basic random variables $\boldsymbol{X}$ (time-invariant random parameters) using Latin Hypercube Sampling (LHS). The domain of LHS is set to $\|\boldsymbol{x}\|_1 \leq \mu_X + 3\sigma_X$.
2. *Generate random samples*: Generate n_k samples $\boldsymbol{x}_k, k = 1, \dots, n_k$ according to the sampling density $f_{\mathbf{x}}(\boldsymbol{x})$. These sample populations are used as candidate locations for computational simulations, that is, candidates for statistical learning. The first-passage probability is determined based on the predictions on these sample points. The population size $n_x = 10^4 \sim 10^5$ seems to be a reasonable choice from the experience.

3. *Perform dynamic analyses*: Perform dynamic analyses under stochastic wind loads and obtain the maximum displacement responses at each DoE point. The datasets of input-output pairs are used to construct the surrogate models. Note that samples of environmental random vector $\boldsymbol{Z}$ are generated to simulate stochastic wind loads for each DoE point.
4. *Estimate the distribution parameter functions by GP-based surrogates*: Obtain the estimates of the optimal augmented hyperparameters, $\widehat{\boldsymbol{\Theta}}_A$ by maximizing the MV approximation bound in Eq. (3.16) using the current DoE points. Then, construct a GP-based surrogate model with heteroscedastic noise. The predictive mean and standard deviation in Eq. (3.18) and Eq. (3.19) are utilized for calculating the first-passage probability in Eq. (3.14).
5. *Train surrogates by active learning process*: Identify the sample point minimizing the learning function as the next best simulation point $\boldsymbol{x}_{best}$ as described in Eq. (3.20). At this stage, the DoE is enriched by acquiring dynamic simulation at $\boldsymbol{x}_{best}$ to update the surrogate model and corresponding predictions on distribution parameter functions.
6. *Check the convergence criteria*: Repeat Steps 2-5 as enriching the DoE until both convergence criteria $\varepsilon^{(1)}$ and $\varepsilon^{(2)}$ become smaller than the predefined tolerances.
7. *End of AL-HGP*: Once converged, AL-HGP stops the iteration and provides the current estimate of the first-passage probability as the final estimate.

3.5 Numerical examples

3.5.1 Application to an eight-story building

The first example investigates an eight-story walled building structure in Figure 3.6 where only the walls contribute to the lateral resistance against the wind loads. The structure is modeled as a linear elastic building subject to dynamic forces caused by fluctuating winds. Table 3.1 and Table 3.2 present the building properties and wind hazard model parameters, respectively, adopted from the final report of the Applied Technology Councils (ATC) project and ASCE 07 (ASCE 2017; FEMA 2018). Figure 3.7 shows one of the simulated fluctuating wind speed time histories, $v(h,t)$ at the eighth-story of the building. The duration of the simulated time history is assumed to be 10 minutes (600 seconds). In this example, the following two cases are considered regarding the type and dimension of random variables.

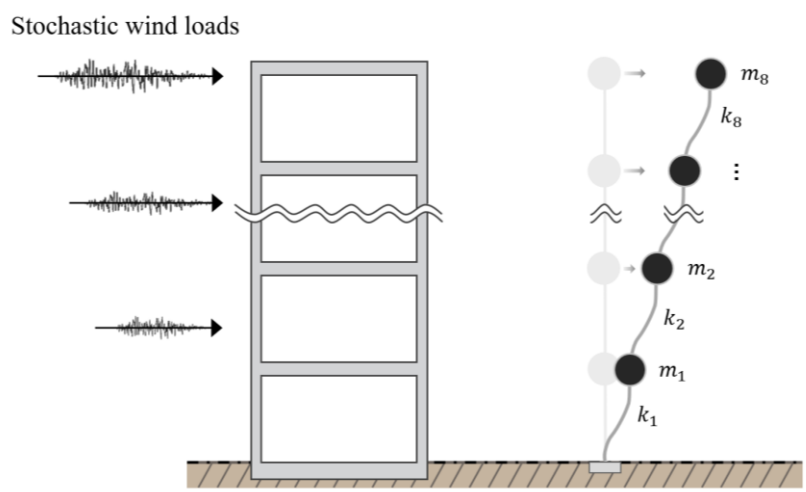

Figure 3.6 Structural model of eight-story building

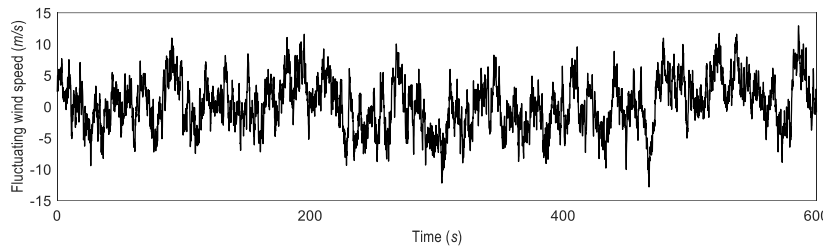

Figure 3.7 Simulated fluctuating wind speed time history at the eighth story

Table 3.1 Structural parameters of eight-story building model

Name	Parameter	Value
Building height (ft)	B_h	106
Building width (ft)	B_d	120
Building weight (kip)	B_w	21,276
The first mode period (s)	T_1	1.13
Story stiffnesses (kip/in)	k_j	6,200
Damping ratios	c_j	0.02

* For $j = 1, \dots, 8$

Table 3.2 Parameters of wind hazard model

Name	Parameter	Value
Basic wind speed (mph)	V_b	95
Air density (kg/m^3)	ρ_a	1.226
Exponent parameter	$\bar{a}$	0.25
Gust parameter	$\bar{b}$	0.45
Drag coefficient	C_D	1.3
Decay coefficient	C_z	10
Von Kármán constant	κ_a	0.4
Spectrum coefficients	a_s	105
	b_s	33

3.5.1.1 Case 1: uncertain parameter in the wind hazard model

Let us first consider the case in which a wind hazard model parameter is considered a random variable. To this end, the basic wind speed (or 3-second gust wind speed) in Eqs. (3.4)-(3.6) is parameterized by $V_b = \tilde{V}_b \varepsilon_v$ where $\tilde{V}_b$ is the nominal value

and ε_v is a non-dimensional random variable, assumed to follow the Gaussian distribution with a mean $\mu_{\varepsilon_v} = 1$ and a standard deviation $\sigma_{\varepsilon_v} = 0.1$, that is, $\varepsilon_v \sim N(1, 0.1^2)$. The nominal value is set to $\tilde{V}_b = 95$ (mph). Thus, ε_v is considered a random variable included in the random vector $\boldsymbol{X}$ in Eq. (3.1).

Following the procedure described in Section 3.4, the AL-HGP method is applied with 50 initial DoEs. The convergence tolerances $\varepsilon_{tol}^{(1)}$ and $\varepsilon_{tol}^{(2)}$ are set to 0.001, which was recommended in a previous study on structural fragility (Kim *et al*. 2021). The responses of interest are eighth-story and first-story drifts whose displacement thresholds are $u_0 = 0.16\ (in)$ and $u_0 = 0.0325\ (in)$, respectively. Figure 3.8 presents initial stages of adaptive learning with the DoEs at top drift, denoted by the red-plus markers. The solid curves show the reference values of distribution parameter functions, i.e., $\hat{\lambda}_{MCS}(x)$ and $\hat{\lambda}_{MCS}(x) \pm \hat{\zeta}_{MCS}(x)$, obtained by 50,000 Monte Carlo Simulation (MCS) on each point x. The distribution parameter functions estimated by GP-based surrogates, $\hat{\lambda}_{GP}(x)$ and $\hat{\lambda}_{GP}(x) \pm \hat{\zeta}_{GP}(x)$ are represented by dashed-line respectively. Based on the estimated parameters, the two conditional distributions of the maximum response at $x = 1$ and $x = 1.3$ are shown in Figure 3.8. It is noted that the relative contributions of the location at $x = 1.3$ are more significant than those at $x = 1$ because of the conditional first-passage failure computed by Eq. (3.13).

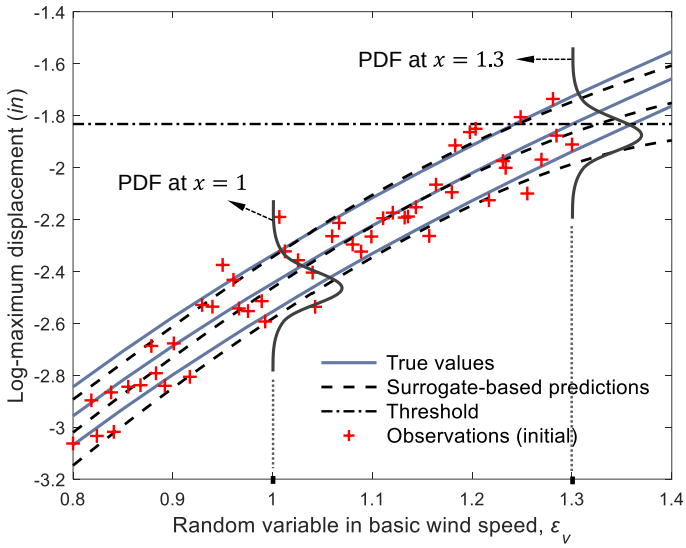

Figure 3.8 Initial stage of adaptive learning with AL-HGP

Figure 3.9 shows the trained surrogates and all DoE points explored up to the final step to illustrate the progress of AL-HGP after 38 simulations for the eighth-story drift. In particular, the blue-cross markers indicate the sample selected by the adaptive procedure in Eq. (3.20), $\boldsymbol{x}_{best}$. The result confirms that most of the sample points selected by AL-HGP reside in the critical domain, improving the prediction accuracy of the surrogate model selectively around the specific region. Therefore, AL-HGP can construct an effective surrogate model from the viewpoint of the first-passage probability problem and thus fit the distribution parameter functions sufficiently well, especially in the region that contributes most to the first-passage probability p_f.

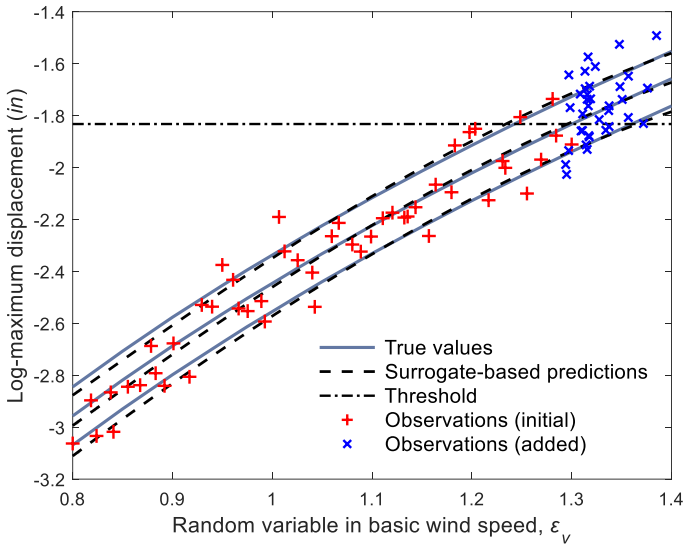

Figure 3.9 Final experimental designs for eight-story building system with basic wind speed as random variable

To investigate the accuracy of the GP-based surrogate, Figure 3.10 plots the KL divergence between the two Gaussian distributions whose parameters are, respectively, obtained by MCS (solid lines in Figures 3.7 and 3.8) and GP-based surrogates (dashed-lines in Figures 3.7 and 3.8). The KL divergence measure D_{KL} (Kurtz and Song 2013; Kanjilal *et al*. 2021) is computed as

$$D_{KL} = \ln \frac{\hat{\zeta}_{GP}(x)}{\hat{\zeta}_{MCS}(x)} + \frac{\hat{\zeta}^2_{MCS}(x) + (\hat{\lambda}_{MCS}(x) - \hat{\lambda}_{GP}(x))^2}{2\hat{\zeta}^2_{GP}(x)} - \frac{1}{2} \tag{3.22}$$

Figure 3.10 shows the changes of the KL divergence in the domain of $x = \varepsilon_v$ over the adaptive learning procedure after identifying 1, 12, and 38 simulations for the eighth-story drift. AL-HGP successfully converges the GP-based surrogate toward the reference distribution by adaptively enriching surrogates, especially in the critical domains, which contributes most to the first-passage failure.

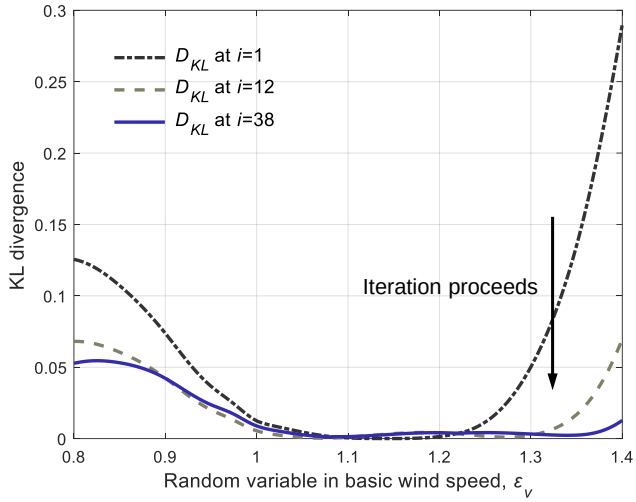

Figure 3.10 KL divergence between the references from the MCS and estimates by GP-based surrogates through iterations

Figure 3.11 compares the first-passage probability by the proposed method (blue-dashed line) with the reference (black-solid line) estimated by MCS (10^5 dynamic simulations leading to a coefficient of variation of 5% at the threshold level). It is noted that only 48 and 33 dynamic simulations are additionally performed to obtain the first-passage probability estimates after 50 simulations on initial DoE points for the eighth-story and first-story drifts, respectively. The results confirm that the proposed method produces accurate estimates with a significantly reduced number of dynamic simulations. The gray curves in the plots are 200 first-passage probabilities, each of which is a surrogate-based prediction based on the randomly selected DoE points. For comparison, each curve uses the same total number of simulations as AL-HGP, i.e., 98(=50+48) and 83(=50+33) simulations, respectively. In detail, the curves show the "non-adaptive" results by surrogate-based predictions using only Steps 1-4 of the algorithm in Section 3.4.5. These curves demonstrate large variability one could introduce by using randomly selected DoE points instead

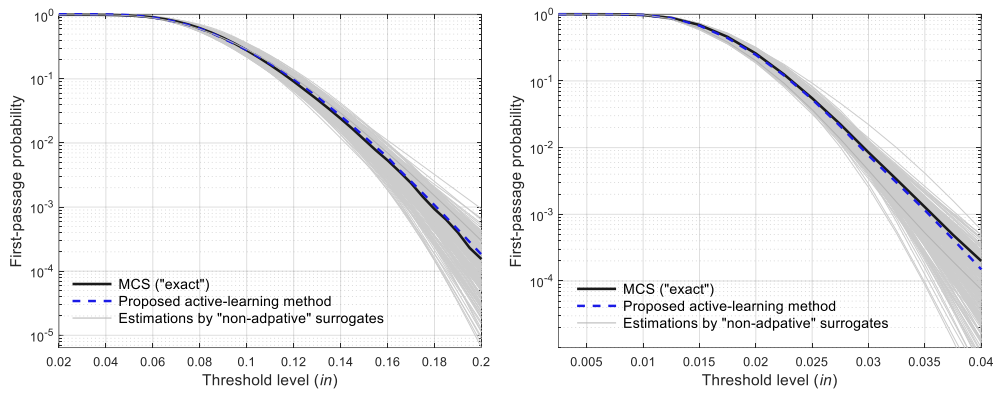

(a) (b)

Figure 3.11 First-passage probabilities by AL-HGP and MCS for (a) eighth-story and (b) first-story drift

of active learning of surrogates.

Figure 3.12 shows the convergence histories of NPD in Eq. (3.21) during the active learning procedure. The red-cross markers show the NPDs between consecutive learning steps whose values decrease as the iteration proceeds. The blue-plus markers are the NPDs between the first-passage probability calculated at each step and the optimal estimates at the final learning stage. It is noted that the blue markers are calculated only to demonstrate that the estimated first-passage probabilities are converging to the final estimates. The convergence histories of the AL-HGP analysis, starting from the initial experimental designs, confirm that the proposed method facilitates convergence to the final values through a small number of iterations.

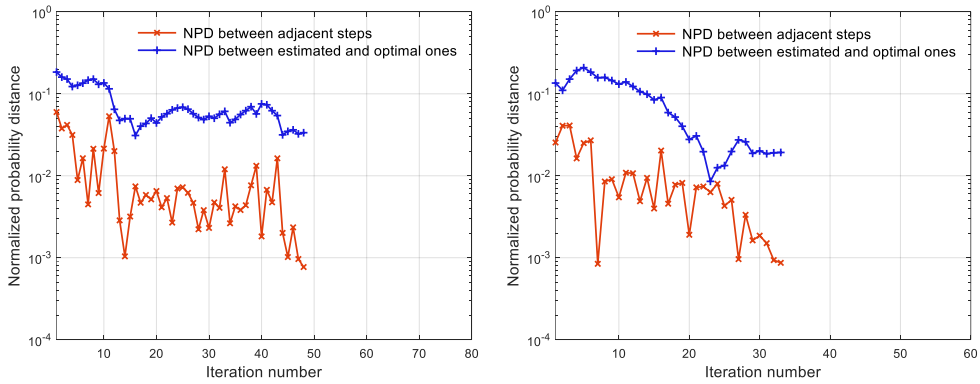

(a) (b)

Figure 3.12 The normalized probability differences (NPDs) of the estimated first-passage probability with respect to the previous learning step and final estimates for (a) eighth-story and (b) first-story drift

3.5.1.2 Case 2: uncertain parameters in both structural system and hazard model

The second case of the example considers the random variables associated with the structural system and wind hazard model. The modal damping coefficients of the building are parameterized by $c_j = \varepsilon_{cj}\tilde{c}_j, j = 1, \ldots, 8$ where $\tilde{c}_j$ are nominal values set to 0.02 and ε_{cj} are random variables following a multivariate Gaussian distribution with means of one and covariance matrix in which the covariance between ε_{cj} and ε_{ck} is defined as $\Sigma_{jk} = (0.2)^2 \exp[-(j-k)^2/2^2]$. The exponential function is introduced to represent the decaying correlation of damping coefficients (Zhang *et al*. 2017). For wind loading, the basic wind speed and air density are also modeled using random variables ε_v and ε_ρ, respectively, i.e., $V_b = \tilde{V}_b\varepsilon_v$ and $\rho_a = \tilde{\rho}_a\varepsilon_\rho$. The nominal values are respectively set to $\tilde{V}_b = 95$ (mph) and $\tilde{\rho} = 1.226\,(kg/m^3)$. The parameters ε_v and ε_ρ are modeled as

Gaussian random variables with the coefficient of variations (c.o.v.) 0.10 and 0.04, respectively (Slot *et al*. 2020; Abdelhady *et al*. 2022). As shown in Table 3.3, the random vector $\boldsymbol{X}$ includes ten variables describing uncertain parameters in the structural system and wind hazard model.

Table 3.3 Random variables associated with the structural system and wind hazard model for an eight-story building example (Case 2)

Random variables	Mean	c.o.v.	Distribution
Damping coefficients, ε_{cj}	1	0.20	Correlated Gaussian
Basic wind speed, ε_v	1	0.10	Gaussian
Air density, ε_ρ	1	0.04	Gaussian

* For $j = 1, \dots, 8$

Figure 3.13 presents the results of the AL-HGP method. The AL-HGP method is applied with 200 initial DoEs and convergence tolerance values 0.001. The response of interest is the eighth-story drift, whose threshold is $u_0 = 0.195\ (in)$. The correlated random samples can be generated by applying proper transformations to samples generated from uncorrelated standard Gaussian variables (Der Kiureghian 2022). The estimated first-passage probabilities and the convergence histories of NPDs are presented in Figures 3.13(a) and 3.13(b). Using the proposed method, only 358(=200+158) dynamic simulations are needed to estimate the first-passage probability whose results are compatible with those by MCS, obtained by 5×10^5 simulations leading to a coefficient of variation of 5% at the threshold. The results indicate that the AL-HGP method successfully addresses the dimension while producing accurate estimates with fewer dynamic analyses

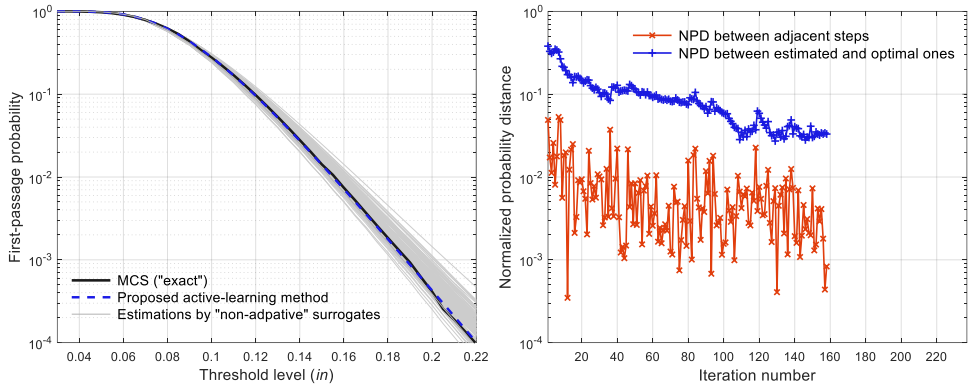

(a) (b)

Figure 3.13 First-passage probabilities of the eighth-story response in the eight-story building example (Case 2): (a) comparison between those by MCS and AL-HGP; and (b) convergence histories of NPDs

The convergence histories of AL-HGP analysis starting from different initial DoE points are given in Figure 3.14. In each case, the first-passage probability at threshold level, $\hat{p}_f(u_0 = 0.195)$ is converged to the reference MCS value after identifying 160, 230, and 256 simulations, despite randomness in the initial DoEs. The convergence histories confirm that the AL-HGP method quickly identifies the area of importance and DoE, enabling rapid convergence to the optimal first-passage probability.

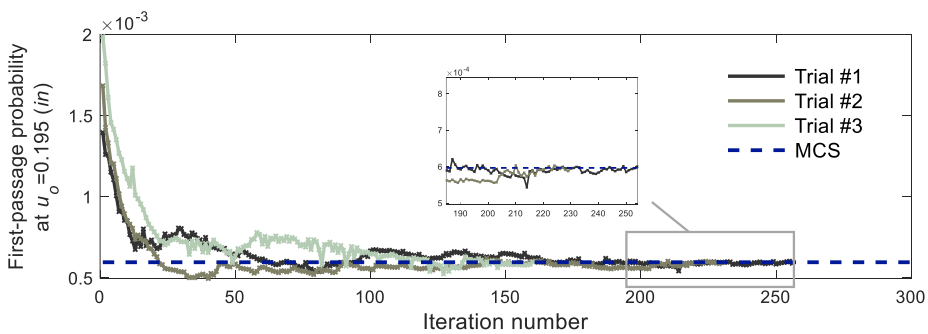

Figure 3.14 Convergence histories of AL-HGP during learning procedure for the eight-story building example (Case 2)

3.5.2 Application to a transmission tower

The next engineering application example investigates a transmission tower structure subjected to stochastic wind loads. Figure 3.15 shows the finite element model of a steel lattice tower structure, created using SAP2000 software to perform the nonlinear time-history analyses under stochastic wind loads. The tower's height is 122.8 m, and each tower section consists of several continuous panels with cross-arms. The tower's foundation is assumed to be rigid, i.e., the model is fixed at the base. The environmental wind forces caused by fluctuating winds are simulated by the stochastic wind-field model in Section 3.2.2 and applied to the transverse direction, as shown in Figure 3.15. Thus, the failure event is defined using the displacement responses of the transverse direction at the top of the tower with a displacement threshold of 1.46 m (Albermani *et al*. 2009; Cai *et al*. 2019). The time duration of consideration is 10 minutes (600 seconds).

The wind model parameters listed in Table 3.2 are used again to simulate the wind loads except for the basic wind speed, which is considered a random variable in this example. The material properties, i.e., modulus of elasticity E and yield strength f_y, of two steel types in the tower structure are also considered random variables, which may have dominant effects on the failure of the tower (Cai *et al*. 2019; Mohammadi *et al*. 2020; Kim *et al*. 2021). Table 3.4 summarizes the types and parameters of the distributions of all random variables.

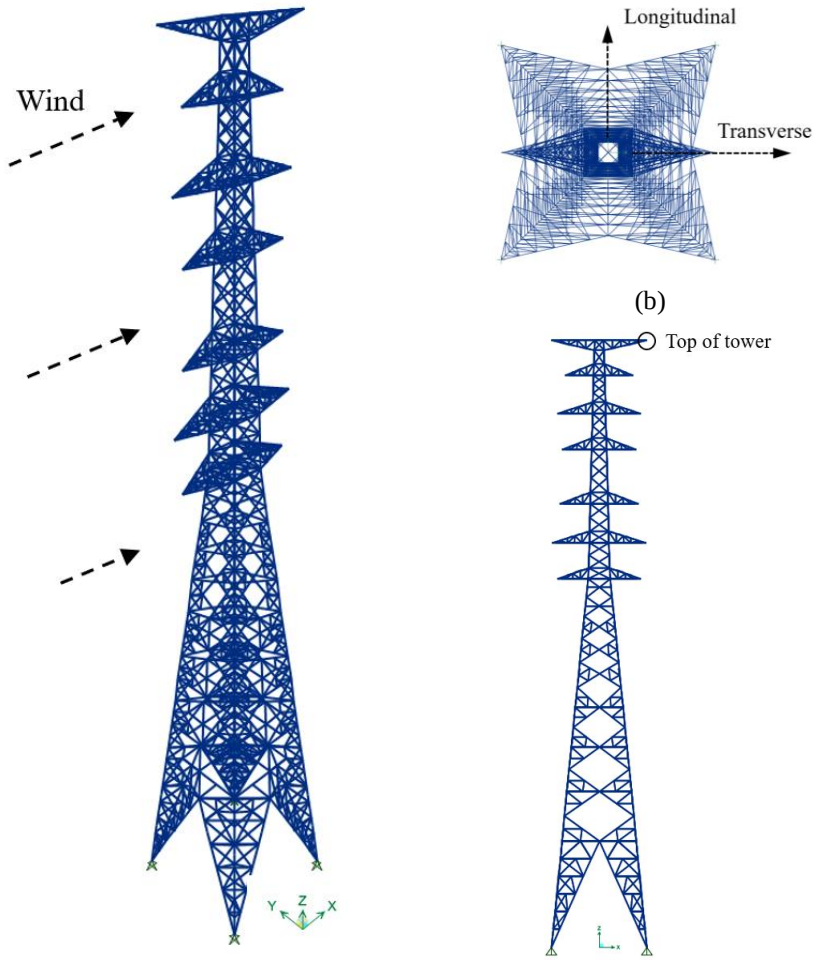

Figure 3.15 Finite element model of transmission tower example: (a) perspective view, (b) plan view, and (c) front view

Table 3.4 Distribution types and parameters of the random variables in a transmission tower example

Random variables	Distribution	Mean	c.o.v.
V_b (mph)	Gaussian	120	0.07
E_{S275} (Mpa)	Lognormal	200000	0.03
E_{S360} (Mpa)	Lognormal	200000	0.03
$f_{y,S275}$ (Mpa)	Lognormal	275	0.05
$f_{y,S360}$ (Mpa)	Lognormal	360	0.05

After the AL-HGP method is initiated with 100 initial DoEs, i.e., 100 time-history analyses of the tower structure, the surrogate models are refined by the proposed active learning procedure. Figure 3.16(a) presents the estimated first-passage probability compared with the MCS result by 5,000 simulation data, while the convergence histories of the NPDs are shown in Figure 3.16(b). The AL-HGP method needs only 236(=100+136) time-consuming simulations to obtain accurate estimates. Figure 3.17 demonstrates that the proposed method facilitates convergence to the optimal first-passage probability requiring only 102, 130, and 139 simulations even if different experimental designs are used in the initial stages. This example confirms that the AL-HGP successfully deals with first-passage problems involving high computational costs.

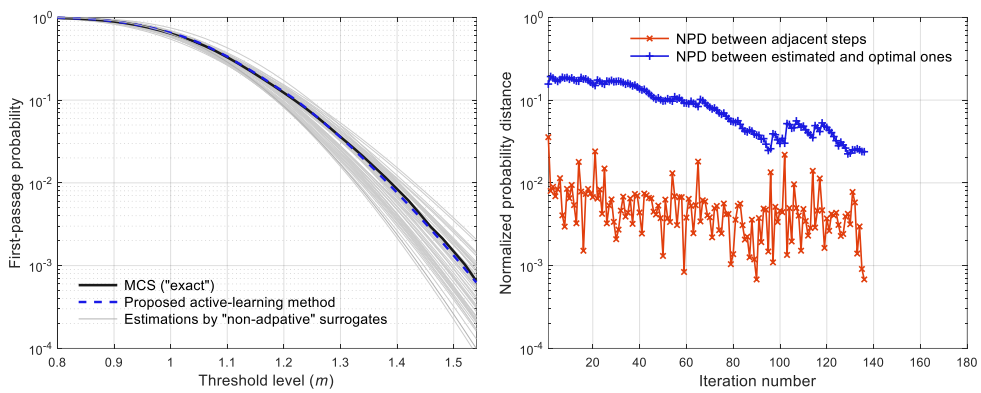

(a) (b)

Figure 3.16 Results of applying AL-HGP to transmission tower example: (a) comparison of the first-passage probability, and (b) convergence histories of NPDs

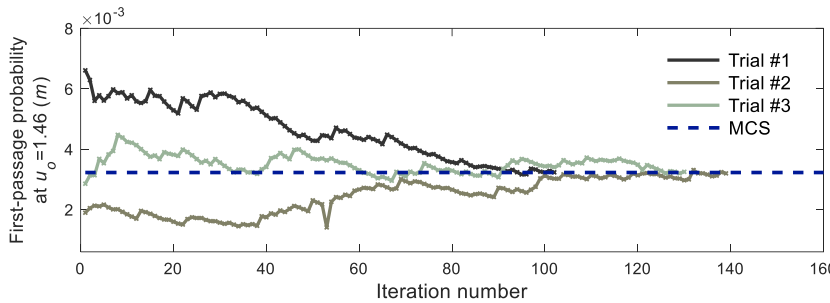

Figure 3.17 Convergence histories of AL-HGP during learning procedure for transmission tower example

3.6 Summary

This chapter proposed a new adaptive surrogate-based analysis framework for first-passage problems, termed active-learning-based method by Gaussian process with heteroscedastic noise (AL-HGP method). The main objective of the AL-HGP is to carry out an adaptive selection of simulation points with low computational costs from the reliability analysis standpoint under stochastic wind loads. The method utilized the Gaussian-process-based surrogates whose predictive mean and variance were employed to capture the conditional distribution of maximum response given the time-invariant basic random variable while handling heteroscedastic noise. This framework considered both uncertainties arising from the structural systems and the environmental wind loads. The proposed active learning framework further reduced the number of computational simulations by identifying the critical design of experiment (DoE) points that contribute most to the first-passage probability. The applications to the eight-story building system and transmission tower structure successfully demonstrated the performance and merits of the proposed method. In each example, the proposed method required fewer dynamic simulations to achieve accurate results, while the "non-adaptive" surrogate-based estimations could produce

inaccurate results with considerable variability. The transmission tower example demonstrated that AL-HGP could deal with high-fidelity computational simulations, e.g., finite element analyses, without losing the benefits and merits of the proposed method. Thus, AL-HGP is expected to effectively deal with such challenging and time-consuming problems in practical engineering.

Chapter 4. Reliability-Based Design Optimization Using Active Learning-based Quantile Surrogates

4.1 Introduction

Uncertainties in engineering systems, arising from lack of data, modeling approximations, or inherent randomness in the systems and their environment, may have a significant impact on the system performance. With the growing complexity of modern engineering systems, it is essential to manage the impact of such uncertainties in their design process. A design procedure that properly handles these uncertainties can assure the reliability of engineering systems by preventing the risk of unexpected failures that may eventually result in catastrophic damage or losses. Thus, appropriate strategies are required for uncertainty quantification and optimization in the design process of structures and other engineering systems. To this end, reliability-based design optimization (RBDO) has been extensively studied to achieve reliable optimal design of systems whose failure probability, i.e., the probability of violating the given constraints is lower than the target level of failure probability (Tu *et al*. 1998; Dubourg *et al*. 2011; Chun *et al*. 2016; Byun and Royset 2021).

However, it is challenging to accurately obtain the reliable optimal design since RBDO needs to evaluate the system's performance repeatedly, which may prevent unique and converged design solutions (Du and Chen 2004; Youn and Choi 2004; Jensen *et al*. 2020). This issue is exacerbated especially when the computational cost

of system performance evaluation is high. Reducing the number of function evaluations, therefore, is an essential task for effective RBDO in engineering practice. In these research efforts, adaptive surrogate methods were employed for efficient RBDO by constructing the "quantile surrogates" directly with Gaussian process model.

To overcome the aforementioned challenges in applications of RBDO, this chapter develops a new adaptive RBDO method employing quantile-surrogates, termed quantile surrogates by adaptive Gaussian process (QS-AGP). To identify the *probability-feasible design domain*, which is formulated in terms of the quantile of the performance function, Gaussian process models are utilized to build surrogates of the quantile. Both inherent randomness of the input random variables and epistemic uncertainty of surrogate model errors are considered in predicting the quantile using the surrogate model. At each step of the adaptive DoE procedure, the quantile estimate and the corresponding prediction variance are derived at each sample of $\boldsymbol{\theta}$ from the mixture distribution based on the GP model and inherent randomness of $\boldsymbol{X}$. In addition, a new learning function is introduced to facilitate the exploration-exploitation trade-off based on the quantile surrogate model in trying to identify the best design of structures.

The chapter first provides a brief overview of the RBDO problem and quantile formulation of probabilistic constraints in RBDO that are employed to represent probability-feasible design domain in the proposed method. Then, the following details of QS-AGP will be introduced: (1) the optimization by design samples, (2) the quantile estimation by mixture distribution, (3) the learning function proposed for exploration-exploitation trade-off, and (4) the adaptive RBDO algorithm.

Through numerical examples of challenging RBDO problems, the QS-AGP will be tested in terms of (1) accuracy for highly nonlinear performance functions, (2) robustness against various distribution types, and (3) efficiency, i.e., the number of performance function evaluations required for convergence. Lastly, a summary and concluding remarks are provided (Kim and Song 2021a).

4.2 Reliability-based design optimization (RBDO)

4.3.1 General RBDO formulation

RBDO generally aims to find the values of design parameters that minimize the cost function while satisfying deterministic and probabilistic constraints representing the given requirements. Given the probabilistic distribution model of the random vector $\boldsymbol{X}$, a general mathematical formulation of RBDO problems can be written as

$$\begin{aligned} &\min_{\boldsymbol{\theta}} \ f(\boldsymbol{\theta}) \\ &s.t. \ P[g_i(\boldsymbol{X};\boldsymbol{\theta}) \le 0] \le P_{f_i}^t, \qquad i = 1, \dots, n_c \\ &\qquad h_j(\boldsymbol{\theta}) \le 0, \qquad j = 1, \dots, n_b, \qquad \boldsymbol{\theta}^L \le \boldsymbol{\theta} \le \boldsymbol{\theta}^U \end{aligned} \tag{4.1}$$

where $f(\cdot)$ denotes the cost (or objective) function; $\boldsymbol{\theta} \in \mathbb{R}^{n_d}$ represents the vector of design parameters, which often includes the means of the random vector $\boldsymbol{X}$; $g_i(\cdot)$ and $P_{f_i}^t$ are respectively the *i*th performance (or limit-state) function indicating the occurrence of the failure event by $g_i(\cdot) \le 0$, and the corresponding target failure probability, $i = 1, \dots, n_c$; $h_j(\cdot)$ is the *j*th deterministic constraint function, $j = 1, \dots, n_b$; and $\boldsymbol{\theta}^L$ and $\boldsymbol{\theta}^U$ are the lower and upper bounds on the vector of design parameters $\boldsymbol{\theta}$, respectively. Since distribution parameters of the random vector $\boldsymbol{X}$ are often considered as design parameters in $\boldsymbol{\theta}$, the design under consideration, represented by $\boldsymbol{\theta}$, should satisfy the probabilistic constraints in Eq. (4.1). To check

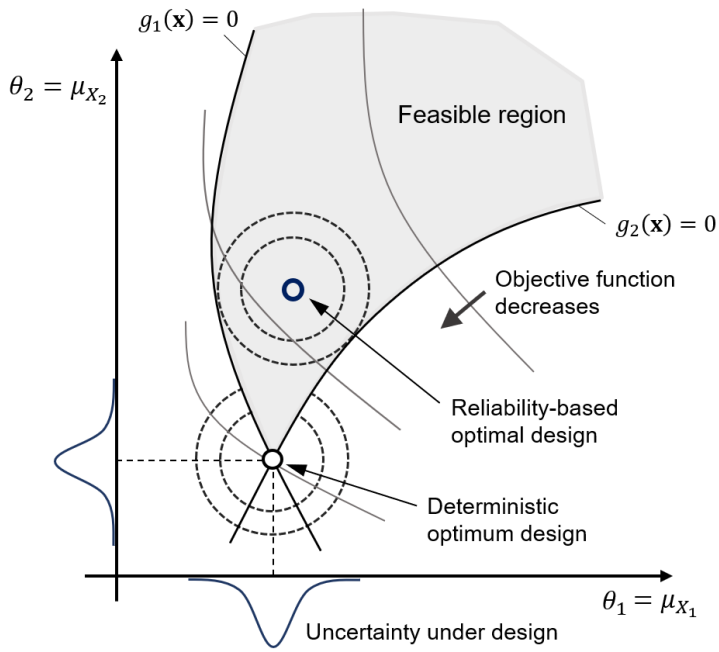

Figure 4.1 Concept of reliability-based design optimization process

whether the design at each iteration step satisfies the probabilistic constraints, RBDO needs to perform reliability analysis repeatedly, which is a main computational challenge in RBDO (Enevoldsen and Sorensen 1994; Youn and Choi 2004; Nguyen *et al*. 2010). The general concept of RBDO is illustrated in Figure 4.1.

4.3.2 Reviews on RBDO methods

In order to handle the probabilistic constraints in RBDO effectively, various approaches have been developed (Enevoldsen and Sorensen 1994; Youn *et al*. 2003; Nguyen *et al*. 2010; Liang *et al*. 2007; Nguyen *et al*. 2010; Chun *et al*. 2019). RBDO methods based on the concept of the First Order Reliability Method (FORM), e.g., Reliability Index Approach (RIA) (Enevoldsen and Sorensen 1994) and Performance Measure Approach (PMA) (Tu *et al*. 1998; Youn *et al*. 2003), perform nonlinear

constrained optimization in standard Gaussian space (Der Kiureghian 2022). The RIA and PMA approaches respectively use Hasofer-Lind Rackwitz-Fiessler (HL-RF) and Advanced Mean Value (AMV) optimization algorithms to identify the reliability measures given design parameters, which may prevent unique and converged design solutions if the RBDO problem features small failure probability and/or high nonlinearity. These approaches are often called a "double-loop" problem since each step of the design iterations involves another iteration for reliability analysis. The double-loop computation, thus, can be prohibitive especially when the cost of function evaluation is high. As an effort to reduce the computational burden of double-loop procedure, many RBDO approaches have been proposed in the literature (Du and Chen 2004; Liang *et al*. 2007; Nguyen *et al*. 2010; Moustapha *et al*. 2016). For example, Sequential Optimization and Reliability Assessment (SORA) (Du and Chen 2004) was proposed to decouple the deterministic design optimization and reliability analysis. The method aims to find the optimal solution by solving a "serial" single loop optimization, which moves the probabilistic constraints toward deterministic constraints by use of shift vectors. Several other single-loop (SL) approaches have been proposed to approximate the solution of the inner-loop optimization. In these approaches, e.g., SL-KKT (using the Karush–Kuhn–Tucker (KKT) optimality condition), SL-SV (using single-loop single-vector method), SL-RDS (using the concept of reliable design space) (Chen *et al*. 1995; Liang *et al*. 2007; Shan and Wang 2008), the inner-loop is replaced by an equivalent deterministic constraint using an approximation scheme. Figure 4.2 provides the concepts of four RBDO methods.

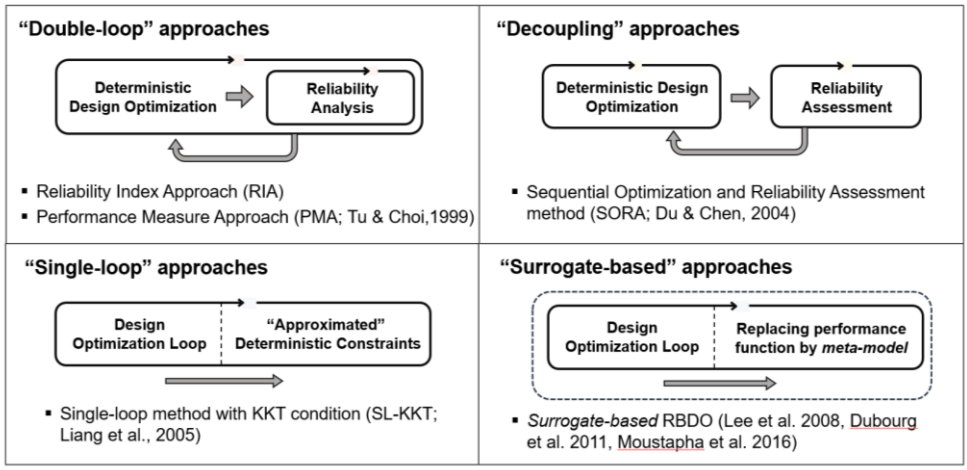

Figure 4.2 Illustration of four RBDO methods

4.3 Quantile-based formulation for RBDO

4.3.1 Performance measure

RBDO aims to find the values of $\boldsymbol{\theta}$ that minimize the cost function while satisfying both probabilistic and deterministic constraints. To check the design at each iteration step with regard to the probabilistic constraints, RBDO algorithms usually rely on the estimates of the failure probability for $\boldsymbol{\theta}$, i.e., $P[g_i(\boldsymbol{X};\boldsymbol{\theta}) \leq 0]$. Therefore, it is desirable to construct surrogates in the design parameter space $\boldsymbol{\theta}$ for computational efficiency. In particular, the proposed method aims to identify the admissible design domain in $\boldsymbol{\theta}$, termed "probability-feasible design domain," where any design choice satisfies the reliability requirements, by use of surrogates representing the quantile of the performance function (Lee and Jung 2008; Shan and Wang 2008; Moustapha *et al*. 2016).

To this end, the probabilistic constraints in Eq. (4.1) is described alternatively by the cumulative distribution function (CDF) of the performance function and the

target reliability index β_i^t, that is,

$$P[g_i(\boldsymbol{X};\boldsymbol{\theta}) \le 0] = F_{g_i(\boldsymbol{X};\boldsymbol{\theta})}(0) \le P_{f_i}^t = \Phi\left(-\beta_i^t\right) \tag{4.2}$$

where $F_{g_i}(\cdot)$ denotes the CDF of the *i*th performance function $g_i(\cdot)$; and $\Phi(\cdot)$ is the CDF of the standard Gaussian distribution. For an alternative description of Eq. (4.2), let us consider the $P_{f_i}^t$-quantile of the performance function, i.e.,

$$g_p(\boldsymbol{\theta}) = F_{g(\boldsymbol{X};\boldsymbol{\theta})}^{-1}\left(P_f^t\right) = \inf\left\{g \in \mathbb{R} : F_{g(\boldsymbol{X};\boldsymbol{\theta})}(g) \ge P_f^t\right\} \tag{4.3}$$

where g_p is the P_f^t-quantile of performance function (often termed "performance measure" (Tu *et al*. 1998; Youn *et al*. 2003)); and $F_g^{-1}(\cdot)$ denotes the inverse CDF of the performance function. During the optimization process, any design choice in $\{\boldsymbol{\theta}|g_p(\boldsymbol{\theta}) = 0\}$ is considered located at the boundary discerning the satisfactory and unsatisfactory designs from viewpoint of reliability requirement (often termed an inverse most probable point (MPP) in PMA method (Tu *et al*. 1998; Youn *et al*. 2003)). On the other hand, the probability-feasible design domain $\mathcal{S}_p$ can be described in terms of the quantile of the performance function as $\mathcal{S}_p = \left\{\boldsymbol{\theta}\middle|g_p(\boldsymbol{\theta}) \ge 0\right\}$. Geometric illustrations of the quantile-based formulation for satisfactory and unsatisfactory design cases are given in Figures 4.3(a) and Figure 4.3(b) respectively.

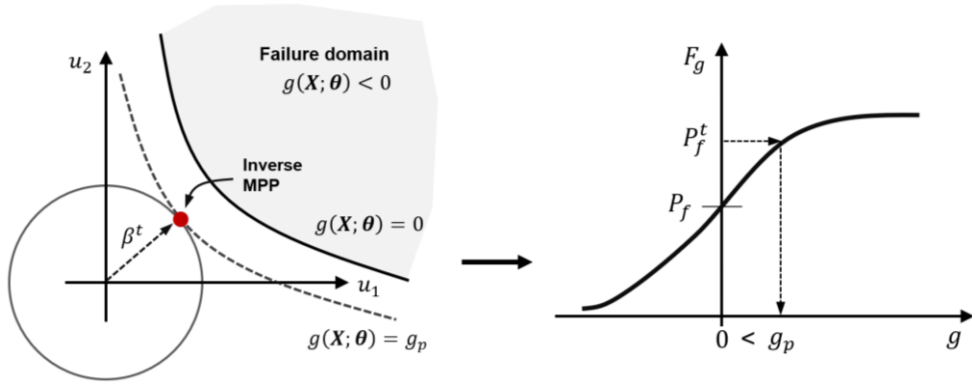

(a) Satisfactory design

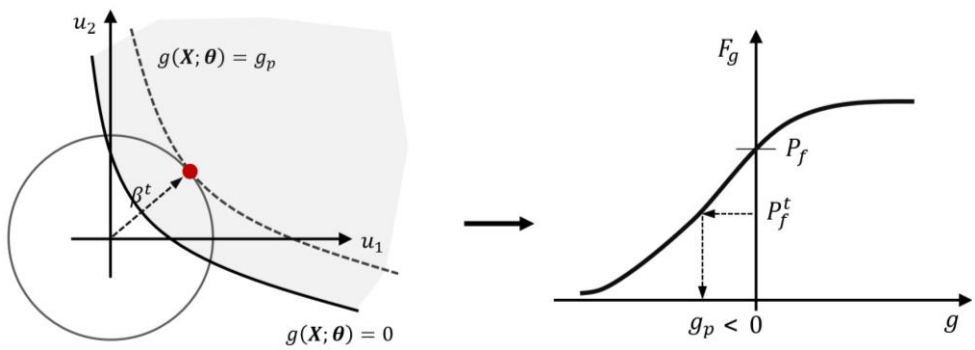

(b) Unsatisfactory design

Figure 4.3 Geometric representations of performance measure g_p for (a) satisfactory design, and (b) unsatisfactory design (Note: u_1 and u_2 in the figure denote the axes of uncorrelated standard Gaussian space transformed from the original random variable space (Der Kiureghian 2022), which are introduced to facilitate illustration of the quantile concept, but not required in the proposed method)

4.3.2 Identification of probability-feasible design domain

The proposed scheme aims to construct a surrogate of the quantile, $\hat{g}_p(\boldsymbol{\theta})$ to approximately identify the boundary of the probability feasible domain, i.e., $\{\boldsymbol{\theta}|g_p(\boldsymbol{\theta}) = 0\}$. This concept is illustrated by Figure 4.4. (In the proposed method, the cost function $f(\boldsymbol{\theta})$ is also approximated by a surrogate $\hat{f}(\boldsymbol{\theta})$ to facilitate the design optimization.) It is noteworthy that the quantiles are the functions of the

design variables $\boldsymbol{\theta}$ only since $\boldsymbol{\theta}$ determines the joint probability density of the input random variables $\boldsymbol{X}$. In order to construct the surrogate models using as small number of simulation points as possible, an *adaptive* DoE scheme (Zhang *et al*. 2017; Marelli and Sudret 2018) is employed in the proposed method. The main goal is to identify the domains in the design space where a further computational simulation, i.e., a performance function evaluation, is expected to be the most effective in terms of finding the optimal design using the quantile surrogate model. The scheme basically guides the simulation locations toward boundaries of the probability-feasible design domain, $\{\boldsymbol{\theta}|g_p(\boldsymbol{\theta}) = 0\}$, because the optimal solutions are usually located at the boundary of a constraint (Shan and Wang 2008; Moustapha *et al*. 2016). Note that, in this chapter, the term "samples" refers to the candidate points in $\boldsymbol{\theta}$, which are generated for the purpose of active-learning, while the term "simulation" means actual evaluation of the true performance function at the sample point selected by the active-learning process.

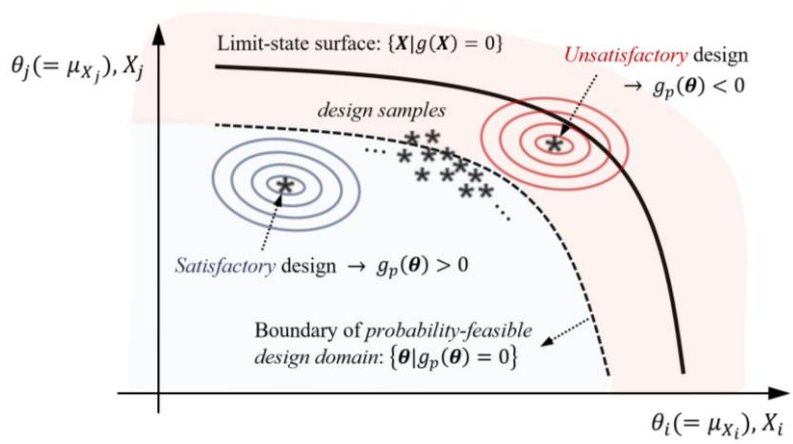

Figure 4.4 Illustration of probability-feasible design domain in QS-AGP method

4.4 Proposed quantile surrogates by adaptive Gaussian process (QS-AGP)

To check if a design belongs to the aforementioned probability-feasible design domain $\{\boldsymbol{\theta}|g_p(\boldsymbol{\theta}) \geq 0\}$, the quantile of the performance function at a given design, $g_p(\boldsymbol{\theta})$ is estimated based on the probabilistic distributions of input random variables $\boldsymbol{X}$. In addition, the model uncertainty of the surrogate-based estimation of the quantile needs to be quantified for the exploration-exploitation trade-off during the active-learning process (Jones *et al*. 1998; Picheny *et al*. 2010). To this end, the proposed QS-AGP constructs quantile surrogates by Gaussian Process. A *learning function* of QS-AGP is also introduced to encourage computational simulations in the vicinity of the boundary $\{\boldsymbol{\theta}|g_p(\boldsymbol{\theta}) = 0\}$ while giving priorities to more desirable domains in $\boldsymbol{\theta}$ from the viewpoint of design optimization, i.e., domains where the cost function is smaller.

4.4.1 Optimization based on design samples

Obtaining the sensitivities (or derivatives) of cost and/or constraint functions with respect to design parameters can be a cumbersome or infeasible task in many engineering practice, which may prohibit the use of gradient-based optimizer. The proposed QS-AGP relies on samples uniformly distributed in the design space, $\boldsymbol{\theta}_l, l = 1, \dots, n_l$, termed *design samples*. These design samples are candidate points for computational simulations, i.e., candidates for statistical learning. Using the computational simulation results at the initial DoE points and those later selected by the GP-based adaptive DoE procedure, the quantile estimate and the corresponding prediction variance are derived at each of the design samples $\boldsymbol{\theta}_l$. To further improve

convergence, this study adopts low-discrepancy samples, often termed quasi-random samples. The improvement of the convergence rate by low discrepancy of samples, e.g., Sobol and Halton sequence, has been discussed in the literature (Caflisch 1998; Wang and Fang 2003).

At each step of the adaptive learning process, the probabilistic constraint feasibility is checked by the signs of the quantile surrogate predictions $\hat{g}_p(\boldsymbol{\theta}_l), l = 1, \dots, n_l$. Then, among the (approximately) feasible samples, the one with the minimal cost according to another GP-surrogate of the cost function, $\hat{f}(\boldsymbol{\theta})$ is determined as an approximately optimal solution. Thus, the proposed RBDO method does not require an additional optimizer or any gradient information regarding the performance and cost function because it aims to identify one of the design *samples* that minimizes $\hat{f}(\boldsymbol{\theta})$ while satisfying the probabilistic constraint according to the surrogate $\hat{g}_p(\boldsymbol{\theta})$ through an active-learning process.

4.4.2 Quantile surrogates by mixture distribution

Using GP-based surrogate models, one can quantify the epistemic uncertainty in the model error caused by the lack of simulations, in the form of GP prediction variance in Eq. (2.8). On the other hand, inherent randomness in the RBDO problem is represented by the probabilistic distributions of $\boldsymbol{X}$. It is essential to handle both types of uncertainties in estimating the quantile of the performance function in RBDO (Girard *et al*. 2003; Der Kiureghian and Ditlevsen 2009; Li and Wang 2019).

To incorporate both uncertainties into the quantile estimation by surrogates, let us first consider the Gaussian distribution of GP in Eq. (2.6), i.e., $p\left(y_*|\boldsymbol{x}_*, \boldsymbol{x}_{\boldsymbol{\mathcal{D}}}, \boldsymbol{y}_{\boldsymbol{\mathcal{D}}}, \widehat{\boldsymbol{\Theta}}\right)$. Replacing the general output y_* by the performance function

g, and introducing $\boldsymbol{\mathcal{D}} = \{\boldsymbol{x}_{\boldsymbol{\mathcal{D}}}, \boldsymbol{g}_{\boldsymbol{\mathcal{D}}}\}$ to represent the pair of simulation inputs and corresponding outputs, the GP-based prediction of the performance function at $\boldsymbol{x} = \boldsymbol{x}_*$ based on simulations at DoE points can be denoted by $p(g|\boldsymbol{x}_*, \boldsymbol{\mathcal{D}}, \widehat{\boldsymbol{\Theta}})$. By the total probability theorem, the predictive distribution of the performance function is derived as (Girard *et al*. 2003)

$$p(g|\boldsymbol{\theta}, \boldsymbol{\mathcal{D}}) = \int p\left(g|\boldsymbol{x}_*, \boldsymbol{\mathcal{D}}, \widehat{\boldsymbol{\Theta}}\right) p(\boldsymbol{x}_*|\boldsymbol{\theta})\, d\boldsymbol{x}_* \tag{4.4}$$

in which $p(\boldsymbol{x}_*|\boldsymbol{\theta})$ is the probability density function (PDF) of the input random variables at $\boldsymbol{x} = \boldsymbol{x}_*$, affected by the design parameters $\boldsymbol{\theta}$. The predictive distribution is then fitted by a mixture of the GP-based densities of g, each of which is obtained at random samples generated from $p(\boldsymbol{x}_*|\boldsymbol{\theta})$, i.e.,

$$p(g|\boldsymbol{\theta}, \boldsymbol{\mathcal{D}}) \cong \frac{1}{n_m} \sum_{k=1}^{n_m} p\left(g|\boldsymbol{x}_*^k, \boldsymbol{\mathcal{D}}, \widehat{\boldsymbol{\Theta}}\right) = \frac{1}{n_m} \sum_{k=1}^{n_m} f_N\left(g; \mu_g^k, \sigma_g^k\right) = f_g(g) \tag{4.5}$$

where $\boldsymbol{x}_*^k$ is the kth random sample generated from $p(\boldsymbol{x}_*|\boldsymbol{\theta})$ representing the aleatoric uncertainty in $\boldsymbol{X}$, $k = 1, \ldots, n_m$; and $f_N(\cdot)$ denotes the PDF of the Gaussian distribution. The distribution parameters μ_g^k and σ_g^k are respectively the predictive mean and standard deviation of the corresponding GP surrogate in Eq. (2.7) and Eq. (2.8). The approximated distribution in Eq. (4.5) converges to the true distribution as the number of the samples randomly generated from $p(\boldsymbol{x}_*|\boldsymbol{\theta})$ grows. It is noted that, as a result of the marginalization in Eq. (4.4), the distribution of the performance function is now given in terms of $\boldsymbol{\theta}$ only. Then, from Eq. (4.5), the CDF of the performance function, denoted by $F_g(g)$, is approximated as

$$F_g(g) \cong \frac{1}{n_m}\sum_{k=1}^{n_m} F_N\left(g;\mu_g^k,\sigma_g^k\right) = \frac{1}{n_m}\sum_{k=1}^{n_m} \Phi\left(\frac{g-\mu_g^k}{\sigma_g^k}\right) \tag{4.6}$$

where $F_N(\cdot)$ is the CDF of a general Gaussian distribution.

Next, the P_f^t-quantile of the performance function can be estimated by solving the equation $F_g(g) = P_f^t$ for g. The equation can be solved numerically as follows:

$$\hat{g}_p(\boldsymbol{\theta}) = \underset{g\in\mathbb{R}}{\operatorname{argmin}}|Q(g)| \tag{4.7a}$$

$$Q(g) = \frac{1}{n_m}\sum_{k=1}^{n_m} \Phi\left(\frac{g-\mu_g^k}{\sigma_g^k}\right) - P_f^t \tag{4.7b}$$

Since the Gaussian CDF $\Phi(\cdot)$ is a monotonically increasing function, Eq. (4.7) can be solved by a line search algorithm using the sensitivity

$$\frac{\partial Q}{\partial g} = \frac{1}{n_m}\sum_{k=1}^{n} \frac{1}{\sigma_g^k}\varphi\left(\frac{g-\mu_g^k}{\sigma_g^k}\right) \tag{4.8}$$

where $\varphi(\cdot)$ is the PDF of the standard Gaussian distribution. In summary, during RBDO, at each of the design samples $\boldsymbol{\theta}_l, l = 1,\dots,n_l,$ the quantile of performance function, $\hat{g}_p(\boldsymbol{\theta})$ can be estimated by using the mixture of Gaussian CDFs in Eq. (4.5) which are derived from the GP surrogate. A geometric representation of the quantile estimation using the GP surrogate is provided in Figure 4.5.

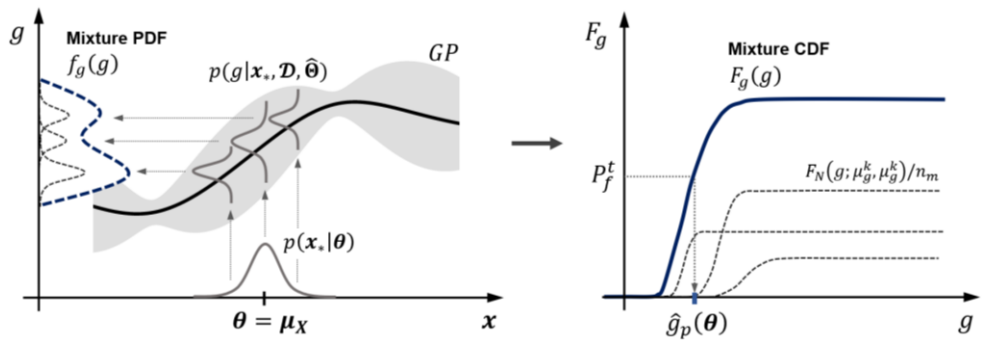

Figure 4.5 Quantile estimation by GP-surrogate-based mixture distribution

Because the quantile is estimated in Eq. (4.7) by use of n_m mixture samples, statistical uncertainty exists in the estimate. Therefore, the solution of Eq. (4.7) is considered as the mean, i.e., $\hat{g}_p(\boldsymbol{\theta}) = \mu_{\hat{g}_p}(\boldsymbol{\theta})$, while the statistical uncertainty is quantified by the variance $\sigma_{\hat{g}_p}^2$, which can be derived using standard order statistics theory (Arnold *et al*. 1992) as follows:

$$\sigma_{\hat{g}_p}^2(\boldsymbol{\theta}) = \frac{P_f^t(1-P_f^t)}{n_m\left[f_g\left(F_g^{-1}(P_f^t)\right)\right]^2} \cong \frac{P_f^t(1-P_f^t)}{n_m\left[f_g(\hat{g}_p)\right]^2} \tag{4.9}$$

where $f_g(\hat{g}_p) = \frac{1}{n_m}\sum_{k=1}^{n_m} f_N(\hat{g}_p; \mu_g^k, \sigma_g^k)$ from Eq. (4.5). It is noted that the estimation variance converges to zero as the probabilistic density at prediction point, $f_g(\hat{g}_p)$ increases or the sample size n_m is large.

4.4.3 Training of quantile surrogates

For efficiency, the proposed RBDO refines the GP surrogate by computational simulations at locations recommended by a learning function instead of trying to fit *all* boundaries of the probability feasible design domain. Inspired by the adaptive

learning procedure that was developed for reliability analysis (Kim and Song 2020), the GP surrogates are trained adaptively using a learning function as follows.

At a given RBDO iteration, based on the surrogate-based estimation of the quantile and cost function, the optimal design $\boldsymbol{\theta}^*$ is identified among the design samples $\boldsymbol{\theta}_l$ as

$$\begin{aligned} &\boldsymbol{\theta}^* = \underset{\boldsymbol{\theta}_l}{argmin}\, \hat{f}(\boldsymbol{\theta}_l) \\ &s.t.\ \hat{g}_{p,i}(\boldsymbol{\theta}_l) \geq 0,\ \ i = 1, \dots, n_c, l = 1, \dots, n_l \end{aligned} \tag{4.10}$$

To enrich the DoE effectively in the next RBDO iteration, the learning criteria is defined so as to fit the boundary of the feasible domain $\{\boldsymbol{\theta} | g_{p,i}(\boldsymbol{\theta}) = 0, i = 1, \dots, n_c\}$ well especially in the areas making significant contribution to the current optimum $\hat{f}^* = \hat{f}(\boldsymbol{\theta}^*)$. To achieve this goal through exploration-exploitation trade-off, the proposed method introduces to select the sample *minimizing* the following learning function featuring a penalty term $\gamma_{\hat{f}}(\boldsymbol{\theta})$, as the next simulation point:

$$\alpha(\boldsymbol{\theta}) = \frac{\left|\mu_{\hat{g}_{p,ct}}(\boldsymbol{\theta})\right|}{\sigma_{\hat{g}_{p,ct}}(\boldsymbol{\theta})} \cdot \gamma_{\hat{f}}(\boldsymbol{\theta}) \tag{4.11}$$

$$with\ \gamma_{\hat{f}}(\boldsymbol{\theta}) = \begin{cases} \left|\dfrac{\hat{f}(\boldsymbol{\theta}) - \hat{f}^*}{\hat{f}^*}\right| & \text{if } \Delta_{o.p} \geq tol \\ 1 & \text{otherwise} \end{cases} \tag{4.12}$$

in which $\mu_{\hat{g}_{p,ct}}(\boldsymbol{\theta})$ and $\sigma_{\hat{g}_{p,ct}}(\boldsymbol{\theta})$ are respectively the mean and standard deviation of the performance quantile derived in Eq. (4.7) and Eq. (4.9); $\gamma_{\hat{f}}(\boldsymbol{\theta})$ is the penalty function; $\hat{f}(\boldsymbol{\theta})$ is the GP-surrogate-based estimate of the cost function at $\boldsymbol{\theta}$; $\Delta_{o.p}$ is the distance between the optimal $\boldsymbol{\theta}$ values obtained by Eq. (4.10) at the current and previous learning-steps; and tol is the prescribed threshold of convergence. The numerator $|\mu_{\hat{g}_{p,ct}}(\boldsymbol{\theta})|$ of the ratio in Eq. (4.11) encourages computational

simulations in the vicinity of the boundary $\{\boldsymbol{\theta}|g_p(\boldsymbol{\theta})=0\}$ while the denominator $\sigma_{\hat{g}_{p,ct}}(\boldsymbol{\theta})$ promotes simulations at less-explored areas, i.e., more uncertain areas. On the other hand, the penalty term helps guide the search toward cost-effective regions which have significant impact on the optimal design. In Eq. (4.11), the learning function is defined for the performance function with the minimum $\mu_{\hat{g}_{p,i}}(\boldsymbol{\theta})$ for $i=1,\dots,n_c$, denoted by the index ct, as proposed by Fauriat and Gayton (2014). The use of the composite index ct means no evaluation for the performance functions that have little or no influence at a current step, and thus only one performance function g_{ct} is evaluated per each iteration.

After the best design point is identified as $\boldsymbol{\theta}_{best}=\underset{\boldsymbol{\theta}_l}{argmin}\,\alpha(\boldsymbol{\theta}_l)$, the location of the performance function evaluation, $\boldsymbol{x}_{best}$ is determined as

$$\boldsymbol{x}_{best}=\underset{\boldsymbol{x}^k}{\operatorname{argmin}}\frac{\left|\mu_{\hat{g}_{ct}}(\boldsymbol{x}^k;\boldsymbol{\theta}_{best})\right|}{\sigma_{\hat{g}_{ct}}(\boldsymbol{x}^k;\boldsymbol{\theta}_{best})} \tag{4.13}$$

where $\mu_{\hat{g}_{ct}}(\boldsymbol{x};\boldsymbol{\theta}_{best})$ and $\sigma_{\hat{g}_{ct}}(\boldsymbol{x};\boldsymbol{\theta}_{best})$ respectively denote the GP-based predictive mean and standard deviation of performance function at $\boldsymbol{x}$ given $\boldsymbol{\theta}_{best}$, which are denoted by μ_g^k and σ_g^k in Eq. (4.5). Thus, Eq. (4.13) represents another GP-based exploration-exploitation trade-off to choose the next location of the performance function evaluation among the random samples $\boldsymbol{x}^k$, $k=1,\dots,n_m$, generated from $p(\boldsymbol{x}|\boldsymbol{\theta}_{best})$ near the approximate limit-state surface. It is noted that the locations of performance function, $\boldsymbol{x}_{best}$ are different from $\boldsymbol{\theta}_{best}$ because of inherent randomness of input uncertainties. In summary, the proposed optimization scheme enriches the DoE by $[\boldsymbol{\theta}_{best}, g_{ct}(\boldsymbol{x}_{best};\boldsymbol{\theta}_{best}), f(\boldsymbol{\theta}_{best})]^{\mathrm{T}}$.

The following convergence criteria are introduced to check the convergence

with regards to the relative increment of optimal cost and refinement of surrogate constraint:

$$\left|\frac{\hat{f}\left(\boldsymbol{\theta}^*_{(m)}\right)-\hat{f}\left(\boldsymbol{\theta}^*_{(m-1)}\right)}{\hat{f}\left(\boldsymbol{\theta}^*_{(m)}\right)}\right| \leq \varepsilon_f \tag{4.14}$$

$$\max_i \left[\sigma_{\hat{g}_{p,i}}\left(\boldsymbol{\theta}^*_{(m)}\right)\right] \leq \varepsilon_p,\ i=1,\dots,n_c \tag{4.15}$$

where $\boldsymbol{\theta}^*_{(m)}$ is the optimal design at the m-th learning step; and ε_f and ε_p are pre-specified tolerance values for the criteria. The tolerance values depend on the target level of accuracy, and $\varepsilon_f, \varepsilon_p \in (10^{-4}, 10^{-2})$ are recommended based on the experience of the authors.

4.4.4 Algorithm of QS-AGP

The algorithm of the proposed QS-AGP is summarized as follows (see Figure 4.6 for the flowchart):

1. *Generate samples in design space*: Generate n_l design samples $\boldsymbol{\theta}_l, l=1,\dots,n_l$ that are uniformly distributed in the design space. These sample populations are used as candidate locations for active-learning, and finally the optimal solution is determined among these samples. The sample population size $n_l = 10^4 \sim 10^5$ seems to be a reasonable choice from the experience.
2. *Construct the initial DoE*: Generate n_0 samples $\boldsymbol{\theta}_{\boldsymbol{\mathcal{D}}} = \left[\boldsymbol{\theta}_1,\dots,\boldsymbol{\theta}_{n_0}\right]^{\mathrm{T}}$ by Latin Hypercube Sampling (LHS) in the design space. Then, corresponding samples $\boldsymbol{x}_{\boldsymbol{\mathcal{D}}} = \left[\boldsymbol{x}_1,\dots,\boldsymbol{x}_{n_0}\right]^{\mathrm{T}}$ are also generated with input variations, i.e.,

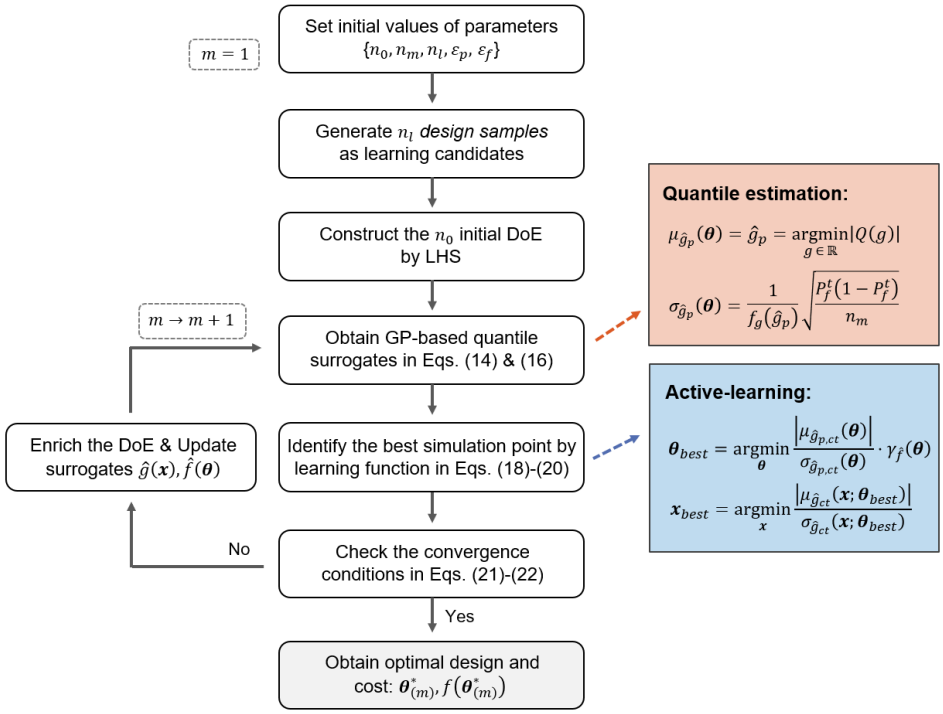

Figure 4.6 Flowchart of QS-AGP algorithm

$\boldsymbol{x}_{\mathcal{D}} = \boldsymbol{\theta}_{\mathcal{D}} + \boldsymbol{\varepsilon}_{\mathrm{x}}$ where $\boldsymbol{\varepsilon}_{\mathrm{x}} \sim N(0, \boldsymbol{\Sigma}_x)$. The cost function $f(\boldsymbol{\theta})$ and each of the performance functions $g_i(\boldsymbol{x}), i = 1, \ldots, n_c$, are respectively evaluated on the DoE points $\boldsymbol{\theta}_{\mathcal{D}}$ and $\boldsymbol{x}_{\mathcal{D}}$ to construct the initial DoE of the surrogate models.

3. *Obtain GP-based quantile surrogates*: Construct GP-based quantile surrogates at the design sample points using the current DoE. That is, for each of the design samples points $\boldsymbol{\theta}_l$, the mean of quantile, $\mu_{\hat{g}_p}(\boldsymbol{\theta})$ in Eq. (4.7) and the corresponding standard deviation of estimated quantile, $\sigma_{\hat{g}_p}(\boldsymbol{\theta})$ in Eq. (4.9) are calculated from the mixture CDF for each performance function. The derived quantities of quantiles are utilized for the exploration-exploitation trade-off in the proposed learning function.

4. *Perform active-learning process*: Identify the sample point where the learning function $\alpha(\boldsymbol{\theta})$ in Eq. (4.11) is minimized, as $\boldsymbol{\theta}_{best}$. Then, the next location of the performance function evaluation, $\boldsymbol{x}_{best}$ is determined by Eq. (4.13). The DoE is enriched by performance function evaluation $\boldsymbol{x} = \boldsymbol{x}_{best}$ and cost function calculation at $\boldsymbol{\theta} = \boldsymbol{\theta}_{best}$. Next, the estimate of the optimal GP hyperparameters, $\widehat{\boldsymbol{\Theta}}$ is obtained again by MLE with the enriched DoE in Eq. (2.5).
5. *Check the convergence criteria*: Once the best simulation point is determined, the convergence conditions in Eq. (4.14) and Eq. (4.15) are calculated to check the convergence in terms of surrogate refinements and learning convergences. If the procedure has not achieved the prescribed level of convergence, repeat Steps 3-5 as enriching the DoE.
6. *End of QS-AGP*: Once converged, QS-AGP stops the iteration to determine the current design $\boldsymbol{\theta}^*_{(m)}$ and cost $f\left(\boldsymbol{\theta}^*_{(m)}\right)$ as the optimal design and cost, respectively.

4.5 Numerical examples

4.5.1 Highly nonlinear performance function

First, consider a two-dimensional RBDO example with highly non-linear performance function, which is formulated as (Lee and Jung 2008; Moustapha and Sudret 2019)

$$
\begin{aligned}
&\min_{\boldsymbol{\theta}} f(\boldsymbol{\theta}) = (\theta_1 - 3.7)^2 + (\theta_2 - 4)^2 \\
&s.t.\ P[g_i(\boldsymbol{X};\boldsymbol{\theta}) \le 0] \le P_{f_i}^t, \qquad i = 1,2 \\
&\qquad 0 \le \theta_1 \le 3.7, 0 \le \theta_2 \le 4.0 \\
&\text{with } g_1(\boldsymbol{x}) = -x_1 \sin(4x_1) - 1.1x_2 \sin(2x_2) \\
&\qquad g_2(\boldsymbol{x}) = x_1 + x_2 - 3
\end{aligned}
\tag{4.16}
$$

where $\boldsymbol{x}$ is realization of the random vector $\boldsymbol{X}$ consisting of two independent Gaussian random variables X_1 and X_2; $\boldsymbol{X}$ has the means $\boldsymbol{\theta}$ and the same constant standard deviation $\sigma = 0.1$, i.e., $X_j \sim N(\theta_j, \sigma^2), j = 1,2$. The generalized target reliability index β_i^t is set to 2 for both constraints. The solid curves in Figures 4.7-4.9 show the limit-state surfaces by the true performance functions.

Table 4.1 shows typical results (among more than 20 independent runs) by the proposed QS-AGP, compared with those by RIA, PMA, SORA and SL-KKT reported in the literature (Enevoldsen and Sorensen 1994; Tu *et al*. 1998; Du and Chen 2004; Liang *et al*. 2007). The accuracy and efficiency of the different methods are compared in terms of the values of the final optimal design parameters ($\boldsymbol{\theta}_{opt}$), the optimal cost ($f_{opt}$), and the numbers of evaluations for the two performance functions (N_{g_1} and N_{g_2}), and the number of the cost function evaluation (N_f). The proposed method obtains an optimal design using fewer function evaluations, i.e., 19 and 12 for the first and second performance functions respectively despite their high nonlinearity. It is noted that the RBDO result by SL-KKT cannot converge to a similar result due to the high non-linearity of the performance function.

Figure 4.7 illustrates the adaptive search process of the proposed method. Figure 4.7(a) presents initial stages of adaptive learning with the initial set of DoE, which is denoted by the circular markers. The limit state surfaces estimated by

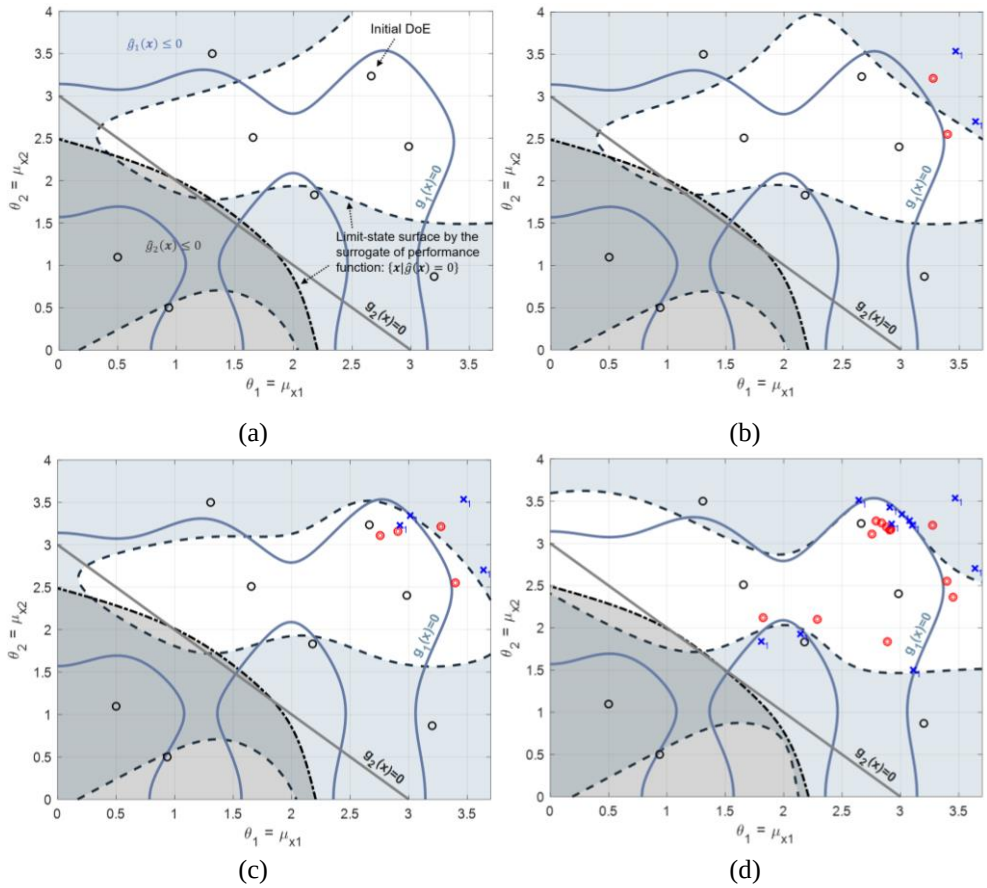

Figure 4.7 Progresses of DoE by QS-AGP for example with highly nonlinear performance functions: (a) $m = 0$ (initial stage), (b) $m = 2$, (c) $m = 4$, and (d) $m = 12$

surrogates are represented by dashed-line for the two performance functions respectively. Figures 4.7(b)-(d) show the progresses after 2, 4 and 12 simulations respectively. In particular, the double red-circle markers are the design samples selected by the adaptive procedure in Eq. (4.11), i.e., $\boldsymbol{\theta}_{best}$. The cross-marker "x" is the corresponding location of function evaluations, i.e., $\boldsymbol{x}_{best}$, and a subscript of the marker denotes the index of the evaluated performance function. For instance, at the location denoted by the marker "x1," QS-AGP evaluates performance function $g_1(\boldsymbol{x})$ only. It is confirmed that the proposed method guides the search so that more

simulations are performed in the near-optimal regions from the viewpoint of RBDO.

Table 4.1 Comparison between the results by the proposed QS-AGP method and other RBDO methods for example with highly nonlinear performance functions

RBDO Method	$\boldsymbol{\theta_{opt}}$	f_{opt}	N_{g_1}/N_{g_2}	N_f
PMA	[2.82, 3.28]	1.30	991/129	24
RIA	[2.82, 3.28]	1.30	588/97	23
SORA	[2.82, 3.28]	1.30	42/53	33
SL-KKT	[2.83, 3.22]	1.37	152/152	76
QS-AGP	**[2.81, 3.28]**	**1.31**	**19/12**	**23**

Figure 4.8 shows the approximate limit-state surface along with all DoE points explored up to the final step. The diamond marker represents the final reliable optimum $\boldsymbol{\theta}_{opt}$ reported in Table 4.1. The result confirms that most of the sample points selected by QS-AGP are located around the true limit-state surface, especially in the cost-effective regions, which facilitates construction of effective surrogate models for the purpose of RBDO. Figure 4.9 provides a close-up of DoE around the optimal design along with refined surrogate-based boundaries of probability-feasible design domain, i.e., $\{\boldsymbol{\theta}|\hat{g}_p(\boldsymbol{\theta}) = 0\}$. It is observed that the final reliable optimum,

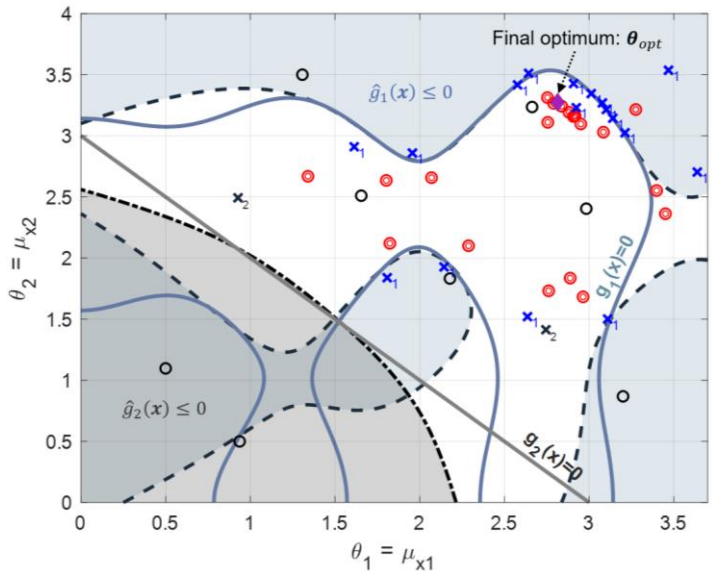

Figure 4.8 Final DoE for example with highly nonlinear performance functions

active on the first performance function constraint, is successfully obtained by the quantile surrogates refined by the adaptive learning. The convergence histories of QS-AGP are given in Figure 4.10 (in which estimated design parameters are normalized by the final optimal solution $\boldsymbol{\theta}_{opt}$). The convergence histories of QS-AGP analysis, starting from the initial experimental designs, confirm that the cost and design parameters are converged to the final values by a small number of iterations through the estimated quantile surrogates constructed by GP-based surrogates.

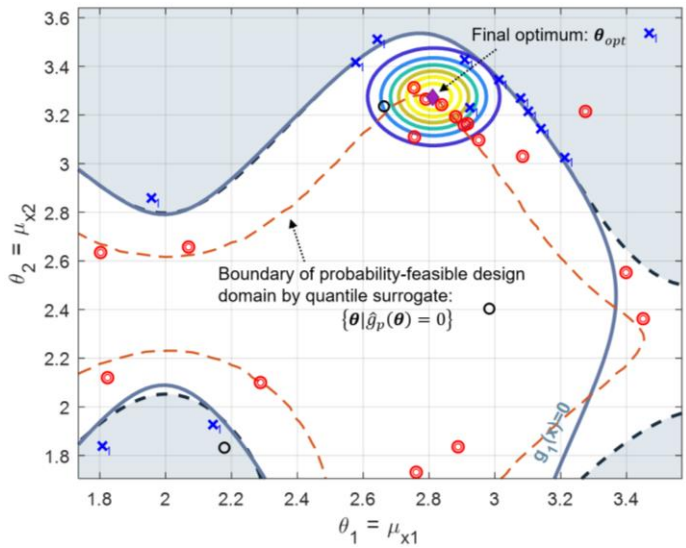

Figure 4.9 Close-ups of DoE around the final optimum along with boundaries of probability-feasible design domain

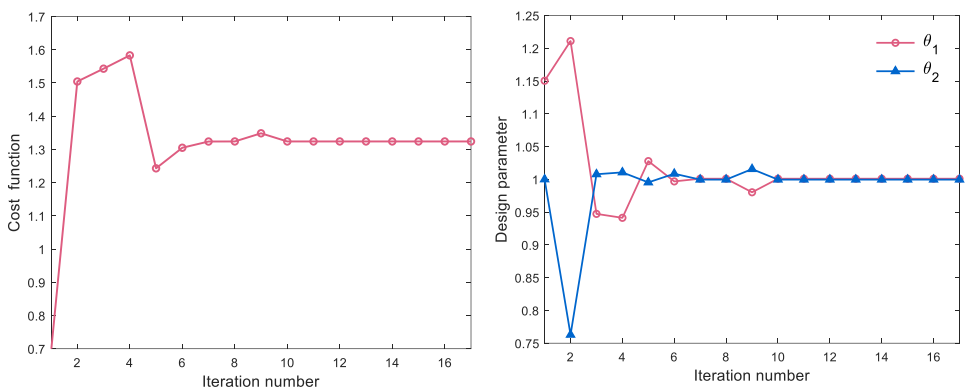

(a) (b)

Figure 4.10 Convergence histories of QS-AGP for example with highly nonlinear performance functions: (a) optimal cost, and (b) design parameters (normalizaed by $\boldsymbol{\theta}_{opt}$)

4.5.2 Passive vehicle suspension design

As an engineering application example, a design of passive vehicle suspension in Figure 4.11 is investigated (Chan *et al*. 2007). The objective of design is to minimize the mean square value of the vertical acceleration of the vehicle body while

satisfying the following four constraints: lower bound on the road-holding ability of the vehicle (g_1), upper bound on the rolling angle (g_2), lower bound on the suspension's dynamic displacement (g_3), and lower bound on tire stiffness (g_4). The means of three random parameters, i.e., the spring stiffness c (kg/cm), tire stiffness c_k (kg/cm), and shock absorber damping coefficient k $(kg/cm \cdot s)$ are considered as design variables, i.e., $\boldsymbol{\theta} = [\mu_c, \mu_{c_k}, \mu_k]$. The RBDO problem is formulated as:

$$
\begin{aligned}
&\min_{\boldsymbol{\theta}=\{\mu_c,\mu_{ck},\mu_k\}} \overline{\ddot{Z}^2} = (\pi AV/m^2)\left(\mu_{c_k}\mu_k + (M+m)\mu_c^2\mu_k^{-1}\right) \\
&s.t.\ P[g_i(\boldsymbol{X};\boldsymbol{\theta}) \le 0] \le P_{f_i}^t, \qquad i = 1, \dots, 4 \\
&\quad 350 \le \mu_c \le 450, 1400 \le \mu_{c_k} \le 1500, 0 \le \mu_k \le 50 \\
&\text{with } g_1(\boldsymbol{x}) = 1 - \left(\frac{\pi AVm}{b_0 g^2 k}\right)\left(\left(\frac{c_k}{M+m} - \frac{c}{M}\right)^2 + \frac{c^2}{Mm} + \frac{c_k k^2}{mM^2}\right) \\
&\quad g_2(\boldsymbol{x}) = 1 - 7.6394(4000(Mg)^{-1.5}C - 1)^{-1} \\
&\quad g_3(\boldsymbol{x}) = 1 - 0.5(Mg)^{0.5}(k^2 c_k c^{-1}(M+m)^{-1} + c)^{-0.5} \\
&\quad g_4(\boldsymbol{x}) = 1 - \left((M+m)g\right)^{0.877} c_k^{-1}
\end{aligned}
\tag{4.17}
$$

where $A = 1\ cm^2/cycle \cdot m$, $b_0 = 0.27$, $V = 10m/s$, $M = 3.2633kg \cdot s^2/cm$ and $m = 0.8158kg \cdot s^2/cm$ are the system parameters of the vehicle suspension. The deterministic optimum solution for the problem was reported as $[c^*, c_k^*, k^*]$= [391.21, 1442.6, 21.27]. Due to manufacturing variability, the stiffness and damping coefficient, i.e., c, c_k and k are considered to be Gaussian random variables with standard deviations $\sigma_{\boldsymbol{X}} = [7.5, 7.5, 5]$. The generalized target reliability index is set as $\beta_i^t = 2$ for all constraints.

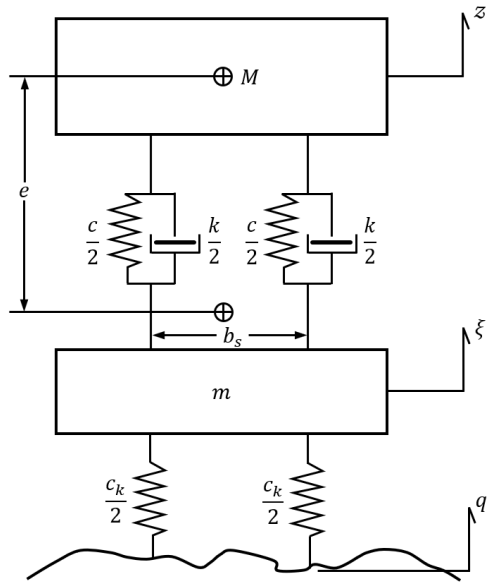

Figure 4.11 Passive vehicle suspension design (Chan *et al*. 2007)

As shown in Table 4.2, QS-AGP needs 9, 12, 16 and 13 evaluations of the four performance functions respectively to obtain a reliable optimal design. The convergence histories of QS-AGP are given in Figure 4.12. The convergence histories demonstrate quick identification of the regions of interest, which enables a rapid convergence to the reliable optimal design.

Table 4.2 Comparison between the results by the proposed QS-AGP method and other RBDO methods for passive vehicle suspension design

RBDO Method	$\boldsymbol{\theta_{opt}}(\times \mathbf{10^2})$	$f_{opt}(\times 10^6)$	$N_{g_1}/N_{g_2}/N_{g_3}/N_{g_4}$	N_f
PMA	[4.06, 14.6, 0.31]	3.16	115/124/112/112	32
RIA	[4.06, 14.6, 0.31]	3.16	104/94/94/92	31
SORA	[4.06, 14.6, 0.31]	3.16	104/114/114/114	101
SL-KKT	[4.06, 14.6, 0.31]	3.16	78/78/78/78	39
QS-AGP	**[4.06, 14.6, 0.31]**	**3.16**	**9/12/16/13**	**26**

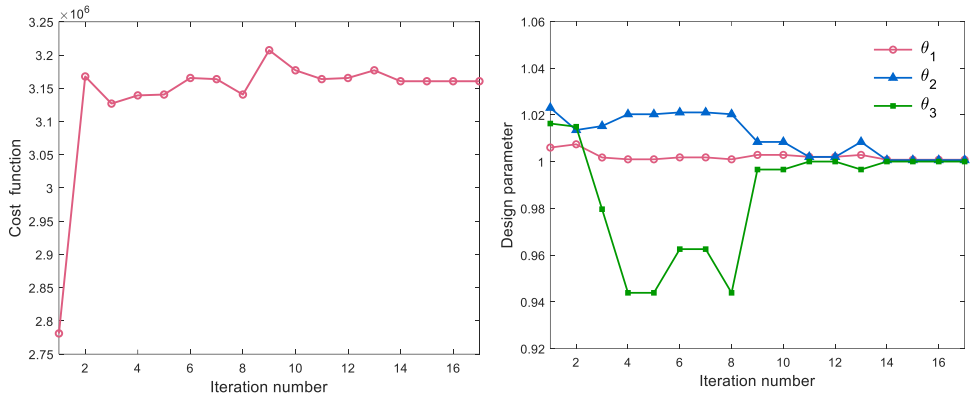

(a) (b)

Figure 4.12 Convergence histories of QS-AGP for passive vehicle suspension design: (a) optimal cost, and (b) design parameters (normalizaed by $\boldsymbol{\theta}_{opt}$)

4.5.3 A welded beam structure

In the next example, QS-AGP is applied to the design of welded beam structure shown in Figure 4.13 (Chen *et al*. 2013). The problem has four design parameters characterizing the depth and size of beam structures, and five probabilistic constraints related to the shear stress $\tau(\boldsymbol{x})$, bending stress $\sigma(\boldsymbol{x})$, buckling load $P_c(\boldsymbol{x})$ and end deflection $\delta(\boldsymbol{x})$. The cost function represents the cost of the design of welded beam. The RBDO formulation is given as

$$
\begin{aligned}
&\min_{\boldsymbol{\theta}} \; f(\boldsymbol{\theta}) = c_1\theta_1^2\theta_2 + c_2\theta_3\theta_4(z_2+\theta_2) \\
&s.t.\; P[g_i(\boldsymbol{X};\boldsymbol{\theta}) \le 0] \le P_{f_i}^t, \qquad i = 1,\dots,5 \\
&\quad 3.175 \le \theta_1 \le 10, 15 \le \theta_2 \le 254, 200 \le \theta_3 \le 220, 3.175 \le \theta_4 \le 10 \\
&\text{with } g_1(\boldsymbol{x}) = 1 - \tau(\boldsymbol{x})/z_6, \qquad g_2(\boldsymbol{x}) = 1 - \sigma(\boldsymbol{x})/z_7 \\
&\quad g_3(\boldsymbol{x}) = 1 - x_1/x_4, \qquad g_4(\boldsymbol{x}) = 1 - \delta(\boldsymbol{x})/z_5 \\
&\quad g_5(\boldsymbol{x}) = P_c(\boldsymbol{x})/z_1 - 1 \\
&\quad \tau(\boldsymbol{x}) = \left[t(\boldsymbol{x})^2 + \frac{2t(\boldsymbol{x})tt(\boldsymbol{x})x_2}{2R(\boldsymbol{x})} + tt(\boldsymbol{x})^2\right]^{0.5}
\end{aligned}
\tag{4.18}
$$

$$t(\boldsymbol{x}) = \frac{z_1}{\sqrt{2}x_1x_2}, \qquad tt(\boldsymbol{x}) = \frac{M(\boldsymbol{x})R(\boldsymbol{x})}{J(\boldsymbol{x})}$$

$$M(\boldsymbol{x}) = z_1(z_2 + 0.5x_2), \qquad R(\boldsymbol{x}) = \sqrt{[x_2^2 + (x_1 + x_3)^2]/4}$$

$$J(\boldsymbol{x}) = \sqrt{2}x_1x_2[x_2^2/12 + (x_1 + x_3)^2/4]$$

$$\sigma(\boldsymbol{x}) = \frac{6z_1z_2}{x_3^2x_4}, \qquad \delta(\boldsymbol{x}) = \frac{4z_1z_2^3}{z_3x_3^3x_4}$$

$$P_c(\boldsymbol{x}) = \frac{4.013x_3x_4^3\sqrt{z_3z_4}}{6z_2^2}\left(1 - \frac{x_3}{4z_2}\sqrt{\frac{z_3}{z_4}}\right)$$

where z and c are the fixed system parameters listed in Table 4.3. The random vector $\boldsymbol{X}$ consists of independent Gaussian random variables with the means $\boldsymbol{\theta}$ and standard deviations $\sigma_{\boldsymbol{X}} = [0.1693, 0.1693, 0.0107, 0.0107]$. The generalized target reliability index β_i^t is set to 3 for all constraints.

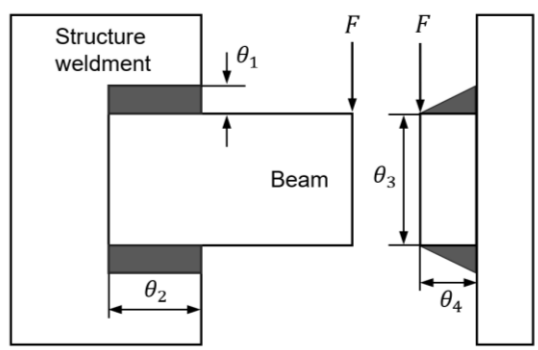

Figure 4.13 A welded beam structure (Chen *et al*. 2013)

Table 4.3 System parameters of the welded beam structure

Parameters	Value	Parameters	Value
z_1	$2.67 \times 10^4\ (N)$	z_5	$9.38 \times 10\ (MPa)$
z_2	$3.56 \times 10^2\ (mm)$	z_7	$2.07 \times 10^2\ (MPa)$
z_3	$2.07 \times 10^5\ (MPa)$	c_1	$6.74 \times 10^{-5}\ (\$/mm^3)$
z_4	$8.27 \times 10^4\ (MPa)$	c_2	$2.94 \times 10^{-6}\ (\$/mm^3)$
z_5	$6.35\ (mm)$		

Table 4.4 presents the estimated optimal design and optimal costs along with the number of function evaluations. The results show that QS-AGP method successfully deals with the dimension while producing accurate results with smaller number of function evaluations. Note that the RIA approach fails to converge because of the inactive probabilistic constraint (g_4), which may yield the reliability index for that constraint, β_4, into infinite value that prohibits the feasibility check of reliability requirement.

Table 4.4 Comparison between the results by the proposed QS-AGP method and other RBDO methods for passive vehicle suspension design

RBDO Method	$\boldsymbol{\theta_{opt}}$	f_{opt}	$N_{g_1}/\ldots/N_{g_4}$	N_f
PMA	$[5.73, 2.01 \times 10^2, 2.11 \times 10^2, 6.24]$	2.59	138/138/138/145/147	46
RIA	-	-	-	-
SORA	$[5.73, 2.01 \times 10^2, 2.11 \times 10^2, 6.24]$	2.59	99/99/110/101/119	96
SL-KKT	$[5.85, 1.95 \times 10^2, 2.11 \times 10^2, 6.24]$	2.57	92/92/92/92/92	46
QS-AGP	$\boldsymbol{[5.72, 2.00 \times 10^2, 2.11 \times 10^2, 6.25]}$	**2.59**	**26/13/20/12/13**	**35**

4.6 Summary

In this chapter, a new RBDO method using quantile surrogates enriched by adaptive Gaussian process (QS-AGP) was proposed. The QS-AGP aims at an adaptive selection of simulation points which would reduce computational costs for RBDO. The method utilized a quantile-based formulation to identify the probability-feasible design domain which satisfies the reliability requirements. The adaptive learning procedure was designed to further reduce the number of computational simulations

by utilizing the exploration-exploitation trade-off based on quantile surrogates. The proposed optimization scheme relies on design samples, and thus does not use an optimization algorithm or gradient information of cost and performance functions. Accuracy and efficiency of the proposed method were successfully tested through several RBDO problems featuring highly nonlinear performance functions, various distribution types and complexity. In each example, the proposed method needed fewer performance function evaluations in achieving convergence to accurate results. QS-AGP is expected to effectively deal with such challenging and time-consuming RBDO problems in engineering practice.

Chapter 5. Development of Active Learning Methods for High-Dimensional RBDO Applications

5.1 Introduction

To obtain the optimal structural design satisfying probabilistic requirements, RBDO has been widely studied and applied. However, its practical applications have been often hampered by huge computational costs. To address the challenge, an RBDO method termed quantile surrogates by adaptive Gaussian process (QS-AGP) in Chapter 4 are developed, which approximates the quantiles of the performance functions adaptively using Gaussian process models to check whether the pre-generated design samples satisfy the reliability requirements. It has been shown that QS-AGP requires much fewer evaluations of performance functions than existing RBDO methods. Although the efficiency of the QS-AGP method was shown superior to that of existing RBDO methods, its applications to high-dimensional systems is limited because the quantiles and objective function are evaluated at each of the pre-generated design samples. If an RBDO problem features many design parameters, the search space becomes high-dimensional, which requires an insurmountable memory to handle design samples generated to cover the space, and thus may degenerate the performance of the method. Moreover, QS-AGP generates Monte Carlo (MC) samples to estimate the quantiles using the mixture distribution (Kim and Song 2021a), which further decreases the computational efficiency.

To promote the application of the ideas in QS-AGP to high-dimensional engineering systems, this chapter proposes a new RBDO method termed, quantile

surrogates and sensitivity by adaptive Gaussian process (QS^2-AGP). The QS^2-AGP method utilizes the Gaussian process model to build quantile surrogates, identifying the admissible design domain concerning reliability requirement. Both inherent randomness of the input variables and epistemic uncertainty of surrogate model errors are incorporated to characterize the system performance, but without requiring any MC samples. The quantile surrogates are trained through adaptive selections of simulation points, and the design optimization is performed with the trained quantile surrogates. To speed up the RBDO iterations, QS^2-AGP uses a gradient-based optimizer based on the parameter sensitivity of the quantile surrogate with respect to design parameters, i.e., without requiring additional training data.

This chapter first provides a primary challenge in high-dimensional applications using QS-AGP method introduced in Chapter 4. Next, the following details of the proposed QS^2-AGP method will be introduced: (1) the proposed kernel-based quantile surrogate model, (2) corresponding adaptive training process, (3) design parameter sensitivity of quantile surrogates, and (4) overall algorithm of RBDO by QS^2-AGP. Through numerical examples of challenging RBDO problems, QS^2-AGP will be tested in terms of (1) accuracy for highly nonlinear performance functions, (2) applicability to high-dimensional problems, and (3) computational efficiency in terms of the number of performance function evaluations required for convergence. Lastly, a summary and concluding remarks are provided (Kim and Song 2021b).

5.2 Challenges in high-dimensional applications using QS-AGP

The method employs the *design samples* $\boldsymbol{\theta}_l, l = 1, \dots, n_l$, which are uniformly distributed in the design parameter space, as candidate points for statistical learning and optimal design solution. Thus, as the quantile surrogates $\hat{g}_p(\boldsymbol{\theta})$ are updated, QS-AGP checks the feasibility of each design sample with respect to the given probabilistic constraints by the signs of the corresponding quantile surrogate predictions $\hat{g}_p(\boldsymbol{\theta}_l), l = 1, \dots, n_l$. Then, among the feasible samples, the one with the minimal cost according to another GP-surrogate of the cost function, $\hat{f}(\boldsymbol{\theta})$ is approximately identified as an optimal solution. At each step of the optimization process, the quantile surrogates $\hat{g}_p(\boldsymbol{\theta})$ are estimated from the mixture distribution based on the GP model, fitted by the random MC samples $\boldsymbol{x}^m,\ m = 1, \dots, n_m$ generated from the input variable distribution $p(\boldsymbol{x}|\boldsymbol{\theta})$. To facilitate the RBDO process by quantile surrogates, the iterative active-learning process is conducted until the design solutions are converged. Thus, the adaptive refinement of quantile surrogates and design optimization are simultaneously performed based on the pre-generated design samples.

To facilitate the RBDO process assisted by quantile surrogates, QS-AGP, employs the pre-generated design samples that are uniformly distributed in the design space. In addition, QS-AGP generates MC samples to identify the distributions of quantile surrogates by the mixture distributions. Consequentially, when the mixture model is fitted by n_m MC samples at each of n_l pre-defined design samples, the total number of MC samples required at each RBDO iteration is $n_l \times n_m$. This approach may demand an insurmountable memory for larger systems

and thus degenerate the performance of the method. Moreover, the number of pre-generated design samples required for accurate estimation exponentially increases, which hampers applications to high-dimensional RBDO problems (Spence and Gioffrè 2012; Li *et al*. 2019; Jerez *et al*. 2022).

5.3 Proposed quantile surrogates and sensitivity by adaptive Gaussian process (QS^2-AGP)

In this chapter, an efficient quantile-surrogate-based RBDO framework named QS^2-AGP is proposed to facilitate applications to high-dimensional problems. In particular, the quantile surrogates that incorporate both the input uncertainties and error of surrogate models are now constructed without generating any MC samples. Moreover, a sensitivity formulation of the quantile surrogate is also introduced to facilitate the use of a gradient-based optimizer in RBDO, without requiring and handling pre-generated design samples.

5.3.1 Kernel-based derivation of quantile surrogates

In RBDO employing surrogate models, it is essential to properly quantify both epistemic uncertainty in the model error caused by the lack of simulations, represented by the prediction variance of GP in Eq. (2.8), and inherent randomness represented by the probabilistic distributions of the input $\boldsymbol{X}$. Therefore, it is an important task to consider both types of uncertainties in constructing the surrogates for probabilistic constraints, i.e., $P[g_i(\boldsymbol{X};\boldsymbol{\theta}) \leq 0]$, in RBDO (Der Kiureghian and Ditlevsen 2009; Li and Wang 2019; Kim and Song 2021a). To this end, a method that can incorporate both uncertainties into the GP surrogate modeling of the quantile

of performance functions g is introduced as follows. Suppose, after a proper transformation (Der Kiureghian 2022), the input distribution is described as Gaussian $\boldsymbol{X}\sim N(\boldsymbol{\theta},\boldsymbol{\Sigma_X})$ where $\boldsymbol{\theta}$ is the mean vector of $\boldsymbol{X}$, used as the design parameter of RBDO; and $\boldsymbol{\Sigma_X}$ is the covariance matrix. By the total probability theorem, the predictive distribution of the performance function is obtained as follows (Girard *et al*. 2003):

$$p(g|\boldsymbol{\theta},\boldsymbol{\mathcal{D}}) = \int p\left(g|\boldsymbol{x}_*,\boldsymbol{\mathcal{D}},\widehat{\boldsymbol{\theta}}\right)p(\boldsymbol{x}_*|\boldsymbol{\theta})\,d\boldsymbol{x}_* \tag{5.1}$$

in which $p(\boldsymbol{x}_*|\boldsymbol{\theta})$ is the probability density function (PDF) of the input random variables at $\boldsymbol{x}=\boldsymbol{x}_*$, affected by the design parameters $\boldsymbol{\theta}$; and $p\left(g|\boldsymbol{x}_*,\boldsymbol{\mathcal{D}},\widehat{\boldsymbol{\theta}}\right)$ is the PDF of the GP-based prediction of g at $\boldsymbol{x}_*$ from Eq. (2.6).

Since the calculation of the integral in Eq. (5.1) is generally intractable due to the complexity of $p\left(g|\boldsymbol{x}_*,\boldsymbol{\mathcal{D}},\widehat{\boldsymbol{\theta}}\right)$, a numerical approximation, e.g., Taylor expansion, MC approach, is often employed (Girard *et al*. 2003). By contrast, QS^2-AGP utilizes the following derivations of the "exact" predictive moments, i.e., mean $m_{\hat{g}}(\boldsymbol{\theta}) = \mathrm{E}_g[p(g|\boldsymbol{\theta},\boldsymbol{\mathcal{D}})]$ and variance $v_{\hat{g}}(\boldsymbol{\theta}) = \mathrm{Var}_g[p(g|\boldsymbol{\theta},\boldsymbol{\mathcal{D}})]$ (Mchutchon and Rasmussen 2011):

$$m_{\hat{g}}(\boldsymbol{\theta}) = \mathrm{E}_{\boldsymbol{x}_*}\left[\mu_{\hat{g}}(\boldsymbol{x}_*)\right] \tag{5.2}$$

$$v_{\hat{g}}(\boldsymbol{\theta}) = \mathrm{E}_{\boldsymbol{x}_*}\left[\sigma^2_{\hat{g}}(\boldsymbol{x}_*)\right] + \mathrm{Var}_{\boldsymbol{x}_*}\left[\mu_{\hat{g}}(\boldsymbol{x}_*)\right] \tag{5.3}$$

where $\mathrm{E}_{\boldsymbol{x}_*}[\cdot]$ and $\mathrm{Var}_{\boldsymbol{x}_*}[\cdot]$ respectively denote the mathematical expectation and variance under $p(\boldsymbol{x}_*|\boldsymbol{\theta})$; and $\mu_{\hat{g}}(\boldsymbol{x}_*)$ and $\sigma^2_{\hat{g}}(\boldsymbol{x}_*)$ are the posterior mean and variance of GP model in Eq. (2.7) and Eq. (2.8). This study adopts zero-mean function and automatic relevance determination (ARD) squared exponential (SE)

covariance function (Rasmussen and Nickisch 2015), expressed as:

$$k(\boldsymbol{x}, \boldsymbol{x}'; \boldsymbol{\Theta}) = \sigma_f^2 \exp\left(-\frac{1}{2}(\boldsymbol{x} - \boldsymbol{x}')^T \boldsymbol{\Lambda}^{-1}(\boldsymbol{x} - \boldsymbol{x}')\right) \tag{5.4}$$

where $\boldsymbol{\Lambda} = \text{diag}[\lambda_1^2, \dots, \lambda_D^2]$; and D is the dimension of input variable $\boldsymbol{x}$. σ_f^2 and $\lambda_i, i = 1, \dots, D$ are hyperparameters in $\boldsymbol{\Theta}$, which respectively denote the process variance and correlation length-scale. The ARD kernel is useful for handling problems composed of different dimensional inputs (Rasmussen and Nickisch 2015) since the kernel facilitates the use of different length-scales on input dimensions.

Then, the exact expressions of the predictive mean and variance can be derived in terms of SE kernel in Eq. (5.4) as follows (Deisenroth 2009):

$$m_{\hat{g}}(\boldsymbol{\theta}) = \boldsymbol{\Omega}^{\mathrm{T}} \boldsymbol{q} \tag{5.5}$$

$$v_{\hat{g}}(\boldsymbol{\theta}) = \sigma_f^2 - \text{tr}([\boldsymbol{K} + \sigma_n^2 \boldsymbol{I}]^{-1} \boldsymbol{Q}) + \boldsymbol{\Omega}^{\mathrm{T}} \boldsymbol{Q} \boldsymbol{\Omega} - m_{\hat{g}}(\boldsymbol{\theta})^2 \tag{5.6}$$

where $\boldsymbol{\Omega} \equiv (\mathbf{K} + \sigma_n^2 \mathbf{I})^{-1} \boldsymbol{g}_{\boldsymbol{\mathcal{D}}}$; $\boldsymbol{g}_{\boldsymbol{\mathcal{D}}}$ are the observations of the performance function; and $\text{tr}(\cdot)$ is the trace operator of the matrix. The terms $\boldsymbol{q}$ and $\boldsymbol{Q}$ are related to the moments of the kernel function, whose elements are determined as

$$q_i = \sigma_f^2 |\boldsymbol{\Sigma}_{\mathbf{x}} \boldsymbol{\Lambda}^{-1} + \boldsymbol{I}|^{-\frac{1}{2}} \exp\left(-\frac{1}{2}(\boldsymbol{x}_i - \boldsymbol{\theta})^{\mathrm{T}} (\boldsymbol{\Sigma}_{\mathbf{x}} + \boldsymbol{\Lambda})^{-1} (\boldsymbol{x}_i - \boldsymbol{\theta})\right) \tag{5.7}$$

$$Q_{ij} = \frac{k(\boldsymbol{x}_i, \boldsymbol{\theta}) k(\boldsymbol{x}_j, \boldsymbol{\theta})}{|2\boldsymbol{\Sigma}_{\mathbf{x}} \boldsymbol{\Lambda}^{-1} + \boldsymbol{I}|^{\frac{1}{2}}} \exp\left((\boldsymbol{z} - \boldsymbol{\theta})^{\mathrm{T}} \left(\boldsymbol{\Lambda} + \frac{1}{2}\boldsymbol{\Lambda}\boldsymbol{\Sigma}_{\mathbf{x}}^{-1}\boldsymbol{\Lambda}\right)^{-1} (\boldsymbol{z} - \boldsymbol{\theta})\right) \tag{5.8}$$

where $\boldsymbol{z} = (\boldsymbol{x}_i + \boldsymbol{x}_j)/2$. Thus, the predictive moments in Eq. (5.5) and Eq. (5.6) provide the surrogate modeling of the performance function for the given design parameter $\boldsymbol{\theta}$ under both aleatoric and epistemic uncertainties. The details of the derivations are provided in the literatures (Deisenroth 2009).

Then, approximating the predictive distribution in Eq. (5.1) as a Gaussian distribution, the quantile in Eq. (4.3) can be described in terms of the predictive moments as

$$\hat{g}_p(\boldsymbol{\theta}) = m_{\hat{g}}(\boldsymbol{\theta}) + \Phi^{-1}\left(P_f^t\right)\sqrt{v_{\hat{g}}(\boldsymbol{\theta})} \tag{5.9}$$

where $\Phi^{-1}(\cdot)$ denotes the inverse CDF of the standard Gaussian distribution. This quantile surrogate $\hat{g}_p(\boldsymbol{\theta})$ incorporates both input variation and surrogate model uncertainty. It is noted that the quantile surrogate in Eq. (5.9) can be computed efficiently using the function of kernel matrix directly, i.e., without generating MC samples as in QS-AGP (Kim and Song 2021a). The error that may occur from the Gaussian assumption of the predictive distribution decreases gradually as the surrogate models are refined. This is because the PDF $p\left(g|\boldsymbol{x}_*, \boldsymbol{\mathcal{D}}, \widehat{\boldsymbol{\theta}}\right)$ in Eq. (5.1) converges to a narrow distribution especially in the area of interests, i.e., the vicinity of the optimal solution. The concept of the proposed GP-based quantile surrogate estimation is illustrated in Figure 5.1.

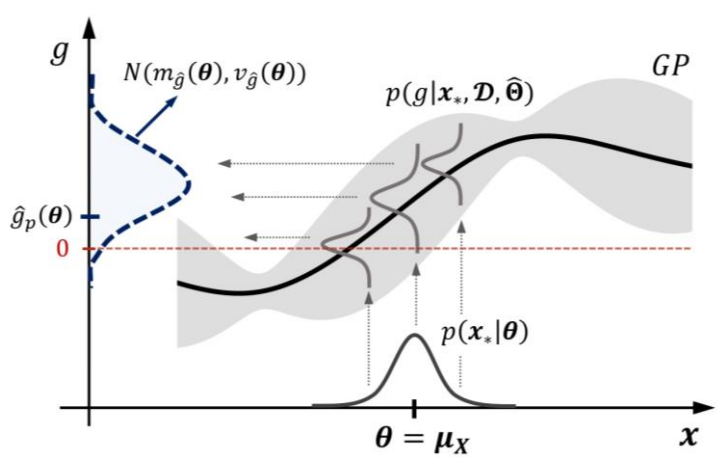

Figure 5.1 Illustration of GP-surrogate-based estimation of the quantile of the performance function by QS-AGP

5.3.2 Learning criteria for adaptive training

For efficiency, the proposed RBDO method employs an adaptive DoE scheme (Dubourg *et al*. 2011; Zhang *et al*. 2017) that refines the quantile surrogates by as few simulation points as possible. To determine the location of the next simulation of the performance function $g(\boldsymbol{X};\boldsymbol{\theta})$, the method uses the two-stage learning described below since RBDO usually incorporates the distribution parameters in the design parameters $\boldsymbol{\theta}$.

First, in the space of the design parameters $\boldsymbol{\theta}$, to focus the simulations around the boundary of the probability-feasible design domain, the best location is determined as

$$\boldsymbol{\theta}_{best} = \underset{\boldsymbol{\theta}}{argmin} \left| m_{\hat{g}_{ct}}(\boldsymbol{\theta}) + \Phi^{-1}\left(P_{f_{ct}}^{t}\right)\sqrt{v_{\hat{g}_{ct}}(\boldsymbol{\theta})} \right| \cdot \gamma_{\hat{f}(\boldsymbol{\theta})} \tag{5.10}$$

where $m_{\hat{g}_{ct}}(\boldsymbol{\theta})$ and $v_{\hat{g}_{ct}}(\boldsymbol{\theta})$ are respectively the predictive mean and variance of the performance function derived in Eq. (5.5) and Eq. (5.6); and ct is the index of the most critical performance function, i.e., the one with the minimum value of $|\mu_{\hat{g}_{p,i}}(\boldsymbol{\theta})/\sigma_{\hat{g}_{p,i}}(\boldsymbol{\theta})|$ for $i = 1, \dots, n_c$, as proposed by Fauriat *et al*. (2014). Using the composite index ct in Eq. (5.10) means that no simulations are performed for the performance functions that have little or no influence at the design iteration step. Namely, only one performance function is evaluated per each iteration. On the other hand, $\gamma_{\hat{f}(\boldsymbol{\theta})}$ in Eq. (5.10) is a penalty function introduced to give priorities to more desirable domains in $\boldsymbol{\theta}$ from the viewpoint of the design optimization, i.e., domains where the cost function is smaller. In detail, the penalty function is defined as

$$\gamma_{\hat{f}}(\boldsymbol{\theta}) = \begin{cases} \left| \dfrac{\hat{f}(\boldsymbol{\theta}) - \hat{f}_*}{\hat{f}_*} \right| & \text{if } \Delta_{o.p} \geq tol \\ 1 & \text{otherwise} \end{cases} \tag{5.11}$$

in which $\hat{f}(\boldsymbol{\theta})$ is the GP-surrogate-based estimate of the cost function at $\boldsymbol{\theta}$; $\hat{f}_* = \hat{f}(\boldsymbol{\theta}_*)$ is the current optimum at a given RBDO iteration; $\Delta_{o.p}$ is the distance between the optimal $\boldsymbol{\theta}$ at the current and previous learning-steps; and tol is the prescribed threshold. In summary, the learning function in Eq. (5.10) guides the search toward the vicinity of the critical boundary of the probability-feasible domain while giving a priority to the objective of the optimal design, instead of trying to improve the quantile surrogate regarding *all* boundaries.

Next, once the best location in the design parameter space, $\boldsymbol{\theta}_{best}$ is identified, the location of the performance function evaluation, $\boldsymbol{x}_{best}$ is determined as

$$\boldsymbol{x}_{best} = \underset{\boldsymbol{x}^m}{\operatorname{argmin}} \frac{\left|\mu_{\hat{g}_{ct}}(\boldsymbol{x}^m; \boldsymbol{\theta}_{best})\right|}{\sigma_{\hat{g}_{ct}}(\boldsymbol{x}^m; \boldsymbol{\theta}_{best})} \tag{5.12}$$

where $\mu_{\hat{g}_{ct}}(\boldsymbol{x}; \boldsymbol{\theta}_{best})$ and $\sigma_{\hat{g}_{ct}}(\boldsymbol{x}; \boldsymbol{\theta}_{best})$ respectively denote the mean and standard deviation of GP predictions for performance function at $\boldsymbol{x}$ given $\boldsymbol{\theta}_{best}$, which are computed by Eq. (2.7) and Eq. (2.8), respectively. Thus, Eq. (5.12) represents GP-based exploration-exploitation trade-off to choose the location of the performance function evaluation among the random samples $\boldsymbol{x}^m$, $m = 1, \dots, n_m$, generated from $p(\boldsymbol{x}|\boldsymbol{\theta}_{best})$, near the approximate limit-state surface, i.e., $\{\boldsymbol{x}|\hat{g}_{ct}(\boldsymbol{x}; \boldsymbol{\theta}_{best}) = 0\}$. Note that the random samples are utilized only one time per each iteration to identify the simulation location of the performance function. To this end, the location of the next performance function is determined as $\boldsymbol{x}_{best}$, and the performance function is enriched with the new simulation point $[\boldsymbol{x}_{best}, g_{ct}(\boldsymbol{x}_{best}; \boldsymbol{\theta}_{best})]^{\mathrm{T}}$ at each iteration.

5.3.3 Design parameter sensitivity

To use efficient gradient-based optimization algorithms for RBDO and facilitate the convergence, it is essential to accurately calculate the sensitivity of the estimated failure probability with respect to design parameters. Since the RBDO formulation involves both random variables and design parameters, the sensitivity analysis often requires the probabilistic transformation of random variables or simulation-based techniques (Youn and Choi 2003; Dubourg *et al*. 2011; Lee at al. 2011). Furthermore, if surrogate models are used in RBDO, it is essential to incorporate the surrogate model uncertainties into sensitivity analysis for successful performance of RBDO. It is noted that QS-AGP (Kim and Song 2021a) relies on pre-generated design samples, and thus does not use the parameter sensitivity of quantile surrogates.

By contrast, QS^2-AGP utilizes the sensitivity of quantile surrogates with respect to design parameters to improve the efficiency of the surrogate model-based RBDO process. The sensitivity of quantile surrogates for the ith performance function with respect to design parameters $\boldsymbol{\theta}$ can be analytically derived by taking the partial derivative of Eq. (5.9), i.e.,

$$\frac{\partial \hat{g}_{p_i}(\boldsymbol{\theta})}{\partial \boldsymbol{\theta}} = \frac{\partial m_{\hat{g}_i}(\boldsymbol{\theta})}{\partial \boldsymbol{\theta}} + \Phi^{-1}\left(P_{f_i}^t\right) \frac{1}{2\sqrt{v_{\hat{g}_i}(\boldsymbol{\theta})}} \frac{\partial v_{\hat{g}_i}(\boldsymbol{\theta})}{\partial \boldsymbol{\theta}} \tag{5.13}$$

which shows that the quantile sensitivity consists of the gradients of the mean $m_{\hat{g}_i}(\boldsymbol{\theta})$ and variance $v_{\hat{g}_i}(\boldsymbol{\theta})$ that are presented in Eq. (5.5) and Eq. (5.6), respectively. Since the predictive moments are defined as functions of the given DoE and GP model, the gradient terms in Eq. (5.13) can be obtained by taking the derivatives of the predictive mean and variance with respect to design parameters $\boldsymbol{\theta}$

as follows:

$$\frac{\partial m_{\hat{g}_i}(\boldsymbol{\theta})}{\partial \boldsymbol{\theta}} = \boldsymbol{\Omega}^{\mathrm{T}} \boldsymbol{q}_{\boldsymbol{\theta}} \tag{5.14}$$

$$\frac{\partial v_{\hat{g}_i}(\boldsymbol{\theta})}{\partial \boldsymbol{\theta}} = -\mathrm{tr}([\boldsymbol{K} + \sigma_n^2 \boldsymbol{I}]^{-1} \boldsymbol{Q}_{\boldsymbol{\theta}}) + \boldsymbol{\Omega}^{\mathrm{T}} \boldsymbol{Q}_{\boldsymbol{\theta}} \boldsymbol{\Omega} - 2 m_{\hat{g}_i}(\boldsymbol{\theta}) \frac{\partial m_{\hat{g}_i}(\boldsymbol{\theta})}{\partial \boldsymbol{\theta}} \tag{5.15}$$

where $\boldsymbol{q}_{\boldsymbol{\theta}}$ and $\boldsymbol{Q}_{\boldsymbol{\theta}}$ respectively denote the Jacobian matrices of $\boldsymbol{q}$ and $\boldsymbol{Q}$, given in Eq. (5.7) and Eq. (5.8). As a result, the derivatives of the predictive mean and variance can be easily obtained through the GP kernel function without additional simulation data. It is noted that the design parameter sensitivities of quantile surrogates do not require any mathematical model of structural response since it is obtained through the constructed surrogate surface. After calculating the predictive moments for the current design point, the required sensitivity of the predictive mean and variance can be obtained based on Eq. (5.14) and Eq. (5.15), and the sensitivity of quantile surrogates can be derived accordingly by Eq. (5.13).

5.3.4 Algorithm of QS²-AGP

The algorithm of the proposed QS²-AGP integrates the adaptive training process of quantile surrogates and gradient-based optimization employing parameter sensitivity of quantile surrogates. Each step of the proposed algorithm, illustrated by the flowchart in Figure 5.2, is summarized as follows:

1. *Construct the initial DoE*: Generate n_0 samples, $\boldsymbol{\theta}_{\boldsymbol{\mathcal{D}}} = \left[\boldsymbol{\theta}_1, \dots, \boldsymbol{\theta}_{n_0}\right]^{\mathrm{T}}$ by Latin Hypercube sampling (LHS) in the design parameter space. Then, the corresponding samples in the random variable space, $\boldsymbol{x}_{\boldsymbol{\mathcal{D}}} = \left[\boldsymbol{x}_1, \dots, \boldsymbol{x}_{n_0}\right]^{\mathrm{T}}$ are also generated as $\boldsymbol{x}_{\boldsymbol{\mathcal{D}}} = \boldsymbol{\theta}_{\boldsymbol{\mathcal{D}}} + \boldsymbol{\varepsilon}_{\mathrm{x}}$ where $\boldsymbol{\varepsilon}_{\mathrm{x}} \sim N(\boldsymbol{0}, \boldsymbol{\Sigma}_{\mathbf{x}})$. The cost

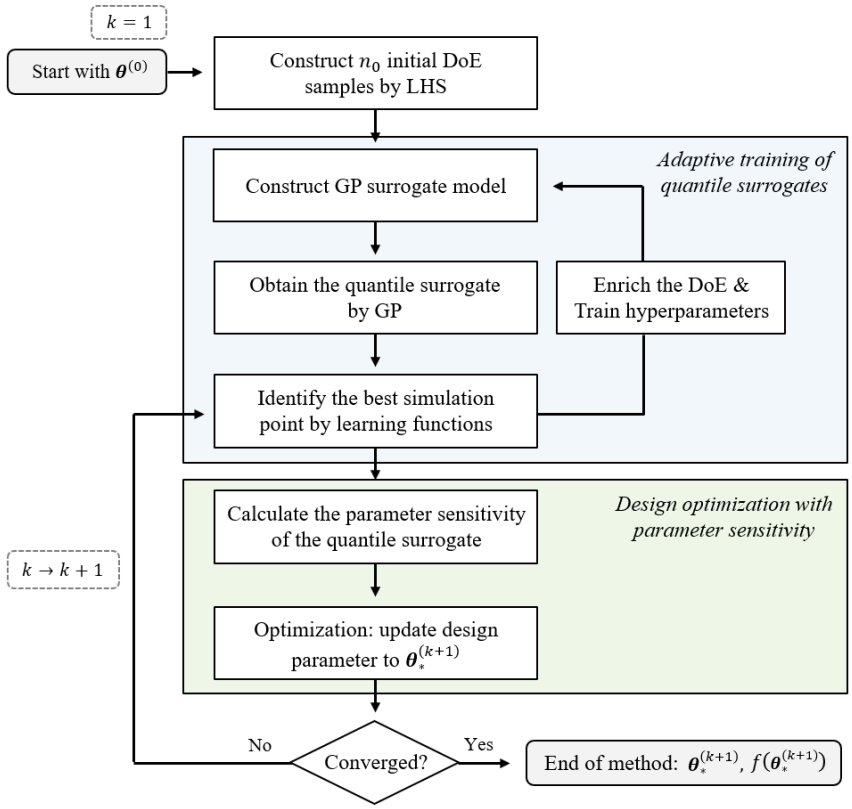

Figure 5.2 Flowchart of RBDO algorithm by QS^2-AGP

function $f(\boldsymbol{\theta})$ and performance functions $g_i(\boldsymbol{x}), i = 1, \dots, n_c$, are respectively evaluated on these points to construct the initial DoE of the surrogate models.

2. *Obtain the quantile surrogate model*: Obtain the estimates of the optimal GP hyperparameters, $\widehat{\boldsymbol{\Theta}}$ by MLE with the current DoE. Then, construct the GP-surrogate of the cost function $\hat{f}(\boldsymbol{\theta})$ and the quantile surrogates $\hat{g}_{p,i}(\boldsymbol{\theta}), i = 1, \dots, n_c$ as described in Eq. (5.9). The quantile surrogates are derived using the predictive moments of GP model in Eq. (5.5) and Eq. (5.6). The derived estimates of quantiles are utilized for both active-learning process and design optimization procedure.

3. *Train the model by active-learning process*: Identify the best design point $\boldsymbol{\theta}_{best}$ by minimizing the learning function in Eq. (5.10). To this end, a global optimization algorithm, e.g., genetic algorithm, particle swarm optimization, can be utilized. Then, the location of the next performance function evaluation, $\boldsymbol{x}_{best}$ is determined by Eq. (5.12). At this stage, the DoE is enriched by performance function evaluation at $\boldsymbol{x} = \boldsymbol{x}_{best}$, and this refinement process is repeated n_a times. From the experience, the recommended number of enrichment points is $n_a \in (2,7)$.
4. *Calculate the parameter sensitivity of surrogate*: Using the quantile surrogates identified from the previous steps, calculate the parameter sensitivity of the surrogate at the current point, as described in Eqs. (5.13)-(5.15). Note that the sensitivity of quantile surrogates can be obtained without additional training data.
5. *Update design parameters by optimization algorithm*: Based on the calculated parameter sensitivity, move on to the next step of design as $\boldsymbol{\theta}_*^{(k)} \rightarrow \boldsymbol{\theta}_*^{(k+1)}$ using a gradient-based optimizer, e.g., interior-point algorithm, sequential quadratic programming. Note that the updated design $\boldsymbol{\theta}_*^{(k+1)}$ is utilized for the penalty function in Eq. (5.11) and enrichment of DoE for cost function surrogate $\hat{f}(\boldsymbol{\theta})$. Steps 2-5 are repeated until the convergence is achieved.
6. *End of Algorithm*: Once the optimization algorithm achieves convergence, the current design $\boldsymbol{\theta}_*^{(k+1)}$ and cost $f\left(\boldsymbol{\theta}_*^{(k+1)}\right)$ are obtained as the optimal design and cost, respectively.

5.4 Numerical examples

5.4.1 Benchmark RBDO problem

First, let us consider a two-dimensional benchmark RBDO example involving three performance functions, which is formulated as (Youn and Choi 2003; Moustapha 2016)

$$\begin{aligned}
&\min_{\boldsymbol{\theta}} \ f(\boldsymbol{\theta}) = \theta_1 + \theta_2 \\
&s.t. \ P[g_i(\boldsymbol{X};\boldsymbol{\theta}) \le 0] \le P_{f_i}^t, \qquad i = 1,\dots,3 \\
&\qquad 0 \le \theta_1 \le 10, 0 \le \theta_2 \le 10 \\
&\text{with } g_1(\boldsymbol{x}) = \frac{x_1^2 x_2}{20} - 1 \\
&\qquad g_2(\boldsymbol{x}) = \frac{(x_1 + x_2 - 5)^2}{30} + \frac{(x_1 - x_2 - 12)^2}{120} - 1 \\
&\qquad g_3(\boldsymbol{x}) = \frac{80}{x_1^2 + 8x_2 + 5} - 1
\end{aligned} \tag{5.16}$$

where $\boldsymbol{x}$ denotes a realization of the random vector $\boldsymbol{X}$ consisting of two independent Gaussian random variables X_1 and X_2; the means of $\boldsymbol{X}$ are design parameters, i.e., $\boldsymbol{\theta} = \boldsymbol{\mu}_{\mathbf{X}}$ while the common standard deviation is given as $\sigma = 0.2$, i.e., $X_j \sim N(\theta_j, 0.2^2), j = 1,2$. The generalized target reliability index β_i^t is set to 3 for both constraints. The solid curves in Figure 5.3 and Figure 5.4 show the exact limit-state surface by the performance functions.

Following the procedure described in Section 5.3, the QS^2-AGP method is applied with an initial design point $\boldsymbol{\theta}^{(0)} = [5,5]^{\mathrm{T}}$ and 10 initial DoEs. Two points are added at each design iteration for surrogate refinement. Figure 5.3 illustrates the adaptive search process of the proposed method. Figure 5.3(a) presents the initial stages of adaptive learning with the initial set of DoE $\boldsymbol{x}_{\boldsymbol{D}}$, which is denoted by the

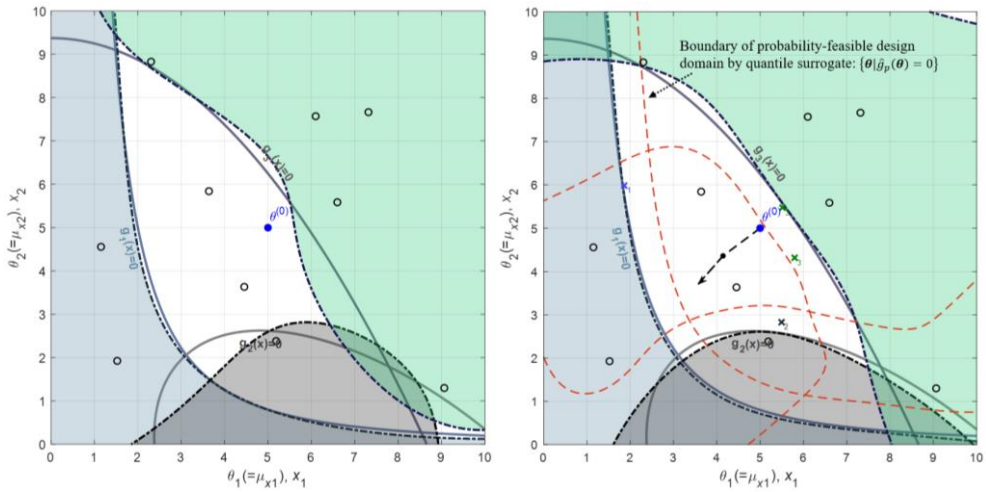

(a) (b)

Figure 5.3 Progresses of RBDO by QS^2-AGP method for benchmark RBDO example: (a) $k = 0$ (initial stage); and (b) $k = 2$.

circular markers. The estimated limit state surfaces are represented by the dash-dotted lines for the three performance functions respectively. Figure 5.3(b) shows the progress after 2 iterations along with the three boundaries of probability-feasible design domain represented by the quantile surrogates, i.e., $\{\boldsymbol{\theta}|\hat{g}_{p,i}(\boldsymbol{\theta}) = 0\}, i = 1, \dots, 3$. Here, the cross-markers "x" indicate the locations of performance function evaluations selected by the adaptive procedure in Eq. (5.12), i.e., $\boldsymbol{x}_{best}$, and a subscript of the marker denotes the index of the evaluated performance function, i.e., *ct* in Eqs. (5.10) and (5.12). For instance, at the location denoted by the marker "x_1," QS^2-AGP evaluates performance function $g_1(\boldsymbol{x})$ only. The black-arrow with dashed lines shows the trajectory of the design parameter starting from the initial design $\boldsymbol{\theta}^{(0)}$ guided by the parameter sensitivity.

Figure 5.4 shows the approximate limit-state surface along with all DoE points explored up to the final step. The purple diamond marker represents the final reliable

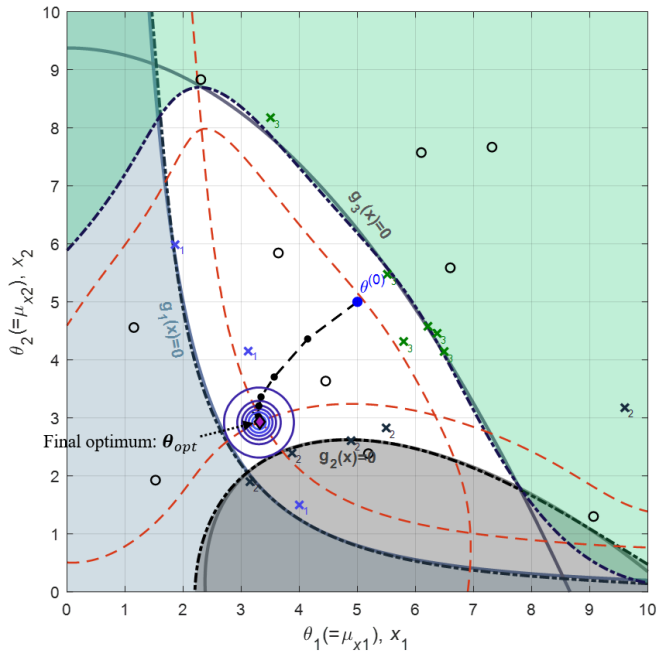

Figure 5.4 Final experimental designs for benchmark RBDO example

optimum $\boldsymbol{\theta}_{opt}$. The results demonstrate that the proposed method guides the search such that more simulations are performed in the near-optimal regions from the RBDO viewpoint. It is also confirmed that most of the training points selected by QS^2-AGP are located around the true limit-state surface, especially in the cost-effective regions, which facilitates construction of effective surrogate models for the purpose of RBDO. It is observed that the final reliable optimum, active on the first and second performance function constraints, is successfully obtained by the proposed method.

Table 5.1 presents the convergence history of design parameters, cost function values and the estimated values of quantiles for the three constraints, i.e., $\hat{g}_{p,i}(\boldsymbol{\theta})$, $i = 1, \dots, 3$, respectively. The positive signs of the quantiles indicate that the corresponding probabilistic constraints are satisfied. An optimal design $\boldsymbol{\theta}_{opt} =$

$[3.31, 2.91]$ is achieved after 10 iterations by QS^2-AGP method. Table 5.2 shows typical results (among more than 20 independent runs) by the proposed QS^2-AGP, compared to those by several RBDO methods reported in Enevoldsen and Sorensen (1994), Youn and Choi (2003), Du and Chen (2004) and Liang *et al*. (2007). The accuracy and efficiency of the different methods are compared in terms of the values of the final optimal design parameters ($\boldsymbol{\theta}_{opt}$), the optimal cost ($f_{opt}$), and the total numbers of performance function evaluations (n_g). The numbers in the parenthesis denotes the those of function evaluations needed for each performance function. Each of the selected methods provides a solution with a good accuracy for the two-dimensional example. It is observed that both surrogate-based RBDO methods, QS-AGP and QS^2-AGP, obtain an optimal design using significantly fewer function evaluations than the other RBDO methods.

Table 5.1 Design convergence history by QS^2-AGP method for benchmark RBDO example

Iteration	Design point	Quantile surrogates for each constraint, $\hat{g}_{p,i}(\boldsymbol{\theta})$			Cost
		$i = 1$	$i = 2$	$i = 3$	
1	[5.00, 5.00]	3.51	0.555	-0.002	10.0
2	[4.14, 4.36]	1.63	0.404	0.200	8.50
3	[3.57, 3.70]	0.53	0.291	0.439	7.27
4	[3.34, 3.36]	0.17	0.141	0.584	6.70
5	[3.30, 3.21]	0.083	0.092	0.645	6.51
6	[3.30, 3.02]	0.009	0.036	0.702	6.32
7	[3.31, 2.96]	0.003	0.014	0.740	6.28
8	[3.31, 2.93]	0.002	0.006	0.727	6.23
9	[3.31, 2.91]	0.002	0.001	0.728	6.21
10	[3.31, 2.91]	0.002	0.001	0.710	6.21

Table 5.2 Comparison between the results by the proposed method (QS^2-AGP) and other RBDO method for benchmark RBDO example

RBDO Method	$\boldsymbol{\theta_{opt}}$	f_{opt}	n_g
PMA	[3.30, 2.90]	6.19	234 (76/78/80)
RIA	[3.30, 2.90]	6.19	175 (63/56/56)
SORA	[3.30, 2.90]	6.19	170 (46/56/68)
SL-KKT	[3.31, 2.90]	6.21	96 (32/32/32)
QS-AGP	[3.30, 2.92]	6.22	42 (16/12/14)
QS^2-AGP	**[3.31, 2.91]**	**6.21**	**46 (11/15/20)**

5.4.2 High-dimensional RBDO problem

The second example deals with a high-dimensional RBDO example, involving 15 design parameters with nonlinear performance functions. The problems are formulated as (Li *et al*. 2019)

$$\begin{aligned}
&\min_{\boldsymbol{\theta}} \ f(\boldsymbol{\theta}) = \theta_{14} + \theta_{15} - \sum_{i=1}^{13} \theta_i \\
&s.t. \ P[g_i(\boldsymbol{X};\boldsymbol{\theta}) \le 0] \le P_{f_i}^t, \qquad i = 1,\dots,12 \\
&\quad 2 \le \theta_j \le 4, \qquad j = 1,\dots,15 \\
&\text{with } g_1(\boldsymbol{x}) = 3x_5^2 + x_7^2 + 2x_{13}^2 + x_1x_{10} + 2x_4x_6 + 3x_2x_9 + 4x_3x_8 \\
&\qquad\qquad + 5x_{11}x_{12} + 0.001(x_{14} + x_{15}) - 200 \\
&\quad g_2(\boldsymbol{x}) = 2x_2^2 + 4x_3^2 + 5x_1x_{10} + 4x_4x_5 + 3x_6x_7 + 2x_9x_8 + x_{11}x_{12} \\
&\qquad\qquad + x_{13}x_{12} + 0.001(x_{14} + x_{15}) - 200 \\
&\quad g_3(\boldsymbol{x}) = 4x_1^2 + x_5^2 + 2x_{10}^2 + 2x_{13}^2 + x_2x_8 + 3x_4x_6 + 2x_3x_7 + 2x_9x_{13} \\
&\qquad\qquad + 3x_{11}x_{12} + 0.001(x_{14} + x_{15}) - 180 \\
&\quad g_4(\boldsymbol{x}) = 2x_2^2 + 1.5x_3^2 + 2x_4^2 + x_7^2 + x_1x_{13} + 2x_8x_{12} + 3x_6x_{11} \\
&\qquad\qquad + 2x_4x_5 + 3x_{10}x_3 + 3x_1x_9 + 0.001(x_{14} + x_{15}) - 180 \\
&\quad g_5(\boldsymbol{x}) = 2x_2^2 + 2x_6^2 + 3x_7^2 + x_{11}^2 + x_{12}x_{13} + 2x_8x_{10} + 3x_3x_9 \\
&\qquad\qquad + 2x_4x_5 + x_1x_3 + 0.001(x_{14} + x_{15}) - 180 \\
&\quad g_6(\boldsymbol{x}) = 10x_1 + 9x_2 + 8x_3 + 7x_4 + 6x_5 + 5x_6 + 4x_7 + 3x_8 + 2x_9 \\
&\qquad\qquad + x_{10} + 6x_{11} + 4x_{12} + 2x_{13} + 0.001(x_{14} + x_{15}) - 200
\end{aligned} \tag{5.17}$$

$$g_7(\boldsymbol{x}) = 10x_1 + 8x_2 + 6x_3 + 4x_4 + 2x_5 + 5x_6 + 4x_7 + 3x_8 + 2x_9 + x_{10} + x_{11} + 3x_{12} + 5x_{13} + 0.001(x_{14} + x_{15}) - 170$$

$$g_8(\boldsymbol{x}) = 4x_1 + 3x_2 + 2x_3 + x_4 + 10x_5 + 9x_6 + 8x_7 + 7x_8 + 6x_9 + 5x_{10} + 4x_{11} + 3x_{12} + 2x_{13} + 0.001(x_{14} + x_{15}) - 200$$

$$g_9(\boldsymbol{x}) = \sum_{i=1}^{13} x_i + 0.001(x_{14} + x_{15}) - 300,$$

$$g_{10}(\boldsymbol{x}) = \sum_{i=1}^{13} x_i + 0.001(x_{14} + x_{15}) - 280$$

$$g_{11}(\boldsymbol{x}) = 0.001\sum_{i=1}^{13} x_i - 10x_{14}^2 x_{15} + 200$$

$$g_{12}(\boldsymbol{x}) = 0.001\sum_{i=1}^{13} x_i - 4(x_{14} + x_{15} - 5)^2 - (x_{14} - x_{15} - 12)^2 + 120$$

where $\boldsymbol{x}$ is a realization of the random vector $\boldsymbol{X}$ composed with 15 independent Gaussian random variables; the means of $\boldsymbol{X}$ are design parameters $\boldsymbol{\theta}$; and the random variables have the common standard deviation $\sigma = 0.3$, i.e., $X_j \sim N(\theta_j, 0.3^2), j = 1, \ldots, 15$. The generalized target reliability index is set as $\beta_i^t = 3.0115$ for all constraints. The performance of the proposed method is demonstrated with the initial design $\boldsymbol{\theta}^{(0)} = [3,3,3,3,3,3,3,3,3,3,3,3,3,3,3]^{\mathrm{T}}$. After building the initial surrogates with 20 DoEs, 5 samples are added at each iteration.

The performance of QS^2-AGP method on the high-dimensional RBDO problem is compared with those by PMA, RIA, SORA and SL-KKT. The results by QS-AGP are not reported because, to fill in the large dimension of the design parameter space, the QS-AGP method required an insurmountable number of design samples, more than 10^9, which resulted in memory problems and inaccurate estimations. Table 5.3 shows the estimated optimal designs obtained by the proposed method and the other RBDO methods. In the table, the results by RIA are not shown because it failed to converge because of the inactive probabilistic constraints (g_7, g_9, g_{10}), which made

the corresponding reliability indices infinity, which prohibits the feasibility check of the reliability requirements. Table 5.4 summarizes the performance regarding the probabilistic constraints, represented by the reliability index computed at the optimal designs along with the objective function values, and total numbers of performance function evaluations. Here, the reliability indices at the optimums are evaluated by using the brute force MCS with 10^6 samples. It is noted that QS^2-AGP properly treats all performance of probabilistic constraints by the quantile surrogates and provides reliable optimal solutions with a significantly reduced number of function evaluations even if the dimension of variables is high. It is confirmed that the performance of QS^2-AGP is not hampered by high-dimensionality, unlike QS-AGP and superior to the other RBDO methods.

Table 5.3 Comparison of optimal designs obtained by the proposed method (QS^2-AGP) and other RBDO methods for high-dimensional RBDO example

RBDO Method	Design parameters														
	θ_1	θ_2	θ_3	θ_4	θ_5	θ_6	θ_7	θ_8	θ_9	θ_{10}	θ_{11}	θ_{12}	θ_{13}	θ_{14}	θ_{15}
PMA	2.00	2.77	2.00	2.51	2.00	2.00	3.42	4.00	4.00	3.05	2.00	4.00	3.09	3.44	3.29
SORA	2.00	2.78	2.00	2.51	2.00	2.00	3.42	3.99	3.99	3.05	2.00	3.99	3.11	3.45	3.29
SL-KKT	2.00	2.78	2.00	2.53	2.01	2.00	3.40	3.99	4.00	3.08	2.02	4.00	3.09	3.43	3.29
QS^2-AGP	**2.00**	**2.78**	**2.00**	**2.50**	**2.00**	**2.00**	**3.40**	**4.00**	**4.00**	**3.05**	**2.00**	**4.00**	**3.06**	**3.47**	3.29

Table 5.4 Reliability index at the optimums and the number of function evaluations for high-dimensional RBDO example

RBDO Method	Reliability index at optimal designs $\boldsymbol{\theta_{opt}}$												f_{opt}	n_g
	g_1	g_2	g_3	g_4	g_5	g_6	g_7	g_8	g_9	g_{10}	g_{11}	g_{12}		
PMA	2.99	4.07	2.95	2.97	4.01	4.50	∞	2.99	∞	∞	3.01	3.04	-30.11	2462
SORA	2.97	3.99	2.93	2.96	4.20	4.35	∞	3.03	∞	∞	2.97	3.07	-30.14	2376
SL-KKT	2.93	4.01	2.94	2.92	4.01	∞	∞	2.99	∞	∞	2.93	3.04	-30.18	2178
QS²-AGP	**3.01**	**4.04**	**3.04**	**3.00**	**4.20**	**4.31**	∞	**3.03**	∞	∞	**3.07**	**3.04**	**-30.03**	**369**

5.4.3 Crashworthiness of vehicle side impact

As an engineering application, crashworthiness model of a vehicle side impact is often used to enhance the side impact crash performance of the vehicle (Youn and Choi 2004; Chakri *et al*. 2018). The system model represents the side impact event of vehicle when it is hit in the side by another vehicle at 49.89 km/h (31 mph). To formulate the RBDO problem, finite element (FE) structure models in Figure 5.5, including side impact dummy model and deformable barrier model, were constructed to simulate the side impact. Then, stepwise response surfaces model was explicitly constructed to approximate the objective function and constraints based on a few selected FE simulation results. The objective is to minimize the weight of vehicle while satisfying the 10 constraints on vehicle safety standard including deflections, velocities at different vehicle and dummy locations. The means of 9 random variables, i.e., the thickness $(\theta_1, \dots, \theta_7)$ and material property (θ_8, θ_9) of the critical part, are considered as design parameters. The RBDO problem of the vehicle side impact is formulated as:

$$
\begin{aligned}
&\min_{\boldsymbol{\theta}} \ \text{Weight}(\boldsymbol{\theta}) \\
&s.t. \quad P[F_{Abdom} \geq 1.0\ kN] \leq P_f^t \\
&\qquad P\left[Def_{rib_j} \geq 32\ mm\right] \leq P_f^t, \qquad j = 1, \dots, 3 \\
&\qquad P\left[VC_{upper_m} \geq 0.32\ m/s\right] \leq P_f^t, \qquad m = 1, \dots, 3 \\
&\qquad P\left[Force_{public} \geq 4.0\ kN\right] \leq P_f^t \\
&\qquad P\left[Vel_{B-pillar} \geq 9.9\ mm/ms\right] \leq P_f^t \\
&\qquad P[Vel_{door} \geq 15.7\ mm/ms] \leq P_f^t \\
&\qquad \boldsymbol{\theta}_L \leq \boldsymbol{\theta} \leq \boldsymbol{\theta}_U
\end{aligned}
\tag{5.18}
$$

The detailed mathematical expressions of the objective function and constraints are

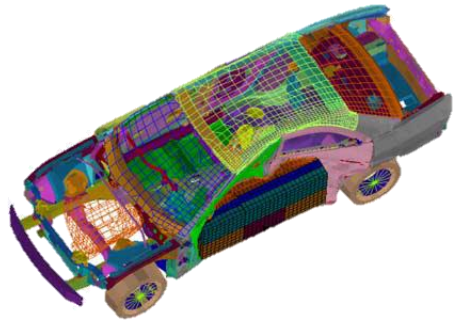

Figure 5.5 Finite element structural models for vehicle side impact (Youn and Choi 2004)

presented in the references (Youn and Choi 2004; Chakri *et al*. 2018). Due to manufacturing variability, the thicknesses and material properties of the critical parts are considered to be Gaussian random variables with standard deviations $\sigma_{\boldsymbol{X}}$. The details of these parameters are listed in Table 5.5. The generalized target reliability index is set as $\beta^t = 3.0$ for all constraints. The performance of QS^2-AGP is demonstrated with the initial design $\boldsymbol{\theta}^{(0)} = [1.0,1.0,1.0,1.0,1.0,1.0,1.0,0.3,0.3]^{\mathrm{T}}$.

Table 5.5 Design parameters for crashworthiness of vehicle side impact

Design parameters	$\boldsymbol{\theta}$	$\boldsymbol{\theta_L}$	$\boldsymbol{\theta_L}$	Standard deviation
Thickness of B-Pillar inner (*mm*)	θ_1	0.5	1.5	0.03
Thickness of B-Pillar reinforcement (*mm*)	θ_2	0.45	1.35	0.03
Thickness of floor side inner (*mm*)	θ_3	0.5	1.5	0.03
Thickness of cross member #1 and #2 (*mm*)	θ_4	0.5	1.5	0.03
Thickness of door beam (*mm*)	θ_5	0.875	2.625	0.05
Thickness of door belt line reinforcement (*mm*)	θ_6	0.4	1.2	0.03
Thickness of roof rail (*mm*)	θ_7	0.4	1.2	0.03
Material property of B-Pillar inner (*mm*)	θ_8	0.333	0.357	0.006
Material property of floor side inner (*mm*)	θ_9	0.180	0.204	0.006

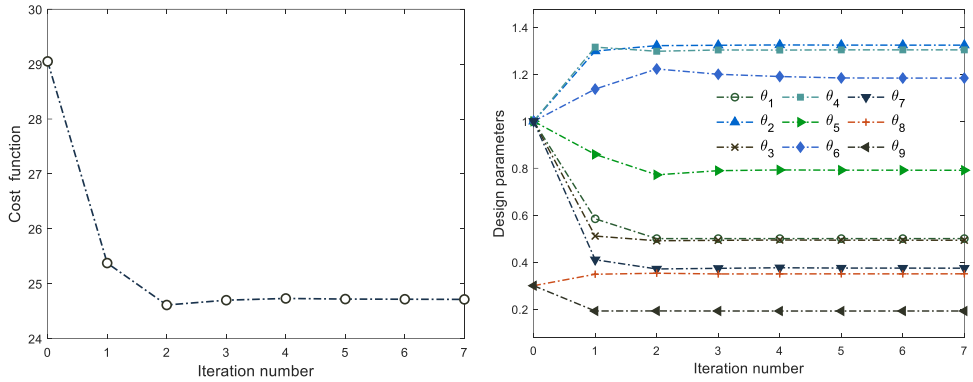

(a) (b)

Figure 5.6 Convergence histories of QS^2-AGP for crashworthiness of vehicle side impact example: (a) cost function; and (b) design parameters

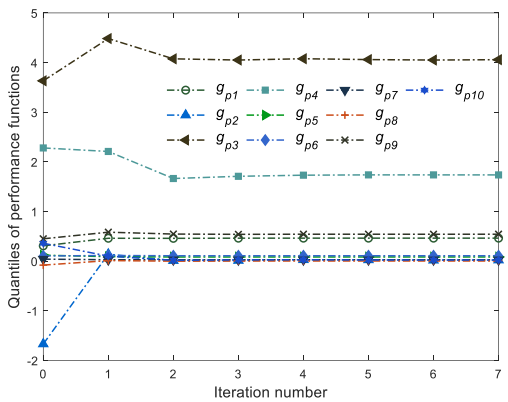

Figure 5.7 Hitories of quantile surrogate estimation by QS^2-AGP for crashworthiness of vehicle side impact example

After QS^2-AGP method is initiated with 15 DoE points, three points are added in surrogate refinement at each iteration. Figure 5.6 presents the convergence histories of cost function and design parameters. Figure 5.7 shows the convergence histories of the quantiles estimated by the surrogate models. The convergence histories of QS^2-AGP analysis confirm that the cost and design parameters are converged to the final values by a small number of iterations. Table 5.6 shows that

QS^2-AGP needs fewer function evaluations than other RBDO methods while producing accurate results.

Table 5.6 Comparison between the results by the proposed method (QS^2-AGP) and other RBDO method for crashworthiness of vehicle side impact example

RBDO Method	PMA	SORA	SL-KKT	QS^2-AGP
θ_1	0.50	0.50	0.50	**0.50**
θ_2	1.32	1.32	1.31	**1.32**
θ_3	0.50	0.50	0.50	**0.51**
θ_4	1.29	1.29	1.30	**1.30**
θ_5	0.87	0.87	0.87	**0.87**
θ_6	1.15	1.14	1.14	**1.13**
θ_7	0.40	0.40	0.40	**0.41**
θ_8	0.36	0.36	0.36	**0.35**
θ_9	0.19	0.19	0.19	**0.19**
Weight($\boldsymbol{\theta}$)	24.5	24.6	24.5	**24.7**
n_g	1064	593	480	**171**

5.5 Comparison of computational time of QS-AGP and QS^2-AGP

The computational costs of the two quantile-surrogates-based RBDO methods, QS-AGP and QS^2-AGP, are compared in Figure 5.8 through the RBDO examples investigated in this chapter and the previous research in Chapter 4 (Kim and Song 2021a). The computational costs are normalized by that of the QS^2-AGP method for the 2-dimensional problem in this chapter. Note that the computational times in Figure 5.8 only incorporate the CPU times for design iterations except those for the performance function evaluations. The results confirm that the proposed QS^2-AGP requires dramatically less computational time than QS-AGP, and effectively deals with high-dimensional RBDO problem while QS-AGP fails to find the optimal designs when the dimension of the design parameter space exceeds 7.

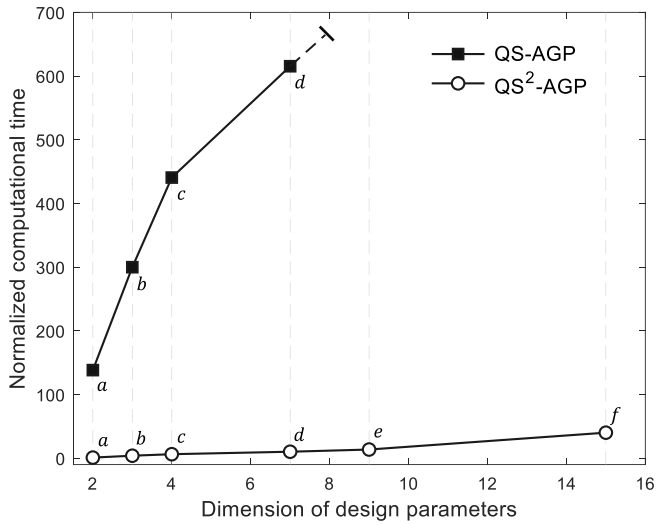

Figure 5.8 Comutational time comparison for RBDO by QS-AGP and QS^2-AGP (*a* = benchmark RBDO problem, *b* = passive vehicle suspension design, *c* = welded beam design, *d* = speed reducer design (Chen *et al*. 2013), *e* = crashworthiness of vehicle side impact, *f* = high-dimensional RBDO problem). Times are normalized with respect to the 2-dimensional problem computation by QS^2-AGP (42 seconds in this case)

5.6 Summary

The new RBDO method proposed in this chapter, termed quantile surrogates and sensitivity by adaptive Gaussian process (QS^2-AGP), aims to find the reliable optimal solution accurately and efficiently by combining the adaptive training process of the quantile surrogates with the design optimization procedure guided by the parameter sensitivity of quantile surrogates. By avoiding the use of pre-generated design samples and the MC-sample based procedure to fit the quantile surrogate in the previous quantile-surrogate-based RBDO method termed QS-AGP, QS^2-AGP achieved a superior level of efficiency especially for RBDO problems with a larger number of design parameters. The formulations of the parameter sensitivity of the

quantile surrogate also helped further reduce the computational costs.

The performance and merits of the proposed method were successfully demonstrated through several numerical examples including high-dimensional RBDO problem up to 15 design parameters and engineering applications. In each example, the proposed method required fewer performance function evaluations in achieving convergence to accurate results than other RBDO methods. QS^2-AGP is expected to effectively deal with a variety of challenging and time-consuming RBDO problems in engineering practice.

Chapter 6. Conclusions

6.1 Summary and contributions of this dissertation

This dissertation focuses on developing active learning methods and applications to reliability assessment and design optimization for challenging and complex engineering systems. The four research objectives proposed in Chapter 1 were fulfilled: (1) PAK-B^n method was developed to assess the reliability of complex structural systems using active learning-based Kriging model; (2) The proposed AL-HGP efficiently estimated first-passage probability under stochastic wind excitations, the high-dimensional reliability problem; (3) QS-AGP method was proposed to identify the reliable optimal design of complex structures by constructing quantile surrogates and training the model; and (4) The further developed method, QS^2-AGP treated high-dimensional RBDO problems using kernel-based quantile surrogates and sensitivity. The major developments and findings of this study are summarized as follows:

- *PAK-B^n* method was developed for structural reliability analyses. The main objective of PAK-B^n was to carry out an active learning process, i.e., adaptive selection of simulation points, with low computational costs from a reliability analysis standpoint. The method utilized a new learning criterion designed to identify important points that are located in the vicinity of the limit-state surface and, at the same time, contribute most to the failure probability. The uniformly

distributed samples in *n*-ball domain could further reduce the number of computational simulations and achieved efficient convergence.

- Several benchmark reliability problems, e.g., a system problem with high non-linearity, small failure probability, and multiple design points, and general engineering problems with moderate dimension, were investigated to demonstrate the accuracy and efficiency of the PAK-B^n method. In each example, the proposed method needed a small number of limit-state function evaluations to achieve accurate and converged estimates. PAK-B^n is expected to effectively deal with such challenging and time-consuming problems in practical engineering with robustness against the types of limit-state surface.
- The first-passage probability problems under stochastic wind loads were solved by the proposed *AL-HGP* method. AL-HGP utilized the Gaussian-process-based surrogates whose predictive mean and variance were employed to capture the conditional distribution of maximum response given the time-invariant basic random variable while handling heteroscedastic noise. This framework considered both uncertainties arising from the structural systems and the environmental wind loads. The proposed active learning framework further reduced the number of computational simulations by identifying the critical design of experiment (DoE) points that contribute most to the first-passage probability.
- The applications to the eight-story building system and transmission tower structure successfully demonstrated the performance and merits of the proposed AL-HGP method. In each example, the proposed method required fewer dynamic simulations to achieve accurate results, while the "non-adaptive"

surrogate-based estimates could produce inaccurate results with considerable variability. The transmission tower example demonstrated that AL-HGP could deal with high-fidelity computational simulations, e.g., finite element analyses, without losing the benefits and merits of the proposed method. Thus, AL-HGP is expected to effectively deal with such challenging and time-consuming problems in practical engineering.

- A new RBDO method using *QS-AGP* was proposed. The method utilized a quantile-based formulation to identify the probability-feasible design domain that satisfies the reliability requirements. An adaptive learning procedure was designed to further reduce the number of computational simulations by utilizing the exploration-exploitation trade-off based on quantile surrogates. The proposed optimization scheme relied on design samples and, thus, did not use an optimization algorithm or gradient information on cost and performance functions.
- The accuracy and efficiency of the QS-AGP were successfully tested through several RBDO problems featuring highly nonlinear performance functions, various distribution types, and complexity. In each example, the proposed method needed fewer performance function evaluations to achieve convergence to accurate results. QS-AGP is expected to effectively deal with such challenging and time-consuming RBDO problems in engineering practice.
- The quantile surrogate-based RBDO framework was further developed to handle the high-dimensional RBDO applications. The proposed *QS^2-AGP* aims to find the reliable optimal solution accurately and efficiently by combining the adaptive training process of the quantile surrogates with the design optimization

procedure guided by the parameter sensitivity of quantile surrogates. By avoiding the use of pre-generated design samples and the MC-sample based procedure to fit the quantile surrogate in the previous QS-AGP, QS^2-AGP achieved a superior level of efficiency, especially for RBDO problems with a larger number of design parameters. The formulations of the parameter sensitivity of the quantile surrogate also helped further reduce the computational costs.

- The performance and merits of the proposed QS^2-AGP method were successfully demonstrated through several numerical examples including high-dimensional RBDO problems up to 15 design parameters and engineering applications. In each example, the proposed QS^2-AGP method required fewer performance function evaluations in achieving convergence to accurate results than other RBDO methods. In addition, the proposed QS^2-AGP demanded dramatically less computational cost than QS-AGP and treated high-dimensional RBDO problems effectively. Thus, QS^2-AGP is expected to effectively deal with a variety of challenging and time-consuming RBDO problems including complex engineering systems and high-dimensional RBDO problems in which the number of the design parameters is considerably large.

6.2 Recommendations for future studies

In order to propose a new active learning-based method that covers more realistic engineering systems and advance the frontiers of applications relevant to this study, the following topics are recommended for future research:

- The performance of PAK-B^n is successfully demonstrated for problems with up to 9 random variables. If the dimension of input random variable space, n is considerably larger, e.g., $n > 40$, the probability density function of standard normal variables will be concentrated around the "important ring" region characterized by $R \approx \sqrt{n}$ (Wang and Song 2016). Just as seen in other reliability analysis approaches, alternative modeling and analysis techniques, such as dimension reduction or sparse surrogate modeling (Zhang and Pandey 2013), need to be incorporated for effective applications of PAK-B^n to high-dimensional problems through future research efforts.
- Although AL-HGP focuses on the estimation of the first-passage probability under stochastic wind loads, the concept and framework can be applied to other engineering fields under various types of natural or human-made hazards, e.g., structural failure caused by a strong earthquake, or wire cable failure due to the mechanical vibration.
- While this study demonstrated that AL-HGP was effective for the reliability assessment of stochastic wind-excited systems, the design optimization considering these reliabilities is also an essential task for desirable decision-making under uncertainties. This can be achieved by extending the applicability of AL-HGP to the reliability-based design optimization of structures subjected to stochastic wind excitations.
- This study solved the RBDO problem to achieve a reliable optimal design of structures whose failure probability, i.e., the probability of violating the given constraints is lower than the target level for each component. However, the structural failure is often described by a system event, i.e., a logical function of

multiple failure modes. A systematic approach incorporating system reliability methods needs to be proposed to handle the complex events and achieve resilience of systems.

- Since the proposed quantile surrogate-based RBDO method, QS^2-AGP finds the optimal solution using a gradient-based optimizer using quantile surrogates and corresponding design parameter sensitivity, the design solution identified by the proposed framework can be local optimum if the performance and/or cost functions of structural systems are complex. Thus, incorporating a global optimization scheme can be a promising future research topic.
- In this study, even though several numerical examples including nonlinear limit-state functions are examined to demonstrate the performance of the proposed methods, their validation to experiment datasets is required to extend the applicability of the active learning methods to real world engineering problems. In addition, refined frameworks are needed to properly predict the structural responses having highly complex and nonlinear behavior, e.g., dynamic response showing hysteric characteristic.
- Since the proposed methods employ GP-based surrogate models for response predictions, the performance may degenerate if the distribution of structural system response is non-Gaussian, which is usually shown in the nonlinear dynamical systems having hysteretic behaviors. Thus, it is expected that incorporating other stochastic surrogate models having non-Gaussian assumptions (Yang and Perdikaris 2019; Zhu and Sudret 2021) will promote the future applications of active-learning methods to a wide class of structural systems.

- To mitigate the damage and losses to structures during severe disasters, it is important to define the damage state and social losses, which can be incorporated into the widely used performance-based engineering frameworks. Therefore, the applications of developed active learning-based methods to performance-based design optimization can be a promising future research topic.
- In structural design optimization, commonly considered design parameters are elements of structural systems, e.g., thickness or cross-sectional areas, and the topology of the design domain is assumed to be fixed. To determine the optimal material layouts and connectivities in a design domain, topology optimization has been widely studied and applied. Therefore, applications of the proposed active learning frameworks to topology optimization can be a promising future research topic in various engineering fields.

References

Abdelhady, A. U., Spence, S. M., and McCormick, J. (2022). Risk and fragility assessment of residential wooden buildings subject to hurricane winds. *Structural Safety*, 94, 102137.

Albermani, F., Kitipornchai, S., and Chan, R. W. (2009). Failure analysis of transmission towers. *Engineering failure analysis*, 16(6), 1922-1928.

Alibrandi, U. (2014). A response surface method for stochastic dynamic analysis. *Reliability Engineering & System Safety*, 126, 44-53.

Andrieu-Renaud, C., Sudret, B., and Lemaire, M. (2004). The PHI2 method: a way to compute time-variant reliability. *Reliability Engineering & System Safety*, 84(1), 75-86.

Arnold, B.C., Balakrishnan, N., and Nagaraja, H. N. (1992). *A first course in order statistics*, Wiley, New York.

ASCE. (2017). *Minimum Design Loads and Associated Criteria for Buildings and Other Structures*. ASCE/SEI 7-16, American Society of Civil Engineers.

Au, S. K., and Beck, J. L. (2003). Subset simulation and its application to seismic risk based on dynamic analysis. *Journal of Engineering Mechanics*, 129(8), 901-917.

Bucher, C. G., & Bourgund, U. (1990). A fast and efficient response surface approach for structural reliability problems. *Structural safety*, 7(1), 57-66.

Byun, J. E., & Royset, J. O. (2022). Data-driven optimization of reliability using buffered failure probability. *Structural Safety*, 98, 102232.

Cadini, F., Santos, F., and Zio, E. (2014). An improved adaptive kriging-based importance technique for sampling multiple failure regions of low probability. *Reliability Engineering & System Safety*, 131, 109-117.

Caflisch, R.E. (1998). *Monte Carlo and quasi-Monte Carlo methods*. Acta numerica, 7, 1–49.

Cai, Y., Xie, Q., Xue, S., Hu, L., and Kareem, A. (2019). Fragility modelling framework for transmission line towers under winds. *Engineering Structures*, 191, 686-697.

Chan, K. Y., S. J. Skerlos, and P. Papalambros. (2007). An adaptive sequential linear programming algorithm for optimal design problems with probabilistic constraints. *Journal of Mechanical Designs*, 129(2), 140–149.

Chakri, A., Yang, X. S., Khelif, R., and Benouaret, M. (2018). Reliability-based

design optimization using the directional bat algorithm. *Neural Computing and Applications*, 30(8), 2381-2402.

Chen, X., Hasselman, T., Neill, D., Chen, X., Hasselman, T., and Neill, D. (1997). Reliability based structural design optimization for practical applications. *In 38th Structures, structural dynamics, and materials conference (p. 1403)*.

Chen, X., and Kareem, A. (2004). Equivalent static wind loads on buildings: New model. *Journal of Structural Engineering*, 130(10), 1425-1435.

Chen, Z., H. Qiu, L. Gao, L. Su, and P. Li. (2013). An adaptive decoupling approach for reliability-based design optimization, *Computers and Structures*, 117, 58–66.

Cheynet, E., Jakobsen, J. B., and Reuder, J. (2018). Velocity spectra and coherence estimates in the marine atmospheric boundary layer. *Boundary-layer meteorology*, 169(3), 429-460.

Chun, M. H., Han, S. J., and Tak, N. I. (2000). An uncertainty importance measure using a distance metric for the change in a cumulative distribution function. *Reliability Engineering & System Safety*, 70(3), 313-321.

Chun, J., Song, J., and Paulino, G. H. (2016). Structural topology optimization under constraints on instantaneous failure probability. *Structural and Multidisciplinary Optimization*, 53, 773-799.

Chun, J., Song, J., and Paulino, G. H. (2019). System-reliability-based design and topology optimization of structures under constraints on first-passage probability. *Structural Safety*, 76, 81-94.

Davenport, A. G. (1967). The dependence of wind loads on meteorological parameters. *In Proc. Int. Res. Seminar, Wind Effects on Buildings and Structures*, Ottawa, Univ. of Toronto Press, 19-82.

Deisenroth, M.P. (2009) *Efficient reinforcement learning using Gaussian Processes*. KIT Scientific Publishing.

Der Kiureghian, A. (2022). *Structural and System Reliability*. Cambridge University Press.

Der Kiureghian, A., and Ditlevsen, O. (2009). Aleatory or epistemic? Does it matter?. *Structural Safety*, 31, 105-112.

Deodatis, G. (1996). Simulation of ergodic multivariate stochastic processes. *Journal of Engineering Mechanics*, 122(8), 778-787.

Du, X., and Chen, W. (2004) Sequential optimization and reliability assessment method for efficient probabilistic design. *Journal of Mechanical Design*,

126, 225-233.

Du, X. (2008) Unified uncertainty analysis by the first order reliability method. *Journal of Mechanical Design*, 130(9), 091401-10.

Dubourg, V., Sudret, B., and Bourinet, J. M. (2011). Reliability-based design optimization using kriging surrogates and subset simulation. *Structural and Multidisciplinary Optimization*, 44, 673-690.

Dubourg, V., Sudret, B., and Deheeger, F. (2013). Metamodel-based importance sampling for structural reliability analysis. *Probabilistic Engineering Mechanics*, 33, 47-57.

Echard, B., Gayton, N., and Lemaire, M. (2011). AK–MCS: an active learning reliability method combining Kriging and Monte Carlo simulation. *Structural Safety*, 33(2), 145–154.

Ellingwood, B. R., Rosowsky, D. V., Li, Y., Kim, J. H. (2004). Fragility assessment of light-frame wood construction subjected to wind and earthquake hazards. *Journal of Structural Engineering*, 130(12), 1921-1930.

Enevoldsen, I., and Sorensen, J. D. (1994). Reliability-based optimization in structural engineering. *Structural Safety*, 15(3), 169-196.

Fauriat, W., and Gayton, N. (2014). AK-SYS: An adaptation of the AK-MCS method for system reliability. *Reliability Engineering & System Safety*, 123, 137-144.

FEMA, P. (2018). *Assessing Seismic Performance of Buildings with Configuration Irregularities*. Calibrating Current Standards and Practices.

Gidaris, I., Taflanidis, A. A., and Mavroeidis, G. P. (2015). Kriging metamodeling in seismic risk assessment based on stochastic ground motion models. *Earthquake Engineering & Structural Dynamics*, 44(14), 2377-2399.

Girard, A., Rasmussen, C. E., Candela, J. Q., and Smith, R. M. (2003). Gaussian process priors with uncertain inputs application to multiple-step ahead time series forecasting. *In Proceedings of the Advances in Neural Information Processing Systems 15*.

Ghosh, S., Roy, A., & Chakraborty, S. (2018). Support vector regression based metamodeling for seismic reliability analysis of structures. *Applied Mathematical Modelling*, 64, 584-602.

Huang, X., Chen, J., and Zhu, H. (2016). Assessing small failure probabilities by AK–SS: An active learning method combining Kriging and Subset Simulation. *Structural Safety*, 59, 86-95.

Jerez, D. J., Jensen, H. A., and Beer, M. (2022). Reliability-based design

optimization of structural systems under stochastic excitation: An overview. *Mechanical Systems and Signal Processing*, 166, 108397.

Jensen, H. A., Jerez, D. J., and Valdebenito, M. (2020). An adaptive scheme for reliability-based global design optimization: A Markov chain Monte Carlo approach. *Mechanical Systems and Signal Processing*, 143, 106836.

Jones, D. R., Schonlau, M., and Welch, W. J. (1998). Efficient global optimization of expensive black-box functions. *Journal of Global Optimization*, 13(4), 455-492.

Kaimal, J. C., Wyngaard, J. C. J., Izumi, Y., and Coté, O. R. (1972). Spectral characteristics of surface-layer turbulence models. *Quarterly Journal of the Royal Meteorological Society*, 98(417), 563-589.

Kanjilal, O., Papaioannou, I., and Straub, D. (2021). Cross entropy-based importance sampling for first-passage probability estimation of randomly excited linear structures with parameter uncertainty. *Structural Safety*, 91, 102090.

Kim, J., and Song, J. (2020). Probability-Adaptive Kriging in n-Ball (PAK-Bn) for reliability analysis. *Structural Safety*, 85, 101924.

Kim J, Kang, S. C., Kim, J. K., and Song, J. (2021). Yield strength estimation of X65 and X70 steel pipe with relatively low t/D ratio. *Steel and Composite Structures*, 38(2), 151-164.

Kim, J., and Song, J. (2021a). Reliability-Based Design Optimization Using Quantile Surrogates by Adaptive Gaussian Process. *Journal of Engineering Mechanics*, 147(5), 04021020.

Kim, J., and Song, J. (2021b). Quantile surrogates and sensitivity by adaptive Gaussian process for efficient reliability-based design optimization. *Mechanical Systems and Signal Processing*, 161, 107962.

Kim, J., Yi, S., and Song, J. Estimation of first-passage probability under stochastic wind excitations by active-learning-based heteroscedastic Gaussian process. Under review.

Kim, T., and Song, J. (2018). Generalized reliability importance measure (GRIM) using Gaussian mixture, *Reliability Engineering & System Safety*, 173, 105-115.

Kim, T., Kwon, O. S., and Song, J. (2020). Probabilistic evaluation of seismic responses using deep learning method. *Structural Safety*, 84, 101913.

Kim, T., Kwon, O.S., and Song, J. (2021). Clustering-based adaptive ground motion selection algorithm for efficient estimation of structural fragilities. *Earthquake Engineering and Structural Dynamics*, 50(6), 1755-1776.

Kurtz, N., and Song, J. (2013). Cross-entropy-based adaptive importance sampling using Gaussian mixture. *Structural Safety*, 42, 35-44.

Kyprioti, A.P., and Taflanidis, A.A. (2021). Kriging metamodeling for seismic response distribution estimation. *Earthquake Engineering and Structural Dynamic,* 50(13), 3550-3576.

Lázaro-Gredilla, M., and Titsias, M. K. (2011). Variational heteroscedastic Gaussian process regression. *In: ICML*, 841-848.

Lázaro-Gredilla, M., Titsias, M. K., Verrelst, J., and Camps-Valls, G. (2013). Retrieval of biophysical parameters with heteroscedastic Gaussian processes. *IEEE Geoscience and Remote Sensing Letters*, 11(4), 838-842.

Lee, T. H., and Jung, J. J. (2008) A sampling technique enhancing accuracy and efficiency of metamodel-based RBDO: Constraint boundary sampling. *Computers and Structures*, 86, 1463-1476.

Lee, I., Choi, K. K., Noh, Y., Zhao, L., and Gorsich, D. (2011). Sampling-based stochastic sensitivity analysis using score functions for RBDO problems with correlated random variables. *Journal of Mechanical Design*, 133(2), 021003.

Lelièvre, N., Beaurepaire, P., Mattrand, C., and Gayton, N. (2018). AK-MCSi: a Kriging-based method to deal with small failure probabilities and time-consuming models. *Structural Safety*, 73, 1–11.

Li, Y., and Kareem, A. (1993). Simulation of multivariate random processes: Hybrid DFT and digital filtering approach. *Journal of Engineering Mechanics*, 119(5), 1078-1098.

Li, M., Sadoughi, M., Hu, C., Hu, Z., Eshghi, A. T., and Lee, S. (2019). High-dimensional reliability-based design optimization involving highly nonlinear constraints and computationally expensive simulations. *Journal of Mechanical Design*, 141(5), 051402.

Li, M., and Wang, Z. (2019). Surrogate model uncertainty quantification for reliability-based design optimization. *Reliability Engineering & System Safety*, 192, 106432.

Liang, J., and Mourelatos, Z. P. (2007) Nikolaidis E. A single-loop approach for system reliability-based design optimization. *Journal of Mechanical Design*, 129(12), 1215-1224.

Lutes, L. D., and Sarkani, S. (2004). *Random vibrations: analysis of structural and mechanical systems*. Butterworth-Heinemann.

Marelli, S., and Sudret, B. (2018). An active-learning algorithm that combines sparse polynomial chaos expansions and bootstrap for structural reliability

analysis. *Structural Safety*, 75, 67–74.

Masoomi, H., Ameri, M. R., van de Lindt, J. W. (2018). Wind performance enhancement strategies for residential wood-frame buildings. *Journal of Performance of Constructed Facilities*, 32(3), 04018024.

Mchutchon, A., and Rasmussen, C. E. (2011). Gaussian process training with input noise. *In Proceedings of the Advances in Neural Information Processing Systems 24*.

Mohammadi, D. Y., Shafieezadeh, A., and Cha, K. (2020). Effect of modelling complexities on extreme wind hazard performance of steel lattice transmission towers. *Structure and Infrastructure Engineering*, 16(6), 898-915.

Moustapha, M., Sudret, B., Bourinet, J. M., and Guillaume, B. (2016). Quantile-based optimization under uncertainties using adaptive Kriging surrogate models. *Structural and Multidisciplinary Optimization*, 54, 1403-1421.

Moustapha, M., and Sudret, B. (2019) Surrogate-assisted reliability-based design optimization: a survey and a unified modular framework. *Structural and Multidisciplinary Optimization*, 60, 2157-2176.

Myers, R. H., Montgomery, D. C., Vining, G. G., Borror, C. M., and Kowalski, S. M. (2004). Response surface methodology: a retrospective and literature survey. *Journal of quality technology*, 36(1), 53-77.

Nguyen, T. H., Song, J., and Paulino, G. H. (2010) Single-loop system reliability based design optimization using matrix-based system reliability method: theory and applications. *Journal of Mechanical Design*, 132, 011005-11.

Nie, J., and Ellingwood, B.R. (2000) Directional methods for structural reliability analysis. *Structural Safety*, 22(3), 233-49.

Picheny, V., Ginsbourger, D., Roustant, O., Haftka, R. T., and Kim, N. H. (2010). Adaptive designs of experiments for accurate approximation of a target region.

Rasmussen, C. E., and Williams, C. K. I. (2006) *Gaussian Processes for Machine Learning*, the MIT Press. Cambridge.

Rasmussen, C. E., and Nickisch, H. (2015). Gaussian processes for machine learning (GPML) toolbox. *Journal of Machine Learning Research*, 11, 3011-3015.

Rogers, T. J., Gardner, P., Dervilis, N., Worden, K., Maguire, A. E., Papatheou, E., and Cross, E. J. (2020). Probabilistic modelling of wind turbine power curves with application of heteroscedastic Gaussian Process regression. *Renewable Energy*, 148, 1124-1136.

Schuëller, G., Pradlwarter, H., and Koutsourelakis, P. A. (2004) Critical appraisal of reliability estimation procedures for high dimensions. *Probabilistic Engineering Mechanics*,19(4), 463–74.

Slot, R. M., Sørensen, J. D., Sudret, B., Svenningsen, L., Thøgersen, M. L. (2020). Surrogate model uncertainty in wind turbine reliability assessment. *Renewable Energy*, 151, 1150-1162.

Shan, S., and Wang, G. G. (2008). Reliable design space and complete single-loop reliability-based design optimization. *Reliability Engineering & System Safety*, 93, 1218-1230.

Spence, S. M., and Gioffrè, M. (2012). Large scale reliability-based design optimization of wind excited tall buildings. *Probabilistic Engineering Mechanics*, 28, 206-215.

Spence, S. M. J., Chuang, W. C., Tabbuso, P., Bernardini, E., Kareem, A., Palizzolo, L., and Pirrotta, A. (2016). Performance-based engineering of wind-excited structures: A general methodology. *In Geotechnical and Structural Engineering Congress 2016*, 1269-1282.

Suksuwan, A., and Spence, S. M. (2018). Efficient approach to system-level reliability-based design optimization of large-scale uncertain and dynamic wind-excited systems. *ASCE-ASME Journal of Risk and Uncertainty in Engineering Systems, Part A: Civil Engineering*, 4(2), 04018013.

Subgranon, A., and Spence, S. M. (2021). Performance-based Bi-objective optimization of structural systems subject to stochastic wind excitation. *Mechanical Systems and Signal Processing*, 160, 107893.

Tu, J., Choi, K. K., and Park, Y. H. (1999). A new study on reliability-based design optimization. *Journal of Mechanical Design*, 121(4), 557-564.

Wang, L., McCullough, M., and Kareem, A. (2013). A data-driven approach for simulation of full-scale downburst wind speeds. *Journal of Wind Engineering and Industrial Aerodynamics*, 123, 171-190.

Wang, X., and Fang, K.T. (2003). The effective dimension and quasi-Monte Carlo integration. *Journal of Complexity*, 19(2), 101-24.

Wang, Z., and Song, J. (2016) Cross-entropy-based adaptive importance sampling using von Mises-Fisher mixture for high dimensional reliability analysis. *Structural Safety*. 59. 45–54.

Wang, Z., Broccardo, M., and Song, J. (2019). Hamiltonian Monte Carlo methods for subset simulation in reliability analysis. *Structural Safety*, 76, 51-67.

Wang, Z., and Broccardo, M. (2020). A novel active learning-based Gaussian process

metamodelling strategy for estimating the full probability distribution in forward UQ analysis. *Structural Safety*, 84, 101937.

Wen, Z., Pei, H., Liu, H., and Yue, Z. (2016). A Sequential Kriging reliability analysis method with characteristics of adaptive sampling regions and parallelizability. *Reliability Engineering & System Safety*, 153,170–179.

Wood, G. S., Kwok, K. C., Motteram, N. A., and Fletcher, D. F. (2001). Physical and numerical modelling of thunderstorm downbursts. *Journal of Wind Engineering and Industrial Aerodynamics*, 89(6), 535-552.

Xiao, N. C., Zuo, M. J., and Zhou, C. (2018). A new adaptive sequential sampling method to construct surrogate models for efficient reliability analysis. *Reliability Engineering & System Safety*, 169, 330-338.

Yang, D. Y., Teng, J. G., and Frangopol, D. M. (2017). Cross-entropy-based adaptive importance sampling for time-dependent reliability analysis of deteriorating structures. *Structural Safety*, 66, 38-50.

Yang, Y., and Perdikaris, P. (2019). Conditional deep surrogate models for stochastic, high-dimensional, and multi-fidelity systems. *Computational Mechanics*, 64(2), 417-434.

Yi, S., and Song, J. (2021). First-passage probability estimation by Poisson branching process model. *Structural Safety*, 90, 102027.

Youn, B. D., Choi, K. K., and Park, Y. H. (2003). Hybrid analysis method for reliability-based design optimization. *Journal of Mechanical Design*, 125(2), 221-232.

Youn, B. D., and Choi, K. K. (2004). A new response surface methodology for reliability-based design optimization. *Computers and Structure*. 82, 241-256.

Zhang, X., and Pandey, M. D. (2013). Structural reliability analysis based on the concepts of entropy, fractional moment and dimensional reduction method. *Structural Safety*, 43, 28-40.

Zhang, J., Taflanidis, A. A., and Medina, J. C. (2017). Sequential approximate optimization for design under uncertainty problems utilizing Kriging metamodeling in augmented input space. *Computer Methods in Applied Mechanics and Engineering*, 315, 369-395.

Zhang, X., Wang, L., and Sørensen, J. D. (2020). AKOIS: an adaptive Kriging oriented importance sampling method for structural system reliability analysis. *Structural Safety*, 82, 101876.

Zhu, X., and Sudret, B. (2021). Emulation of stochastic simulators using generalized lambda models. *SIAM/ASA Journal on Uncertainty Quantification*, 9(4),

1345-1380.

Zuev, K. M., Beck, J. L., Au, S. K., and Katafygiotis, L. S. (2012). Bayesian post-processor and other enhancements of Subset Simulation for estimating failure probabilities in high dimensions. *Computers and structures*, 92, 283-296.

초 록

김정호
건설환경공학부
서울대학교 대학원

현대사회의 재난 복원력을 확보하기 위해서는 구조 시스템이 설계 및 유지보수 과정에서 적절한 수준의 신뢰도를 확보하는 것이 필수적이다. 이러한 설계 절차는 궁극적으로 치명적인 손상이나 손실을 초래할 수 있는 예기치 않은 고장의 위험을 방지함으로써 구조 시스템의 신뢰도를 보장할 수 있다. 따라서, 구조물 및 기타 공학시스템의 설계 과정에서 신뢰성 평가 및 최적화를 위한 방안 구축이 필수적이다. 하지만 신뢰성 해석은 반복적인 시스템 성능 평가를 요구하기 때문에 높은 계산 비용을 초래한다. 이 문제는 특히 구조 시스템이 시스템 성능을 정확하게 모사하기 위해 복잡하고 고차원적인 모델을 필요로 할 때 더욱 악화된다. 다양한 불확실성 하에서 복잡한 구조 시스템을 효율적으로 설계하고 평가하기 위해, 본 학위논문은 신뢰도 평가 및 신뢰도 기반 최적 설계(Reliability-based Design Optimization; RBDO)를 위해 계산 시뮬레이션 데이터로 학습된 시스템 성능의 적응형 대리모델을 활용하는 능동학습(Active learning) 기법을 제안하고자 한다.

최소한의 실험 데이터로 구조물의 신뢰도를 추정하기 위해 능동학습 기반 신뢰도 평가 기법을 제안하였다. 제안된 Probability-Adaptive Kriging in *n*-Ball (PAK-B^n) 방법은 크리깅(Kriging), 혹은 가우시안 프로세스(Gaussian Process; GP)로 알려진 대리모델을 활용하여 한계상태함수를 근사하고 이를 적응형 능동학습으로 학습시켰다. 제안된 PAK-B^{n}은 무작위 변수 공간의 확률적 밀도를 근사 한계상태함수를 식별하는 적응형 학습 절차에 통합하였다. 또한 통계적 학습을 위한 후보점으로 *n*차원 구체, *n*-ball 샘플링 기법을 도입하여, 구조물의 신뢰도 평가에 가장 큰 영향을 미치는 최적의

학습 후보를 결정하였다. 수치 예제를 통하여 개발된 PAK-B^n 방법의 적용 가능성 및 정확성을 입증하였다.

앞서 개발된 PAK-B^{n}은 10개까지의 확률변수를 포함하는 신뢰성 문제에 효과적이지만, 고차원 적용은 제한적이며, 이 문제는 풍하중, 지진 및 충돌과 같은 자연 및 인위적 위험에 노출되는 구조 시스템의 신뢰도를 평가하는 데 필수적이다. 이러한 문제를 해결하고 확률적 바람 가진 구조 시스템에 대한 적용 가능성을 확장하기 위해 Active learning-based Heteroscedastic Gaussian process (AL-HGP)를 제안하였다. 각각 최대 응답의 조건부 분포를 나타내는 가우스 혼합 분포에 의해 제안된 공식은 구조 시스템과 환경 풍하중에서 발생하는 불확실성을 고려하며 이분산 노이즈를 갖는 GP 대리모델에 의한 신뢰성 예측을 가능하게 하였다. 또한 대리모델의 적응형 학습 과정을 통해 효율적인 수렴을 달성하는 최적의 실험 배치를 수립하였다. 공학시스템 응용 사례는 제안된 AL-HGP 방법의 성능을 입증하였다.

복잡 구조물의 신뢰도 기반 최적 설계안을 도출하기 위해 능동학습 기반 RBDO 방법을 개발하였다. 개발된 RBDO 방법, 즉 Quantile Surrogates by Adaptive Gaussian Process (QS-AGP)는 한계상태 함수의 분위(Quantile)를 효율적인 대리모델로 근사하여 목표 신뢰도를 만족하는 허용 설계 공간을 식별하였다. 유도한 분위 대리모델은 내재적 불확실성과 대리모델 오차를 모두 고려하여 탐색-활용(Exploration-Exploitation) 트레이드오프를 통해 적용형으로 학습시켰다. 이 과정에서 신뢰도 기반 최적 설계 도출에 가장 큰 영향을 미치는 영역으로 적응형 학습이 수행되도록 학습 함수를 제안하였다. 제안된 QS-AGP는 기존 RBDO 접근법보다 신뢰도 기반 최적 설계안을 도출하는 데 있어 더 적은 수의 성능 평가가 필요함을 확인하였다.

개발된 QS-AGP의 아이디어를 고차원 공학시스템의 신뢰도 기반 설계 최적화에 적용하기 위해 Quantile Surrogates and Sensitivity by Adaptive Gaussian Process (QS^2-AGP) 기법을 제안하였다. 한계상태함수의 분위 예측식을 가우시안 프로세스의 커널(Kernel) 함수로 구축하고 비표본 기반 최적화

절차를 제안하였다. 또한, 미리 생성된 샘플에 의존하지 않고 고차원 신뢰도 기반 최적 설계를 수행하기 위해 설계변수 민감도를 수치 식으로 제시하였다. 고차원 RBDO를 포함한 다양한 예제로 개발된 QS^2-AGP 기법의 적용 가능성과 효율성을 입증하였다.

제안된 방법론의 성능은 높은 충실도(High Fidelity)의 계산 시뮬레이션을 포함한 수치 예시로 입증하였다. 본 학위논문에서 개발된 능동학습 기반 신뢰도 평가 및 신뢰도 기반 최적화 방법론은 현대 인프라구조 시스템의 설계 및 유지보수 결정 지원과 재난 복원력 향상에 기여할 것으로 기대된다.

주요어: 가우시안 프로세스, 구조신뢰성, 능동 학습, 의사 결정, 대리모델, 신뢰도 평가, 신뢰도 기반 최적 설계, 실험계획법, 위험 기반 설계, 최적화, 추계학적 하중

학번: 2016-26343